

Automated prediction of tailings areas at historic gold mine districts in Nova Scotia
using multispectral images and a random forest classifier

By
Daniel A. Jewell

A Thesis Submitted to
Saint Mary's University, Halifax, Nova Scotia
in Partial Fulfillment of the Requirements for
the Degree of Master of Science in Applied Science

September 2023, Halifax, Nova Scotia

Copyright Daniel A. Jewell, 2023

Approved: Dr. Linda Campbell
Supervisor

Approved: Dr. H. Peter White
Co-Supervisor

Approved: Dr. Michael Parsons
Committee Member

Approved: Dr. Erin Adlakha
Committee Member

Approved: Dr. Sylvain Leblanc
External Examiner

Date: September 6th, 2023

Automated prediction of tailings areas at historic gold mine districts in Nova Scotia
using multispectral images and a random forest classifier

by Daniel A. Jewell

Abstract

Satellite imagery can be analyzed to offer a preliminary regional assessment of mine tailings indicators, enabling identification before performing in-depth fieldwork. Nova Scotia, Canada, still retains mine tailings produced in the 1860s to the 1940s in 64 historic gold districts, which exceed soil guidelines for arsenic (As) and mercury (Hg) levels. Tailings data often relies on historical maps, which may not accurately depict the current extent due to wind and rain transportation. This study employs historical data to train a classifier, enabling the classification of multispectral satellite images from Sentinel-2. Both pixel-wise and object-based methods were evaluated, yielding a median F1-score above 0.7 for most tested methods at two case study sites. Accuracy varied at other sites, particularly those with significant proportions of wetland areas. Lastly, we investigate false positives and propose future research to create a more resilient classifier.

September 6th, 2023

Acknowledgements

I would like to first acknowledge that this work took place in Mi'kma'ki, which is the ancestral and unceded territory of the Mi'kmaq People. Mi'kma'ki is covered by the Peace and Friendship Treaties, signed between 1725 and 1779. These treaties were signed between the British Crown and the Mi'kmaq, Wəlastəkwewiyik (Maliseet), and Passamaquoddy Peoples, as well as other members of the Wabanaki Confederacy, and did not include the surrender of lands or resources.

Thank you to my supervisors, Dr. Linda Campbell, and Dr. H. Peter White. You have been unwaveringly supportive and patient, even as I started to wonder if I would finish this. You have given me an incredible opportunity, for which I will always be grateful. I'd additionally like to thank the other members of my committee, Dr. Michael Parsons, and Dr. Erin Adlakha, for sharing their expertise and providing much-needed edits. I have learned much from each of you, not limited to your scientific knowledge.

A huge thank you to the members of the DEEHR lab, past and present. To Sarah Kingsbury and Michael Smith, thank you for your advice and encouragement when I began this program just as the pandemic was starting. Those were uncertain days, and though it may not have seemed like much I wouldn't have got off the ground without your support. Thanks also to David M. Lewis, Jenna Campbell, Heidi Gavel, Lucinda Laskey, Emily Chapman, and everyone else who helped with field or lab work, or who just provided their time and company.

Thank you to faculty and staff at Saint Mary's University, including Dr. Xiang Yang and Dr. Mitchell Kerr for help in the Electron Microscopy Center, Greg Baker at MP_SpARC, Ashley Campbell and members of the Faculty of Science Interpreting Services, and many others.

Thanks to Ernie Hennick at the Nova Scotia Department of Natural Resources and Renewables, whose knowledge of the province's historic mines was incredibly helpful. Thank you as well to the rest of the team that put the Nova Scotia Mine Tailings Database together. It was an invaluable resource.

I gratefully acknowledge the various sources of funding for this project. Natural Resources Canada's Earth Observation for Cumulative Effects Program, via the Research Affiliate Program, an NSERC Discovery Development Grant provided to Dr. Campbell, EcoCanada, and The Hewitt Foundation.

Lastly, thank you to my friends and family who have supported me throughout these last few years. Thanks especially to Kate.

Contents

Abstract	i
Acknowledgements	ii
Table of Abbreviations	vii
Chapter 1: Introduction and Research Objectives	1
1.1. <i>Historic Gold Mining and Modern Secondary Minerals</i>	2
1.1.1. Regional Mining History.....	2
1.1.2. Tailings Mineralogy.....	4
1.1.3. Spectrally Active Minerals.....	4
1.1.4. Mobility of As and Environmental Impact.....	6
1.2. <i>Mapping Mine Tailings Indicators Using Multispectral Remote Sensing</i>	7
1.2.1. Remote Sensing Types and Platforms.....	7
1.2.2. Sentinel-2.....	9
1.3. <i>Existing Data at Nova Scotia’s Historic Gold Mines</i>	10
1.3.1. Nova Scotia Mine Tailings Database.....	11
1.3.2. Select Mine Studies.....	11
1.3.3. Google Earth Engine.....	13
1.4. <i>Summary and Future Work</i>	13
1.5. <i>References</i>	15
Chapter 2: Historical Gold Mine Tailings Indicators: Pixel and Object-Based Classification Models	1
2.1. <i>Introduction</i>	1
2.1.1. Historic Mining and Present Contaminants.....	3
2.1.2. Geology of Nova Scotia Gold Deposits.....	5
2.1.3. Spectral Reflectance and Pixel Mixing.....	6
2.1.4. Detecting Gold Mine Tailings at Historic Mines Using Space-Based Remote Sensing.....	8
2.1.4.1. Sentinel-2 Mission and Sensors.....	8
2.1.4.2. Google Earth Engine.....	9
2.1.5. Study Area.....	10
2.2. <i>Methods</i>	11
2.2.1. Data Acquisition and Initial Processing.....	11
2.2.1.1. Pre-Processing of Sentinel-2 Images.....	11
2.2.1.2. Nova Scotia Mine Tailings Database.....	12
2.2.1.3. Masking Vegetation and Water Pixels.....	13
2.2.2. Characterization of Historic Gold Mine Waste Samples.....	16

2.2.2.1. Tailings Sample Collection	16
2.2.2.2. Scanning Electron Microscope (SEM) Analysis	17
2.2.3. Image Sampling for Training and Classification	18
2.2.3.1. Remote-Sensing Image Sample Design	18
2.2.3.2. Non-Tailings Sampling Using Stratified Random Sampling	18
2.2.3.3. Sampling Tailings Areas in Sentinel-2 Images	19
2.2.3.4. Splitting Training and Test Areas for Cross-Validation	19
2.2.4. Classification	20
2.2.4.1. Random Forest Classifier	20
2.2.4.2. Accuracy Assessment: F-Score	21
2.2.4.3. Variable Importance and Selection	22
2.2.4.4. Pixel-Wise Classification of Test Areas	25
2.2.5. Object-Based Classification	25
2.3. Results	27
2.3.1. Physical Analysis of Tailings	27
2.3.1.1. Mineralogy and bulk geochemistry	27
2.3.1.2. SEM Results	28
2.3.2. Vegetation and Water Masks	28
2.3.3. Variable Optimization	30
2.3.4. Pixel-Wise Classification	31
2.3.4.1. Montague and Goldenville Districts	31
2.3.4.2. All Districts Using Random Testing and Training Subsets	31
2.3.5. Object-Based Classification	31
2.4. Discussion	33
2.4.1. Data Sources for Training and Validation	33
2.4.2. Variable Importance	35
2.4.3. Pixel-Wise Classification	36
2.4.4. Object-Based Classifier	38
2.5. Conclusion	40
2.6. Figures	42
2.7. Tables	60
2.8. References	62
Chapter 3: Exploring the Causes of False Positives from a Tailings Classifier	72
3.1. Historic Gold Mining and Modern Secondary Minerals	73
3.1.1. Historical Gold Mine Tailings Mineralogy	74
3.2. Mapping Historical Mine Tailings Indicators Using Multispectral Remote Sensing	75

3.2.1.	Collecting Training Data from Images	77
3.2.2.	Spectrally Active Minerals	77
3.2.3.	The Mine Tailings Classification Model	79
3.2.4.	Google Earth Engine	81
3.3.	<i>Applying Remote Sensing Model to Historic Gold Mine Sites</i>	82
3.3.1.	Montague Gold Mine District	82
3.3.2.	Oldham Gold Mine District	83
3.3.3.	Waverley Gold Mine District: Muddy Pond	84
3.4.	<i>Mapping Indicators of Tailings</i>	84
3.4.1.	Possible Causes of Positive Classification	85
3.4.1.1.	Sediments of Estuarine Environments Downstream of Mine Districts	87
3.4.1.2.	Wetlands	89
3.4.2.	Comparison of Land Cover Reflectance	90
3.5.	<i>Results and Discussion</i>	91
3.6.	<i>Conclusion</i>	93
3.7.	<i>Figures</i>	95
3.8.	<i>Tables</i>	102
3.9.	<i>References</i>	103
	Appendix A: Raw Data	1
	Appendix B: Additional Maps	5

Note: This thesis was written in manuscript style, with the intent to publish separately. Chapters are formatted according to the style guide of *Remote Sensing of Environment*. Some details are presented in both chapters. Chapter 1 presents a case study in which big data techniques are applied to indicate the presence of tailings at two mine sites. Chapter 2 provides an exploration of potential causes of false positives following classification using the methods described in Chapter 1.

Table of Abbreviations

Abbreviation	Definition
BSE	Backscattered Electron
CCME	Canadian Council of Ministers of the Environment
EDS	Energy Dispersive Spectroscopy
EM	Electromagnetic
ESA	European Space Agency
FII	Ferric Iron Index
GEE	Google Earth Engine
GSC	Geological Survey of Canada
IFD	Iron Feature Depth
MNDWI	Modified Normalized Difference Water Index
NDVI	Normalized Difference Vegetation Index
NDWI	Normalized Difference Water Index
NIR	Near-Infrared
NSMTD	Nova Scotia Mine Tailings Database
RF	Random Forest
SCL/SCM	Scene Classification Layer/Scene Classification Map
SEM	Scanning Electron Microscope
SNIC	Simple Non-Iterative Clustering
VNIR	Visible-to-Near-Infrared

Chapter 1: Introduction and Research Objectives

Mining and processing of gold ore has historically been an economic driver in many regions around the world, but a poor understanding of the environmental impact of mine waste, or tailings, has often led to inadequate long-term management. Waste from mines active over a century ago often contain contaminants, such as arsenic (As), at quantities well above recommended soil guidelines (CCME, 1997). Contaminated sediment at these sites may also be transported by streams or wind, increasing the potential area of their negative environmental impact. In regions where historic mine waste is prevalent it may be impractical to remediate all sites at once. Sites must first be assessed to determine which pose the greatest risk. In Nova Scotia, Canada, over 300 mines were developed between the 1860s and 1940s, organized into 64 historic gold mine districts. In many cases, the best available data are historical records that may no longer accurately depict tailings areas. Sending researchers to the field to observe all 64 districts and collect and test sediment samples would be expensive and time consuming. Analysing satellite images using remote sensing techniques can provide a preliminary assessment of mine tailings areas, helping to better plan fieldwork and make more efficient use of resources.

Identifying mine tailings across a large region using passive remote sensing satellites requires that tailings comprise spectrally active minerals, and that those minerals are distinct from those of background sediment. In the following chapters of this thesis these concepts are explored, as well as several methods developed to classify Sentinel-2 images and identify mine

tailings areas within them. This introductory chapter describes the problem addressed by this study and provides fundamentals of remote sensing analysis, as well as a brief overview of relevant existing literature.

1.1. Historic Gold Mining and Modern Secondary Minerals

1.1.1. Regional Mining History

Most of the gold in Nova Scotia has been historically mined in the Meguma Supergroup. The Meguma Group shares its name with the Meguma Terrane which makes up about half of the mainland of Nova Scotia, the other half being the older Avalon Terrane to the northwest. The high-grade gold consist mainly of quartz, though sulphide minerals are common as well and their quantities vary directly with that of gold (Sangster et al., 2007). These sulphide minerals have been the main source of As released by mining and processing and are generally the greatest threat to human and ecosystem health of any mining by-product (Ngole-Jeme and Fantke, 2017; Walker et al., 2009).

Ore rock was extracted mainly from shafts in the ground and crushed in stamp mills. In many cases, particularly in the 19th century, mercury (Hg) was used to separate gold from the crushed material (Bates, 1987; LeBlanc et al., 2020; Parsons et al., 2012). The leftover waste rock and sand to silt-sized sediment, called tailings, was deposited in streams, wetlands, or nearby depressions with little to no regard for potential environmental impacts (LeBlanc et al., 2020). In these tailings dumping areas, sulphide minerals were exposed to oxygen and surface water, leading to oxidation and dissolution of As and other metals (DeSisto et al., 2017). This As, as well as the Hg introduced in processing, may be capable of travelling long distances. New

minerals may incorporate available As, or it may be adsorbed onto existing minerals, either temporarily under certain local environmental conditions, or long-term as more stable secondary minerals (Jamieson et al., 2015; Walker et al., 2009). Though it can be transported via fine particles, Hg has been found to concentrate along watercourses in or near tailings sources (Lane et al., 1989). While Hg does pose a risk to human and ecosystem health and may be associated with mine tailings at these sites, it is neither visible via spectral analysis (using the methods and sensors explored in this study) nor associated with secondary minerals that are visible. This study focuses instead on As and its associated minerals.

In the early days of mining in the province, the government formed 64 gold mine districts. These districts were intended to expedite mining projects as well as keep claims organized. An estimated 3 000 000 tonnes of tailings were produced from these districts (Parsons et al., 2012), almost all of which has sat untouched since its deposition, with the exception of recreational vehicle use at some sites. Though the districts are no longer formally used, modern exploration and operations typically coincide with the historic districts, with modern open pit mines often existing alongside or even displacing historic tailings. The Government of Nova Scotia has initiated remediation plans, and at the time of this writing two sites have been selected for cleanup. The first is Montague Gold District, just north of Nova Scotia's capital city of Halifax. Bulk geochemical analysis of tailings at Montague has shown that tailings contain a median of approximately 11 000 ppm As (Parsons et al., 2012). The second site is Goldenville Gold District, which the same study showed has a median of approximately 7000 ppm As. This study looked at 14 sites in total, finding an overall median of 2550 ppm As

across all tailings samples. 99% of samples exceeded the Canadian Council of Ministers of the Environment (CCME) recommended limit of 12 ppm As (CCME, 1997; Parsons et al., 2012).

1.1.2. Tailings Mineralogy

Though no two sites have exactly the same mineralogy, the gold mines of mainland Nova Scotia do share similar bedrock geology and processing methods. Most mines targeted auriferous quartz veins present in slate and metasilstone. Common accessory minerals tend to include chlorite, biotite, muscovite, and plagioclase, which are present alongside carbonates and sulphides (Walker et al., 2009). Environmental impact was not a consideration in this period, and tailings were routinely left exposed to the environment. This study explores whether tailings, left exposed in some cases for over a century, are sufficiently different in mineralogy from natural sediment to be identified via spectral analysis.

1.1.3. Spectrally Active Minerals

Although the classifier used in this study relies on image sampling and does not depend on prior knowledge of the components of tailings, it is still important to understand what minerals are expected to be present and how they might contribute to the reflectance of tailings as a whole. Though tailings are made up of bedrock local to a site, they differ from bedrock in grain size and concentration. By increasing surface area, concentrating sulphides, and leaving this mixture exposed to the elements, mineralogy will begin to diverge from naturally occurring nearby sediment. If spectrally active minerals form in tailings, or the concentration of existing spectrally active minerals changes, it will be possible to determine tailings from background sediment.

Sulphide minerals, primarily arsenopyrite, are the primary source of As at these sites, and therefore are the most important minerals to identify. Ideally, these could be target directly by colour on the tailings surface, or by their reflectance spectra in the remote sensing imagery. Unfortunately, sulphide minerals are not considered spectrally active. They have fairly flat spectra and overall low reflectance, making them poor targets for this kind of analysis. They also are often covered in a rim of iron oxide, iron hydroxide, or hydrous iron arsenate (Corriveau et al., 2011; Walker et al., 2009). Fortunately, these rims are spectrally active. Iron oxides and iron oxyhydroxides have distinct absorption features between 750 and 910 nm, known as the iron absorption feature (Davies and Calvin, 2017; Mielke et al., 2014), that makes them viable remote sensing targets. Sentinel-2 imagery lacks the spectral resolution to determine the specific location of these absorption features, but it does have several bands placed in this range with geological applications in mind, including the narrow band 8A at 860 nm (European Space Agency, 2015). It may be able to detect, broadly, colour differences in this range that could differentiate pixels with these absorption features from those without.

The classifier used in this study assigns binary labels (tailings vs. non-tailings) to each pixel, defining tailings in the broadest sense and likely containing large inter-class variability in mineral composition. Interpreting the results of the classifier is dependent largely on understanding mineralogy typical at these sites, and which minerals are actually contributing to the spectral reflectance values in the imagery. This mineralogy is obtained either from previously published sources, or it could be gathered from field sampling designed around the classifier's results. The classifier may describe the extent of tailings, and with expert knowledge of a site mineralogy may be inferred, but the classifier itself cannot provide mineralogy.

1.1.4. Mobility of As and Environmental Impact

Arsenopyrite, which is the main As host mineral at these sites, occurs naturally throughout the Meguma Group. Meguma rocks contain elevated As, regardless of mining history, however, the process of mining gold ore brings arsenopyrite to the surface, concentrating it and increasing surface area (Corriveau et al., 2011; Weisener, 2003), making it more prone to oxidation and weathering.

The impact of As and its stability at surface depends primarily on mineral host, pH, and exposure to the atmosphere. Arsenopyrite is vulnerable to oxidation and frequently weathers to form scorodite ($\text{FeAsO}_4 \cdot 2\text{H}_2\text{O}$), amorphous ferric arsenate-sulphate or pharmacosiderite ($\text{KFe}_4(\text{AsO}_4)_3(\text{OH})_4 \cdot 6-7\text{H}_2\text{O}$), and, rarely, arsenolite (As_2O_3) (DeSisto et al., 2017; Walker et al., 2009).

Without proper containment using liners, fill, or other engineering techniques, As is likely to move in and out of solution and minerals over time. Meteoric water and groundwater changes may dissolve minerals and salts which may change pH drastically. This, in turn, will alter the solubility of minerals containing As and other metals. Fluctuating water levels due to regular seasonal changes, or long-term due to climate change or other major impacts to hydrological regimes, may leave minerals exposed to oxygen, changing their oxidation states. Ferrous iron (Fe^{3+}) can be a powerful oxidizing agent in certain pH ranges. Bacterial activity can increase oxidation in some cases by several orders of magnitude (Seal and Hammarstrom, 2003). The interplay of these factors is complex and cannot be fully described by the snapshot provided by the remote sensing methods proposed in this study. The proposed classification

model is meant to observe sites in their current state, taking in the sum of all these factors, though not describing any of them quantitatively.

1.2. Mapping Mine Tailings Indicators Using Multispectral Remote Sensing

The objective of this study is to indicate areas which exhibit similar spectral reflectance to tailings and should be investigated further to determine levels of contaminants. There are many options available for retrieving the spectra of a material, whether handheld or mounted on an aircraft or satellite. This section provides an overview of different kinds of sensors and a more detailed description of the Sentinel-2 satellite used in this study.

1.2.1. Remote Sensing Types and Platforms

Remote sensing images have been used extensively at historic and modern mine sites around the world since the 1970s. Broadly, remote sensing images can be captured by three kinds of platforms: field/lab instruments, aerial (planes and remotely-piloted aircraft), and space-based (satellites). Remote sensing images differ from other remote sensing or spectroscopic data in that they are composed of a grid of pixels, each of which has a stack of values (called data number, brightness value, grey level, etc.) corresponding to various bands. The meaning of those pixel values depends on the type of sensor being used. Sensors can be divided into active and passive, sometimes referred to as direct and apparent, respectively (Schowengerdt, 2007). Active sensors emit a signal which reaches a target and returns to the sensor. Information is derived from the difference between the emitted and received light. Active sensors include radar and lidar. Passive sensors only receive a signal, relying on light from the sun or an artificial, external source to illuminate their target. Radar signals can

penetrate clouds, some vegetation cover, and even certain sediments, but provide information in a limited electromagnetic range. Atmospheric effects, including thin, high-altitude clouds, can be removed from passive sensor images, but otherwise data from these sensors represent only the topmost surface of the earth. Passive sensors, however, provide information from a wide range of the electromagnetic spectrum. Specific sensor ranges vary widely, but generally range from 450 nanometres (nm) (visible range) to 2500 nm (shortwave-infrared range), with some sensors exceeding 10 000 nm (thermal range – e.g., NASA's ASTER). Passive sensors can be further divided by the number of bands that they have. Hyperspectral sensors contain anywhere from 40 to 400 or more contiguous bands, each of which spans only a few nanometers. Multispectral sensors contain a small number of relatively wide, non-contiguous bands. Landsat 9 contains a total of 11 bands between its 2 sensors, with bandwidths ranging from about 100 nm to 2000 nm. Sentinel-2 contains 13 bands, with bandwidths ranging from 200 nm to 1850 nm. Generally, bands at higher wavelengths have larger bandwidths due to lower emission from the sun in that range, and less sensitivity at the sensor. The broader bandwidth captures more photons, increasing signal-to-noise ratio. A sensor with narrower and more numerous bands is said to have a higher spectral resolution. This may allow greater discrimination of target materials. Often, higher spectral resolution comes at the cost of spatial resolution, resulting in larger pixels.

The trade-off between spectral and spatial resolutions is an important consideration when choosing a sensor for a study. Identifying materials in remote sensing imagery relies on the presence of distinct absorption and reflectance features, that may not be captured by the broader bands available from multispectral sensors. Sensors with low spatial resolution,

however, produce pixels that cover a larger area on the ground. In real-world applications this means that pixels are very unlikely to be pure, and more materials being mixed into a pixel may make it harder to identify a target.

There are other technical and practical considerations when choosing a sensor for a remote sensing study. While some platforms provide current and historical data free of charge, images from others must be purchased and costs can quickly become prohibitive. Some sensors capture images continuously, meaning that large libraries are already available and there is no need to requisition data for a study area. Others only capture data on request, making them inappropriate for time series analyses if past conditions are being considered. Depending on orbital parameters, it may be some time before an image is captured, and there is no guarantee of a cloud-free capture at that date. On the point of time series, revisit time may be an important consideration. Whether images are captured continuously or not, a platform's orbit varies. Revisit time is the frequency at which a satellite returns to the same point on the earth. Landsat 9's revisit time is 16 days, while Sentinel-2's is 10 days, which is cut to 5 days as the mission comprises a pair of nearly-identical satellites, offset in orbit by 180°.

1.2.2. Sentinel-2

Images from Sentinel-2 were selected for this study. The Sentinel-2 mission comprises a pair of nearly-identical satellites launched by the European Space Agency in 2015 and 2017 (Sentinel-2A and Sentinel-2B, respectively). Each has a return frequency of 10 days at the equator, and slightly less at higher latitudes. Their orbits are offset by 180°, and a new image is acquired at a given location every 5 days with the same viewing conditions, and more frequently with different viewing conditions (European Space Agency, 2015).

Sentinel-2 has 13 bands in varying spatial resolutions and bandwidths. It differs in this way from hyperspectral sensors which may contain several hundred contiguous bands, often at very narrow bandwidths (as small as ~2-5 nm). The 13 bands were chosen carefully based on observations from previous missions such as Landsat and to fulfill specific objectives (van der Meer et al., 2014). In general, Sentinel-2's bands are narrower than Landsat's to reduce the influence of water vapour in the atmosphere. Sentinel-2's band 8A (a near infrared band centered at 865 nm) was carefully placed to avoid water vapour, target peak NIR reflectance in vegetation, and be sensitive to iron oxides in soil (European Space Agency, 2015; van der Meer et al., 2014; Van der Werff and Van der Meer, 2015). For the purposes of this study, this represents a significant advantage for the Sentinel-2 over Landsat satellites. More accurate discernment of vegetation improves the ability of the model to filter out vegetation on the surface, and iron oxides are an important indicator when classifying tailings.

Sentinel-2 bands come in varied spatial resolutions. 4 bands are provided in 10 m resolution, 6 in 20 m, and 3 in 60 m. This is another advantage over the Landsat mission, which has a resolution of 30 m (excluding its panchromatic band). Many of the tailings areas at the historic mine sites in this study are less than 100 m wide. These are relatively small targets, and it is important to maximize the number of pixels within the target areas.

1.3. Existing Data at Nova Scotia's Historic Gold Mines

The gold mines throughout Nova Scotia have a long history, and a large quantity of data has been produced, ranging from the earliest collection of surveys in the early 20th century (Faribault, 1900) to present. The amount of data already available allows for a range of experimentation when creating a remote sensing model of the mine sites.

1.3.1. Nova Scotia Mine Tailings Database

An invaluable collection of data used in this study is the Nova Scotia Mine Tailings Database (NSMTD) (Hennick and Poole, 2020). This database is an aggregation of data of studies and surveys from all gold mine districts in the province. Tailings extents have been compiled into a spatial data format, alongside information on ore types, processing methods, and quantities of crushed rock. These tailings polygons were used as training and validation data in this study.

1.3.2. Select Mine Studies

In addition to the broad collection of tailings found in the NSMTD, studies of individual mines have been used for reference, geochemical, and mineralogical data. These sites have been the subject of considerable research efforts since the first environmental studies in the 1970s connected a case of As intoxication to the Waverley Gold Mine District (Hindmarsh et al., 1977; LeBlanc et al., 2020). Numerous studies have since been published describing sediments, As and Hg contamination, and biological accumulation. This section describes just a few key presenting data pertaining to the sites at large, or those that focus directly on Montague and Goldenville, which will be described in more detail in a later section.

Parsons et al., 2012, is an influential regional study of modern tailings extent and conditions. The researchers analyzed sediment from 14 sites for geochemistry and water quality. A total of 482 tailings and sediment samples were collected and analyzed for metal concentrations, showing a range in As from 10 to 312 000 ppm, and a median of 2250 ppm (LeBlanc et al., 2020; Parsons et al., 2012). This study prompted the province to create the Historic Gold Mines Advisory Committee in April 2005.

Chemistry of tailings will reveal metal concentrations, including As, which is the main focus of most environmental studies, but geochemical studies do not always include mineralogical data. Total As is a good measure of potential environmental and human health risk, it can be determined quickly, and it is easy to compare across multiple mine sites. Understanding As stability and transport potential requires mineralogical data. Understanding site mineralogy is important for remote sensing assessment because minerals in tailings, and not bulk chemistry, are what determine spectral absorption and reflection features in the visible to short-wave infrared region. Many studies have sought to determine mineralogy at Nova Scotia's historic gold mine sites, often explicitly focusing on minerals that contain As or influence its dissolution, precipitation and/or adsorption. In Walker et al., 2009, researchers determined mineralogy of tailings at 3 mine sites: Montague, Goldenville, and Caribou. DeSisto et al., 2016 likewise assessed As minerals at Montague and Goldenville. They identified 4 categories of tailings in which to sample: hardpan, oxic, wetlands, and high-Ca. Cores collected for this study included pore water, which was analyzed for pH and soluble metal concentration, as well as other aqueous parameters. By including near-surface and deeper (~50-200 cm) mineralogy, a better understanding is gained of the relationship between sediments exposed to the atmosphere and those at depth, especially if they exist within the saturated zone. This connection is especially important when drawing conclusions from optical remote sensing images, which only describe the topmost sediment.

At the time of this writing, Percival et al., 2013 is the only paper in which indicators of tailings are mapped at Nova Scotia's historic gold mines using remote sensing methods.

Samples were collected at the Dufferin, Lower Seal Harbour, and Upper Seal Harbour gold mine

districts. Mineralogy of these samples was determined, and a linear spectral unmixing technique was used on a hyperspectral image from the (no longer operational) EO-1 Hyperion satellite. Linear spectral unmixing is a method in which the spectra of known endmembers are combined to recreate the composite spectra found within a pixel. In this case, the endmembers were selected from the image. Areas showing 14 land cover classes, including a tailings endmember, were chosen based on field observations. Linear unmixing provides not only an indicator of endmembers present in a pixel, but their areal proportion. This paper includes a discussion of the spectral reflectance of minerals observed in tailings, which is useful in explaining classifier results.

1.3.3. Google Earth Engine

Desktop analysis, including data pre-processing, image acquisition, image sampling, classification, and accuracy assessment, was performed in Google Earth Engine (GEE) (Jewell, 2021). GEE is a cloud platform created by Google for remote sensing analysis (Gorelick et al., 2017). It is available in web browsers or as a Python package. GEE allows uploading of spatial data and imagery, though there are many datasets available in its built-in library. Sentinel-2 surface reflectance images are available, allowing for easy selection of images from a range of dates and locations that have already been corrected to remove atmospheric effects. In addition to the data library, GEE has a large selection of functions which can be implemented in its JavaScript and Python application programming interfaces (APIs). Computation performed in GEE is run on Google's cloud servers, allowing for the rapid processing of massive datasets.

1.4. Summary and Future Work

The goals of this study were to test if multispectral images could be used to classify mine tailings, and to determine if historic data could provide adequate training data for said classifier. The mine sites throughout Nova Scotia presented an excellent setting for these objectives. Many of the sites are well studied, and the NSMTD provides a thorough database of previously recorded tailings areas. All of the historic gold mine sites in the mainland of the province contain Meguma Group bedrock and similar processing histories and long-term storage methods. Though mineralogy is not exactly the same at any two sites, these similarities provide partial control over mineralogy and allow us to treat all tailings as one material. By combining Sentinel-2 imagery and the NSMTD tailings polygons, we can test the viability of using a broad spatial dataset to obtain image pixels and train a classifier. The spatial dataset requires no information whatsoever on the nature of tailings beyond a boundary. This allows historical and modern data to be combined, increasing the range of available training information. The classifier is trained and tested on images representing modern conditions, even if the tailings boundaries were recorded long ago.

Spectral variation of tailings training pixels, as well as spatial autocorrelation, are not measured directly in this study, but they are to some degree inherently linked to the accuracy of the classifier. A valuable question to explore in a future study would be the applicability of this method, perhaps even using this training data, to other areas. Is there a distance at which training data begins to produce a less accurate classifier, even in similar bedrock? Is distance irrelevant, so long as the target is tailings resulting from hydrothermal gold deposits? How much does grain size and storage facility type affect spectral variation?

1.5. References

Achanta, R., Süssstrunk, S., 2017. Superpixels and Polygons Using Simple Non-iterative Clustering, in: 2017 IEEE Conference on Computer Vision and Pattern Recognition (CVPR). pp. 4895–4904.

<https://doi.org/10.1109/CVPR.2017.520>

Azizur Rahman, M., Hasegawa, H., 2012. Arsenic in freshwater systems: Influence of eutrophication on occurrence, distribution, speciation, and bioaccumulation. *Appl. Geochem.* 27, 304–314.

<https://doi.org/10.1016/j.apgeochem.2011.09.020>

Bates, J.L.E., 1987. Gold in Nova Scotia, Canadian Cataloguing in Publication Data. Nova Scotia Dept. of Mines and Energy, Halifax.

Branco, P., Torgo, L., Ribeiro, R., 2015. A Survey of Predictive Modelling under Imbalanced Distributions. *ArXiv150501658 Cs*.

Breiman, L., 2001. Random Forests. *Mach. Learn.* 45, 5–32. <https://doi.org/10.1023/A:1010933404324>

CCME, 1997. Canadian Soil Quality Guidelines for the Protection of Environmental and Human Health - Arsenic (Inorganic). *Can. Environ. Qual. Guidel.* 7.

Clark, A.J., Labaj, A.L., Smol, J.P., Campbell, L.M., Kurek, J., 2021. Arsenic and mercury contamination and complex aquatic bioindicator responses to historical gold mining and modern watershed stressors in urban Nova Scotia, Canada. *Sci. Total Environ.* 787, 147374.

<https://doi.org/10.1016/j.scitotenv.2021.147374>

Clark, R.N., Lucey, P.G., 1984. Spectral properties of ice-particulate mixtures and implications for remote sensing: 1. Intimate mixtures. *J. Geophys. Res. Solid Earth* 89, 6341–6348.

<https://doi.org/10.1029/JB089iB07p06341>

Clark, R.N., Roush, T.L., 1984. Reflectance spectroscopy: Quantitative analysis techniques for remote sensing applications. *J. Geophys. Res. Solid Earth* 89, 6329–6340.

<https://doi.org/10.1029/JB089iB07p06329>

Clark, R.N., Swayze, G.A., Livo, K.E., Kokaly, R.F., Sutley, S.J., Dalton, J.B., McDougal, R.R., Gent, C.A., 2003. Imaging spectroscopy: Earth and planetary remote sensing with the USGS Tetracorder and expert systems. *J. Geophys. Res. - Planets* 108, 5131-n/a. <https://doi.org/10.1029/2002JE001847>

Cleaver, A.E., Jamieson, H.E., Rickwood, C.J., Huntsman, P., 2021. Tailings dust characterization and impacts on surface water chemistry at an abandoned Zn-Pb-Cu-Au-Ag deposit. *Appl. Geochem.* 128, 104927. <https://doi.org/10.1016/j.apgeochem.2021.104927>

Corriveau, M.C., Jamieson, H.E., Parsons, M.B., Hall, G.E.M., 2011. Mineralogical characterization of arsenic in gold mine tailings from three sites in Nova Scotia. *Geochem. Explor. Environ. Anal.* 11, 179–192. <https://doi.org/10.1144/1467-7873/09-246>

DeSisto, S.L., Jamieson, H.E., Parsons, M.B., 2017. Arsenic mobility in weathered gold mine tailings under a low-organic soil cover. *Environ. Earth Sci.* 76, 773. <https://doi.org/10.1007/s12665-017-7041-7>

DeSisto, S.L., Jamieson, H.E., Parsons, M.B., 2016. Subsurface variations in arsenic mineralogy and geochemistry following long-term weathering of gold mine tailings. *Appl. Geochem.* 73, 81–97.

<https://doi.org/10.1016/j.apgeochem.2016.07.013>

DeSisto, S.L., Jamieson, H.E., Parsons, M.B., 2011. Influence of hardpan layers on arsenic mobility in historical gold mine tailings. *Appl. Geochem.* 26, 2004–2018.

<https://doi.org/10.1016/j.apgeochem.2011.06.030>

Díaz-Uriarte, R., Alvarez de Andrés, S., 2006. Gene selection and classification of microarray data using random forest. *BMC Bioinformatics* 7, 3. <https://doi.org/10.1186/1471-2105-7-3>

Drage, J., 2015. Review of the Environmental Impacts of Historical Gold Mine Tailings in Nova Scotia. Open File Rep. ME 2015-004 15.

Du, Y., Zhang, Y., Ling, F., Wang, Q., Li, W., Li, X., 2016. Water Bodies' Mapping from Sentinel-2 Imagery with Modified Normalized Difference Water Index at 10-m Spatial Resolution Produced by Sharpening the SWIR Band. *Remote Sens.* 8, 354. <https://doi.org/10.3390/rs8040354>

European Space Agency, 2015. Sentinel-2 User Handbook 64.

Faribault, E.R., 1900. The gold measures of Nova Scotia and deep mining / by E.R. Faribault. Together with other papers bearing upon Nova Scotia gold mines. Mining Society of Nova Scotia, Halifax, N.S.

Genuer, R., Poggi, J.-M., Tuleau-Malot, C., 2010. Variable selection using random forests. *Pattern Recognit. Lett.* 31, 2225–2236. <https://doi.org/10.1016/j.patrec.2010.03.014>

Goetz, A.F.H., Curtiss, B., Shiley, D.A., 2009. Rapid gangue mineral concentration measurement over conveyors by NIR reflectance spectroscopy. *Miner. Eng.* 22, 490–499.

<https://doi.org/10.1016/j.mineng.2008.12.013>

Gorelick, N., Hancher, M., Dixon, M., Ilyushchenko, S., Thau, D., Moore, R., 2017. Google Earth Engine: Planetary-scale geospatial analysis for everyone. *Remote Sens. Environ.* 202, 18–27.

<https://doi.org/10.1016/j.rse.2017.06.031>

Gregorutti, B., Michel, B., Saint-Pierre, P., 2017. Correlation and variable importance in random forests. *Stat. Comput.* 27, 659–678. <https://doi.org/10.1007/s11222-016-9646-1>

Groves, D.I., Goldfarb, R.J., Gebre-Mariam, M., Hagemann, S.G., Robert, F., 1998. Orogenic gold deposits: A proposed classification in the context of their crustal distribution and relationship to other gold deposit types. *Ore Geol. Rev.* 13, 7–27. [https://doi.org/10.1016/S0169-1368\(97\)00012-7](https://doi.org/10.1016/S0169-1368(97)00012-7)

Guha, A., 2020. Mineral exploration using hyperspectral data, in: Pandey, P.C., Srivastava, P.K., Balzter, H., Bhattacharya, B., Petropoulos, G.P. (Eds.), *Hyperspectral Remote Sensing, Earth Observation*. Elsevier, pp. 293–318. <https://doi.org/10.1016/B978-0-08-102894-0.00012-7>

Hartlen, J., 1988. *Gold! The Wealth of Waverley*. Lancelot Press, Hantsport, Nova Scotia.

Hennick, E.W., Poole, J.C., 2020. Nova Scotia Mine Tailings Database.

Hindmarsh, J., McLetchle, O.R., Heffernan, L., Hayne, O., Ellenberger, H.A., Mccurdy, R., Thiébaux, H.J., 1977. Electromyographic Abnormalities in Chronic Environmental Arsenicalism. <https://doi.org/10.1093/JAT/1.6.270>

Homem Antunes, M.A., Bolpato, I.F., 2018. Atmospheric Correction and Cirrus Clouds Removal from MSI Sentinel 2A Images, in: *IGARSS 2018 - 2018 IEEE International Geoscience and Remote Sensing Symposium*. Presented at the IGARSS 2018 - 2018 IEEE International Geoscience and Remote Sensing Symposium, IEEE, Valencia, pp. 9145–9148. <https://doi.org/10.1109/IGARSS.2018.8518824>

Intrinsic Corp, EcoMetrix, Crippen Berger, K., Wood, 2020. Human Health Risk Assessment of Sediment, Surface Water, and Fish from Barry’s Run, Halifax Regional Municipality.

Intrinsic Corp, EcoMetrix, Crippen Berger, K., Wood, 2019a. Conceptual Closure Plan For The Historic Goldenville Tailings Areas Goldenville, Nova Scotia Final Report (Consulting).

Intrinsic Corp, EcoMetrix, Crippen Berger, K., Wood, 2019b. Conceptual Closure Study For The Historic Montague Mines Tailings Areas. Halifax, Nova Scotia. Final Report (Consulting). NS Lands Inc.

Jamieson, H.E., Walker, S.R., Parsons, M.B., 2015. Mineralogical characterization of mine waste. *Appl. Geochem.*, *Environmental Geochemistry of Modern Mining* 57, 85–105.

<https://doi.org/10.1016/j.apgeochem.2014.12.014>

Jewell, D.A., 2021. Tailings Classification NS Repository. <https://doi.org/10.5281/zenodo.8273117>

Joshi, A.V., 2023. Decision Trees, in: Joshi, A.V. (Ed.), *Machine Learning and Artificial Intelligence*. Springer International Publishing, Cham, pp. 73–87. https://doi.org/10.1007/978-3-031-12282-8_7

Kamal, M., Phinn, S., 2011. Hyperspectral Data for Mangrove Species Mapping: A Comparison of Pixel-Based and Object-Based Approach. *Remote Sens.* 3, 2222–2242. <https://doi.org/10.3390/rs3102222>

Koch, I., McPherson, K., Smith, P., Easton, L., Doe, K.G., Reimer, K.J., 2007. Arsenic bioaccessibility and speciation in clams and seaweed from a contaminated marine environment. *Mar. Pollut. Bull.* 54, 586–594. <https://doi.org/10.1016/j.marpolbul.2006.12.004>

Kokaly, R.F., Clark, R.N., Swayze, G.A., Livo, K.E., Hoefen, T.M., Pearson, N.C., Wise, R.A., Benzel, W.M., Lowers, H.A., Driscoll, R.L., Klein, A.J., 2017. USGS Spectral Library Version 7: U.S. Geological Survey Data Series 1035. *US Geol. Surv. Data Ser.*, *Data Series 1035*, 61. <https://doi.org/10.3133/ds1035>

Kontak, D.J., Jackson, S.J., 1999. Documentation of variable trace- and rare-earth-element abundances in carbonates from auriferous quartz veins in Meguma lode gold deposits, Nova Scotia. *Can. Mineral.* 37, 469–488.

Lane, P.A., Pett, Robert J., Crowell, M. J., MacKinnon, D. S., Graves, Milton C., 1989. Further studies on the distribution and fate of arsenic and mercury at a site contaminated by abandoned gold mine tailings. *CANMET Spec. Publ.* 89–9, 77–107.

LeBlanc, M.E., Parsons, M.B., Chapman, E.E.V., Campbell, L.M., 2020. Review of ecological mercury and arsenic bioaccumulation within historical gold mining districts of Nova Scotia. *Environ. Rev.* 28, 187–198.

<https://doi.org/10.1139/er-2019-0042>

Lekner, J., Dorf, M., 1988. Why some things are darker when wet. *Appl. Opt.* 27, 1278–80.

<https://doi.org/10.1364/AO.27.001278>

Li, H., 2014. Smile.

Little, M.E., Parsons, M.B., Law, B.A., Milligan, T.G., Smith, J.N., 2015. Impact of historical gold mining activities on marine sediments in Wine Harbour, Nova Scotia, Canada. *Atl. Geol.* 51, 344.

<https://doi.org/10.4138/atlgeol.2015.016>

Lyons, M.B., Keith, D.A., Phinn, S.R., Mason, T.J., Elith, J., 2018. A comparison of resampling methods for remote sensing classification and accuracy assessment. *Remote Sens. Environ.* 208, 145–153.

<https://doi.org/10.1016/j.rse.2018.02.026>

Mielke, C., Muedi, T., Papenfuss, A., Boesche, N.K., Rogass, C., Gauert, C.D.K., Altenberger, U., de Wit, M.J., 2016. Multi- and hyperspectral spaceborne remote sensing of the Aggeneys base metal sulphide mineral deposit sites in the Lower Orange River region, South Africa. *South Afr. J. Geol.* 119, 63–76.

<https://doi.org/10.2113/gssajg.119.1.63>

Montero, I.C., Brimhall, G.H., Alpers, C.N., Swayze, G.A., 2005. Characterization of waste rock associated with acid drainage at the Penn Mine, California, by ground-based visible to short-wave infrared reflectance spectroscopy assisted by digital mapping. *Chem. Geol., Geochemistry of Sulfate Minerals: A tribute to Robert O. Rye* 215, 453–472. <https://doi.org/10.1016/j.chemgeo.2004.06.045>

Mountrakis, G., Im, J., Ogole, C., 2011. Support vector machines in remote sensing: A review. *ISPRS J. Photogramm. Remote Sens.* 66, 247–259. <https://doi.org/10.1016/j.isprsjprs.2010.11.001>

<https://doi.org/10.1016/j.isprsjprs.2010.11.001>

Mudroch, A., Clair, T.A., 1986. Transport of arsenic and mercury from gold mining activities through an aquatic system. *Sci. Total Environ.* 57, 205–216. [https://doi.org/10.1016/0048-9697\(86\)90024-0](https://doi.org/10.1016/0048-9697(86)90024-0)

Ngole-Jeme, V.M., Fantke, P., 2017. Ecological and human health risks associated with abandoned gold mine tailings contaminated soil. *PLOS ONE* 12, e0172517.
<https://doi.org/10.1371/journal.pone.0172517>

Nolet, C., Poortinga, A., Roosjen, P., Bartholomeus, H., Ruessink, G., 2014. Measuring and Modeling the Effect of Surface Moisture on the Spectral Reflectance of Coastal Beach Sand. *PLoS ONE* 9, e112151.
<https://doi.org/10.1371/journal.pone.0112151>

Olofsson, P., Foody, G.M., Herold, M., Stehman, S.V., Woodcock, C.E., Wulder, M.A., 2014. Good practices for estimating area and assessing accuracy of land change. *Remote Sens. Environ.* 148, 42–57.
<https://doi.org/10.1016/j.rse.2014.02.015>

Otsu, N., 1979. A Threshold Selection Method from Gray-Level Histograms. *IEEE Trans. Syst. Man Cybern.* 9, 62–66. <https://doi.org/10.1109/TSMC.1979.4310076>

Parsons, M.B., LeBlanc, K.W.G., Hall, G.E.M., Sangster, A.L., Vaive, J.E., Pelchat, P., 2012. Environmental geochemistry of tailings, sediments and surface waters collected from 14 historical gold mining districts in Nova Scotia (No. 7150). <https://doi.org/10.4095/291923>

Parsons, M.B., Little, M.E., 2015. Establishing geochemical baselines in forest soils for environmental risk assessment in the Montague and Goldenville gold districts, Nova Scotia, Canada. *Atl. Geol.* 51, 364.
<https://doi.org/10.4138/atlgeol.2015.017>

Percival, J.B., White, H.P., Goodwin, T.A., Parsons, M.B., Smith, P.K., 2013. Mineralogy and spectral reflectance of soils and tailings from historical gold mines, Nova Scotia. *Geochem. Explor. Environ. Anal.* Vol. 14, 3–16. <http://dx.doi.org/10.1144/geochem2011-071>

Riaza, A., Müller, A., 2010. Hyperspectral remote sensing monitoring of pyrite mine wastes: a record of climate variability (Pyrite Belt, Spain). *Environ. Earth Sci.* 61, 575–594. <https://doi.org/10.1007/s12665-009-0368-y>

Richards, J.A., 2013. *Remote Sensing Digital Image Analysis*. Springer Berlin Heidelberg, Berlin, Heidelberg. <https://doi.org/10.1007/978-3-642-30062-2>

Roussel, C., Néel, C., Bril, H., 2000. Minerals controlling arsenic and lead solubility in an abandoned gold mine tailings. *Sci. Total Environ.* 263, 209–219. [https://doi.org/10.1016/S0048-9697\(00\)00707-5](https://doi.org/10.1016/S0048-9697(00)00707-5)

Sangster, A.L., Smith, P.K., Goodfellow, W.D., 2007. *Metallogenic Summary of the Meguma Gold Deposits, Nova Scotia (Special Publication No. 5), Mineral Deposits of Canada: A Synthesis of Major Deposit-Types, District Metallogeny, the Evolution of Geological Provinces, and Exploration Methods*. Geological Association of Canada, Nova Scotia.

Sasaki, Y., 2007. The truth of the F-measure. *Conf. Pap.*

Schowengerdt, R.A., 2007. *Remote Sensing : Models and Methods for Image Processing*, 3rd ed. Academic Press, Burlington, MA.

Seal, R.R., Hammarstrom, J.M., 2003. Geoenvironmental Models of Mineral Deposits: Examples from Massive Sulfide and Gold Deposits, in: *Environmental Aspects of Mine Waste, Short Course Series*. Mineralogical Association of Canada, pp. 11–50.

Smeds, J., Mats & Ouml, quist, Nilsson, M.B., Bishop, K., 2022. A Simplified Drying Procedure for Analysing Hg Concentrations. *Water Air Amp Soil Pollut.* 233, NA-NA. <https://doi.org/10.1007/s11270-022-05678-7>

Stehman, S.V., 2009. Sampling designs for accuracy assessment of land cover. *Int. J. Remote Sens.* 30, 5243–5272. <https://doi.org/10.1080/01431160903131000>

- Stehman, S.V., Foody, G.M., 2019. Key issues in rigorous accuracy assessment of land cover products. *Remote Sens. Environ.* 231, 111199. <https://doi.org/10.1016/j.rse.2019.05.018>
- Svetnik, V., Liaw, A., Tong, C., Wang, T., 2004. Application of Breiman's Random Forest to Modeling Structure-Activity Relationships of Pharmaceutical Molecules, in: Roli, F., Kittler, J., Windeatt, T. (Eds.), *Multiple Classifier Systems, Lecture Notes in Computer Science*. Springer Berlin Heidelberg, Berlin, Heidelberg, pp. 334–343. https://doi.org/10.1007/978-3-540-25966-4_33
- Swayze, G.A., Clark, R.N., Goetz, A.F.H., Livo, K.E., Breit, G.N., Kruse, F.A., Sutley, S.J., Snee, L.W., Lowers, H.A., Post, J.L., Stoffregen, R.E., Ashley, R.P., 2014. Mapping Advanced Argillic Alteration at Cuprite, Nevada, Using Imaging Spectroscopy. *Econ. Geol.* 109, 1179–1221. <https://doi.org/10.2113/econgeo.109.5.1179>
- Swayze, G.A., Smith, K.S., Clark, R.N., Sutley, S.J., Pearson, R.M., Vance, J.S., Hageman, P.L., Briggs, P.H., Meier, A.L., Singleton, M.J., Roth, S., 2000. Using Imaging Spectroscopy To Map Acidic Mine Waste. *Environ. Sci. Technol.* 34, 47–54. <https://doi.org/10.1021/es990046w>
- Tou, J.T., 1974. *Pattern recognition principles, Applied mathematics and computation*, no. 7. Addison-Wesley Pub. Co., Reading, Mass.
- van der Meer, F., 2004. Analysis of spectral absorption features in hyperspectral imagery. *Int. J. Appl. Earth Obs. Geoinformation* 5, 55–68. <https://doi.org/10.1016/j.jag.2003.09.001>
- van der Meer, F.D., van der Werff, H.M.A., van Ruitenbeek, F.J.A., 2014. Potential of ESA's Sentinel-2 for geological applications. *Remote Sens. Environ.* 148, 124–133. <https://doi.org/10.1016/j.rse.2014.03.022>
- Van der Werff, H., Van der Meer, F., 2015. Sentinel-2 for Mapping Iron Absorption Feature Parameters. *Remote Sens.* 7, 12635–12653. <https://doi.org/10.3390/rs71012635>
- Van Rijsbergen, C.J., 1979. *Information retrieval*, 2d ed. ed. Butterworths, London ; Boston.

von der Heyden, B.P., Roychoudhury, A.N., 2015. Application, Chemical Interaction and Fate of Iron Minerals in Polluted Sediment and Soils. *Curr. Pollut. Rep.* 1, 265–279. <https://doi.org/10.1007/s40726-015-0020-2>

Walker, S.R., Parsons, M.B., Jamieson, H.E., Lanzirotti, A., 2009. ARSENIC MINERALOGY OF NEAR-SURFACE TAILINGS AND SOILS: INFLUENCES ON ARSENIC MOBILITY AND BIOACCESSIBILITY IN THE NOVA SCOTIA GOLD MINING DISTRICTS. *Can. Mineral.* 47, 533–556. <https://doi.org/10.3749/canmin.47.3.533>

Weisener, C.G., 2003. Novel Spectroscopic Techniques to Characterize Mine Waste, in: *Environmental Aspects of Mine Waste, Short Course Series*. Mineralogical Association of Canada, pp. 181–202.

Wilkin, R.T., Barnes, H.L., 1997. Formation processes of framboidal pyrite. *Geochim. Cosmochim. Acta* 61, 323–339. [https://doi.org/10.1016/S0016-7037\(96\)00320-1](https://doi.org/10.1016/S0016-7037(96)00320-1)

Willick, F., 2021. Cost estimate for cleanup of abandoned N.S. mines still “a few years” away. CBC.

Chapter 2: Historical Gold Mine Tailings Indicators: Pixel and Object-Based Classification Models

2.1. Introduction

Multiple gold rushes took place in Nova Scotia, Canada during the 19th and early 20th centuries. Though technologies, methods, and yields changed over time, for much of this period a lack of environmental regulations meant that waste rock and tailings resulting from processing were often discharged directly into the environment (Drage, 2015). This is true in the 64 historical gold districts in Nova Scotia, where gold mining and amalgamation practices between the 1860s and the 1940s have left behind tailings containing arsenic (As) and mercury (Hg) concentrations that frequently exceed the recommended guidelines, posing a risk to human and ecosystem health (CCME, 1997; LeBlanc et al., 2020; Parsons et al., 2012). If sites are to be remediated, they must first be surveyed to determine the extent of tailings and degree of contamination (Intrinsik Corp et al., 2020, 2019b, 2019a). There are over 360 individual historic gold mines within the province's 64 historic gold districts, and surveying these has been a time-consuming and expensive process, often relying on a foundation of historical records. In many cases, the surficial extent of tailings, as recorded in these documents, may no longer be accurate due to decades of wind and water transport of tailings, weathering reactions, mixing with natural soils and sediments, and overgrowth from vegetation. Following the preprocessing steps described in this paper, these historical data can

be used to train a classifier that can indicate the present extent of exposed tailings, including areas that may not have been recorded previously. This will help identify and prioritize potential tailings areas before planning fieldwork, which can be expensive in terms of equipment, time, labour, and logistics.

Much of the work in remote sensing analysis of mine waste sites has been performed using hyperspectral imagery, which tends to have pixels of approximately 30 m or more. Recently, researchers have begun exploring the use of multispectral images for identifying mine waste and adapting hyperspectral methods for use with multispectral imagery. Multispectral satellite missions such as Landsat (30 m pixels, excluding panchromatic) and Sentinel-2 (10-20 m pixels) provide free images at frequent intervals, with new images captured as often as every five days for Sentinel-2. These platforms capture images continuously and make them available almost instantly, with no need to submit a request beforehand and wait for the images to be processed. This means that images can be acquired from almost anywhere on the planet without having to first build an image library while waiting for the satellite to acquire cloud-free data within the desired date range.

In this study, images from the Sentinel-2 mission were used to create a classification model to provide a first look at mine sites to help guide sampling and mapping efforts for abandoned historical tailings. This model was developed using Google Earth Engine (GEE), a cloud-supported platform that allows instant access to a massive and expanding collection of satellite images and the creation of apps that can be easily shared with users. Many past studies using passive remote sensing to detect mine waste have used hyperspectral images, containing up to several hundred very narrow wavelength, contiguous bands. In this study, we

explore the viability of using multispectral images containing a small number of wide (15-175 nm), noncontiguous bands to identify pixels that may indicate the presence of tailings. To indicate the presence of a material using remote sensing images, our target must have one or more distinctive spectral features that coincide with one or more bands. Two models were developed in GEE: (1) a pixel-based model, where each pixel was labelled as tailings or non-tailings with no regard to the labels of neighbouring pixels; and (2) an object-based model, including a segmentation step in which seed points were placed within the tailings regions and then grown according to an algorithm that considered distance and spectral similarity (Achanta and Süsstrunk, 2017). With these models, we attempt to show that the Sentinel-2 bands are well-placed to capture the spectral features present in tailings, which can be used to train a classifier that can indicate tailings elsewhere in the image.

2.1.1. Historic Mining and Present Contaminants

Three distinct gold rushes took place in the Canadian province of Nova Scotia between the 1860s and the 1940s. This gold was mainly extracted from quartz-carbonate veins present throughout the Cambro-Ordovician metasedimentary rocks of the Meguma Supergroup in mainland Nova Scotia (Little et al., 2015; Sangster et al., 2007). In addition to gold, these veins contain abundant sulphide minerals, particularly arsenopyrite (FeAsS).

In the late 1800s, mined ore was crushed in stamp mills, and gold was concentrated using mercury (Hg) amalgamation. Beginning in the 1890s, some mills also started using cyanidation to recover additional gold as well as more efficient milling techniques (e.g. ball milling) (Bates, 1987; LeBlanc et al., 2020; Parsons et al., 2012). After gold was extracted, the waste rock and sand- to silt-sized sediment, called tailings, was slurried into streams, wetlands,

or nearby depressions with little to no regard for potential environmental impacts (Drage, 2015). In the decades following tailings deposition, sulphide minerals were exposed to oxygen and surface water, leading to the dissolution of As and other metal(loid)s (DeSisto et al., 2017). This As, as well as the Hg introduced in gold processing, may be transported long distances via air as dust or via water as dissolved or suspended sediment load (Cleaver et al., 2021; Mudroch and Clair, 1986). New minerals may form via weathering reactions at these sites, incorporating As, or As can be adsorbed onto existing minerals, either temporarily under certain local environmental conditions or long-term as more stable secondary minerals (DeSisto et al., 2017; Montero et al., 2005). Inorganic As compounds can be toxic, as well as carcinogenic in humans. Invertebrates may bioaccumulate As, though its bioavailability is highly dependent on speciation and geochemical conditions (Azizur Rahman and Hasegawa, 2012; Walker et al., 2009). Some forms of Hg can pose a risk to humans and the environment. In particular, the methylation of Hg to methylmercury by iron- or sulphate-reducing bacteria in anoxic conditions is of most concern (LeBlanc et al, 2020). Analysis has shown that Hg is common in tailings in the region, however, it has not been observed in spectrally active minerals at these sites. The remainder of this paper focuses on As and its mineral hosts.

An estimated 3,000,000 tonnes of tailings were produced by over 360 mines in 64 historical gold districts across the province between the 1860s and 1940s (Parsons et al., 2012). Most sites have been abandoned for decades, with tailings left exposed and subject to weathering and transport into the surrounding and downstream environments.

In recent years, concerns about ecosystem and human health risks due to tailings have led to site assessments and the development of cleanup plans at some historic gold

minedistricts. Assessment and remediation plans were initiated by the Government of Nova Scotia in 2018, and as of 2023 two sites, Montague Gold District and Goldenville Gold District, have been selected for cleanup with a budget of over \$60 million for both sites (Intrinsic Corp et al., 2019a, 2019b). These sites have been prioritized due to their elevated level of As contamination and, in the case of Montague, proximity to residential communities (Willick, 2021). The Montague Gold District is in a suburban region within the city limits of Halifax. Tailings samples at Montague have been found to contain a median of approximately 11 000 ppm As (Parsons et al., 2012). The Goldenville Gold District is near the village of Sherbrooke on the eastern shore of Nova Scotia and tailings at this site have a median As concentration of approximately 7000 ppm (Parsons et al., 2012). In Parsons et al. (2012), 14 gold districts were surveyed, finding an overall median of 2550 ppm As across all 482 tailings samples. Almost all (99%) samples exceeded the Canadian Council of Ministers of the Environment recommended soil quality guideline of 12 ppm As (CCME, 1997; Parsons et al., 2012).

2.1.2. Geology of Nova Scotia Gold Deposits

All 64 gold mine districts are found in the Halifax and Goldenville Groups within the Meguma Supergroup. The Meguma Supergroup shares its name with the Meguma Terrane, which forms the southern portion of mainland Nova Scotia. The Cambro-Ordovician Meguma Supergroup has an exposed section over 480 km long by 120 km wide, with east-west trending folds (Sangster et al., 2007). It has a base of Cambrian metagreywacke, metasilstone, and slate belonging to the Goldenville Group, overlain by black slate and metasilstone of the Halifax Group (Percival et al., 2013) (Figure 1).

The high-grade gold deposits that were the main target of historic mining are in quartz-

carbonate veins found in the hinges of these folds, where gold has been concentrated by hydrothermal fluids (Sangster et al., 2007). The concentration of minerals may vary by site, but their common bedrock should provide similar mineralogy overall. One study of tailings at Goldenville and Montague found mostly quartz (SiO_2), muscovite ($\text{KAl}_2(\text{AlSi}_3\text{O}_{10})(\text{F},\text{OH})_2$), plagioclase ($(\text{Na},\text{Ca})[(\text{Si},\text{Al})\text{AlSi}_2\text{O}_8]$), and chlorite group minerals, with occasional calcite (CaCO_3), ankerite ($(\text{Na},\text{Ca})[(\text{Si},\text{Al})\text{AlSi}_2\text{O}_8]$), and vermiculite ($\text{Mg}_{0.7}(\text{Mg},\text{Fe},\text{Al})_6(\text{Si},\text{Al})_8\text{O}_{20}(\text{OH})_4 \cdot 8\text{H}_2\text{O}$) (Walker et al., 2009). In some cases, these represent up to 90% of mineralogy in gold veins, with sulphides and other minor phases making up most of the remainder (Kontak and Jackson, 1999; Walker et al., 2009).

Though sulphide minerals have a relatively low concentration in tailings (~5%), they are the main source of As and acid rock drainage (Jamieson et al., 2015). Sulphides are a threat to both human and ecosystem health near many mine sites around the world (Ngole-Jeme and Fantke, 2017). Ideally, we would be able to target sulphide minerals directly using remote-sensing methods. Sulphide minerals, however, have fairly flat, low-magnitude reflectance spectra (Kokaly et al., 2017), and are not considered spectrally active. At our study sites, sulphides are typically coated in a rim of iron oxide, iron hydroxide, or iron arsenate which often have absorption features around 700 to 1000 nm, making them viable spectral targets (DeSisto et al., 2016; Van der Werff and Van der Meer, 2015). Minerals with this feature that appear at these mine sites include hematite (Fe_2O_3), goethite ($\text{FeO}(\text{OH})$), scorodite ($\text{FeAsO}_4 \cdot 2\text{H}_2\text{O}$), and others.

2.1.3. Spectral Reflectance and Pixel Mixing

The goal of this study was to develop a remote-sensing methodology to identify areas that have similar spectral reflectance to gold mine tailings, and in turn, may be associated with elevated levels of As, which is also correlated to heightened Hg in the study region due to historical processing techniques. If successful, these methods could be used to identify and prioritize sites of concern before costly and time-consuming on-the-ground assessments. The methods used in this paper were not intended to obtain mineralogical data or quantify contaminant concentrations. Though mineralogical analysis is common using spectroscopy, this typically requires hyperspectral sensors with a spatial resolution on the millimetre to centimetre scale, which is currently only possible via laboratory tools, hand-held spectrometers, or possibly remotely piloted aircraft. Space-based hyperspectral sensors have been effective in some cases, depending on the mineral being targeted (Clark et al., 2003; Mielke et al., 2016; Swayze et al., 2014; van der Meer, 2004) As the surficial materials represented in the pixels of our images are poorly sorted, otherwise known as intimate mixtures, even if one could obtain centimeter-scale pixels via remote sensing technology, those pixels would still represent a mixture and not one pure material (Clark and Lucey, 1984; Stehman, 2009). Therefore, due to the nature of tailings at these sites, and the limitations of the Sentinel-2 satellite's spatial resolution, we treat tailings as a single mixed material, rather than trying to separate it into different tailings types or mineral groups. This adds versatility and follows guidance of other studies attempting to detect tailings in satellite imagery, though it reduces our descriptive ability.

All surface materials within the ground area captured within a pixel contribute to the apparent reflectance factor of that pixel. The apparent reflectance factor is the measure of

upwelling radiance normalized by the downwelling irradiance of the sun and sky, resampled from the continuous EM spectrum to a sensor's discrete bands by wavelength (Percival et al., 2013). This will be referred to simply as "reflectance" in this study. When assessing mine sites across a large area, surface materials are likely to vary in composition and thus reflectance. Even tailings from two nearby sites may contain different minerals and will not have the same spectral signature, so some generalization is required. Such is the case between Goldenville and Montague gold districts, which have similar levels of As concentration in the tailings but variable mineralogy, degrees of water saturation, and vegetative overgrowth at each site (Corriveau et al., 2011; DeSisto et al., 2016; Walker et al., 2009). By treating tailings from across all gold districts as one material, we can sample these areas to create a broad tailings class. Sentinel-2's sensors lack the spectral resolution to discern individual tailings minerals from one another, so here we test its ability to discriminate a wider tailings class from the background non-tailings class. We take advantage of the ease of acquiring new Sentinel-2 images using Google Earth Engine (GEE), to include data from a large region.

2.1.4. Detecting Gold Mine Tailings at Historic Mines Using Space-Based Remote Sensing

2.1.4.1. Sentinel-2 Mission and Sensors

Images from Sentinel-2's MultiSpectral Instrument were selected for this study. The Sentinel-2 mission comprises a pair of identical satellites launched by the European Space Agency (ESA) in 2015 and 2017 (Sentinel-2A and Sentinel-2B, respectively). Each has a return frequency of 10 days at the equator. Their orbits are offset by 180°, such that a new image is acquired at a given location every five days with the same viewing conditions, and more

frequently with different viewing conditions, based on latitude (European Space Agency, 2015). Sentinel-2 has 13 bands in varying spatial resolutions and bandwidths ranging from 15 to 175 nm (Table 1). It differs in this way from hyperspectral sensors that may contain several hundred bands at very narrow bandwidths (~2 to 5 nm) and have continuous or near-continuous spectral coverage. The locations of Sentinel-2's 13 bands were chosen carefully to avoid atmospheric absorption, target peak NIR reflectance in vegetation, and be sensitive to iron oxides in soil (European Space Agency, 2015). In general, bands are narrower than those of Landsat's sensors to avoid atmospheric water vapour absorption bands. Accurate discernment of vegetation improves the ability of the model to mask out vegetation on the surface, and an indication of iron oxides is important for discriminating tailings from non-tailings. Sentinel-2's bands come in different spatial resolutions. Four bands are provided in 10 m resolution, six in 20 m, and three in 60 m for atmospheric analysis. The 10 and 20 m bands were used in this study, with the 10 m bands resampled to 20 m. Spatial resolution is another advantage over the Landsat mission, which has a maximum resolution of 30 m, excluding the panchromatic band. The sites in this study are typically less than 100 to 200 m wide, so smaller pixels allow for better capture of areas in the center of sites, with less mixing from edges that may contain vegetation or water.

2.1.4.2. Google Earth Engine

Desktop analysis in this study was performed using Google Earth Engine (GEE), a cloud-based platform launched by Google in 2010 that allows access to and analysis of a huge collection of satellite images (Gorelick et al., 2017). There are application programming interfaces (APIs) available for GEE using JavaScript or Python. The JavaScript API is web-based

and includes a graphical user interface with search functions for datasets, console output, an interactive map including geometry drawing/import tools, and a documentation browser. Scripts written on GEE can also be exported as standalone apps that can be shared with others without requiring them to register for the platform themselves (Jewell, 2021). Sentinel-2 data is included in GEE's collection, including images corrected from top-of-atmosphere to at-surface reflectance. This collection can easily be filtered to obtain images by, e.g., date ranges, low cloud cover, etc., while requiring no preprocessing by the user.

2.1.5. Study Area

Though the purpose of this study is to create a model that can incorporate tailings data from mine districts across the province, Goldenville and Montague were the target districts used for validation. The remaining 62 districts were available for sampling training data and were used when they intersected the Sentinel-2 image containing either of the target districts (Figure 2). Since the two test districts are approximately 125 km apart and Sentinel-2 images are roughly 100 km by 100 km, each test district required its own image and therefore used different training districts. There are eight districts with exposed gold mine tailings in the image containing Montague, and nine in the image containing Goldenville. Moose River Gold District is in the small overlap between the images, so it was used in the analyses of both images and counted twice. The buffered circle around Goldenville was intersected slightly by the edge of the image, reducing the analysis area, though this did not remove any of the historic tailings areas mapped in the Nova Scotia Mine Tailings Database (NSMTD), which would later be used to obtain training data (Figure 2).

2.2. Methods

2.2.1. Data Acquisition and Initial Processing

2.2.1.1. Pre-Processing of Sentinel-2 Images

Sentinel-2 images are available to end users mainly as two products: Level-1C and Level-2A. Level-1C products have undergone radiometric and geometric corrections and represent top-of-atmosphere reflection. Level-2A images have been further processed to create surface reflectance, or “bottom-of-atmosphere” images. As photons pass through the Earth’s atmosphere and reach a satellite’s sensor, the reflectance signal is altered by water vapour and other atmospheric constituents, even on cloudless days. Water vapour, as well as cirrus clouds, can be effectively removed via atmospheric correction methods (Homem Antunes and Bolpato, 2018). Around 1.4 and 1.9 μm , respectively, are absorption features where water vapour absorbs light, rendering that EM region opaque and unusable for analyzing the Earth’s surface, even with corrections (Richards, 2013).

ESA began automatically generating Level-2A products globally in December 2018. Previously, a user had to take a Level-1C product and perform corrections either manually or by using specialized software such as the ESA’s Sentinel Application Platform. Automatic generation of surface reflectance imagery has made it possible to quickly swap out input images in models. The methods used to perform atmospheric corrections on Sentinel-2 images are continually refined and may not be the same across all datasets available in Google Earth Engine.

In addition to atmospheric correction, Level-2A imagery contains several added data

products. The scene classification map is a coarsely classified land cover data layer (provided as an imagery band) which includes vegetation, bare soil, water, and cloud classes at a 20 m resolution (European Space Agency, 2015). This band will be used to distribute sample points for the classifier across land cover types.

2.2.1.2. Nova Scotia Mine Tailings Database

In 2020, the Nova Scotia Department of Energy and Mines, now the Department of Natural Resources and Renewables, developed the NSMTD, derived from historical maps and modern surveys (Hennick and Poole, 2020). A total of 219 historic mineral processing sites were identified, out of which 194 processed gold. This project was an effort to update the previous map database, produced in 2009 by digitizing 64 maps originally produced between 1884 and 1919. These original maps were largely based on the work of E.R. Faribault at the Geological Survey of Canada (Drage, 2015; Faribault, 1900). These historical maps lack tailings from modern mining operations and may no longer be accurate due to the transport of tailings downstream from mine sites, or the burial of historic tailings by later mine wastes. The NSMTD compiled data from the digitized Faribault maps in a spatial data format and updated it with additional data from modern studies, where available. While the NSMTD is a thorough product, using data from across such a large area and period to classify modern images presents several challenges. Filtering and preprocessing were necessary before it could be used to train a classification model.

NSMTD tailing polygons and accompanying metadata were imported to GEE for processing and to be used as reference and validation data for the classification models. Relevant metadata properties used in the initial filter included metal mined and quantity of ore

extracted. From these, gold tailings could be specified and mine areas with no waste rock could be excluded. While polygon layers of the boundaries of mine districts were available, abandoned historic tailings often exist beyond those boundaries, according to the NSMTD. Rectangular mine district boundaries were converted to buffered circles with a 2.5 km radius, extending from the original district centroid. The radius was chosen based on a visual inspection of tailings maps. Too small, and the buffer would not capture all tailings around a mine point. Too large, and the buffer would overlap with nearby districts. The area of exposed tailings at mine districts varies greatly, impacting the amount of training data available in each district. Since the model relies on a random selection of districts for training and testing, districts with fewer than five tailings pixels, or 2000 m² were excluded. Overlapping within a small area was especially a problem around Goldboro, which contains the Upper Seal Harbour, Isaacs Harbour, and Lower Seal Harbour historic gold districts within a small region.

2.2.1.3. Masking Vegetation and Water Pixels

For classification, only pixels containing mine tailings exposed at the surface were viable for training and detection of the target class. Many of the NSMTD's tailings pixels were at least partially covered by vegetation or water. These areas have either been overgrown since they were mapped, or they were surveyed by removing vegetation and testing the sediment. In some cases, historic tailings were deposited directly into lakes or wetlands. This is commonly represented in the NSMTD as a fan-shaped polygon corresponding to the documented deposition location (Hennick and Poole, 2020). In other cases, shallow temporary pools are common, at least seasonally, and these may be deep enough to obscure tailings from detection within the reflectance imagery. Tailings polygons were converted to a raster image and

vegetation and water masks were applied as described below.

Normalized difference vegetation index (NDVI, Equation 1) and modified normalized difference water index (MNDWI, Equation 2) images were generated from the Sentinel-2 surface reflectance image. A threshold was set for each, chosen via histogram inspection, with any pixel with a value (NDVI or MNDWI) below this threshold used to create the mask. The histogram for NDVI was bimodal, with peaks around 0.0 and 0.8, likely corresponding to bare pixels (including water) and healthy, green vegetation, respectively. The flat area of the histogram between these peaks represents the range of viable NDVI thresholds. Choosing a value closer to the leftmost peak (lower NDVI) would make the mask more restrictive. A threshold value closer to the rightmost peak (higher NDVI) would allow pixels with more vegetation, increasing sample area but also introducing noise to the training data. MNDWI was chosen for the water mask over the normalized difference water index (NDWI) because it has been demonstrated to be better at differentiating water and built-up areas (Du et al., 2016). The MNDWI histogram also showed a bimodal distribution, with peaks around 0.0 and 0.35, likely corresponding to dry land and shallow water, respectively.

$$NDVI = \frac{(NIR - Red)}{(NIR + Red)} = \frac{(Band\ 8 - Band\ 4)}{(Band\ 8 + Band\ 4)} \quad (1)$$

$$MNDWI = \frac{(Green - SWIR)}{(Green + SWIR)} = \frac{(Band\ 3 - Band\ 11)}{(Band\ 3 + Band\ 11)} \quad (2)$$

The accuracy of these NDVI and MNDWI masks was tested by training a classifier at the threshold values and classifying the Montague mine district. The precision metric (Equation 4) was used, which is the ratio of true positives out of combined true and false positives. Precision

was used over recall or F1-Score for this test, as it penalizes false positives, and the goal was not to predict new tailings areas at this time (Branco et al., 2015; Van Rijsbergen, 1979).

Precision is explained in more detail in section 2.2.4.2.

Several threshold values were tested for the vegetation and water masks applied to the rasterized NSMTD polygons. The two masks removed pixels indicating green vegetation and water. Threshold values were tested by repeating classification at various values and obtaining precision. To ensure that the difference in accuracy was a result of the thresholds, input variables and target district were kept the same. Twenty metre Sentinel-2 bands were used as variables, and only Montague was used as the target district. Each test consisted of 25 iterations, and a summary of the results was obtained (Figure 3 and Figure 4). The values chosen to test the thresholds were based on the histograms of NDVI and MNDWI, respectively. These histograms were bimodal, and the distribution of test values targets the space between histogram peaks.

Additional methods were tested to remove waterbodies. Sentinel-2's SCM is a general land cover classification that is generated with the level 2A data products and includes a water class. GIS layers of waterbodies were imported from a provincial database, rasterized, and used as a mask. This data was based on either field surveys, or digitization of existing maps, and didn't reflect seasonal fluctuations in surface area. Though they might have provided a more accurate water body extent in some cases, there was no ability to locate temporary standing water on sites.

Before training and testing, districts were filtered one last time to remove those with little or no exposed tailings. Pixels were counted in each district and a filter was then used to

select only mine districts with at least five pixels or 2000 m² at a scale of 20 m. Tailings pixels from districts that were filtered out were still available to be sampled for the training dataset.

2.2.2. Characterization of Historic Gold Mine Waste Samples

2.2.2.1. Tailings Sample Collection

Tailings samples were collected at the Montague, Oldham, and Waverley historic gold mine districts (Figures 5a, 5b, and 5c, respectively) near Halifax (Figure 6). Sample locations were chosen based on visual inspection of tailings areas to target different colours of tailings at the surface. This was based on the assumption that tailings colour is a result of differing mineralogy (Percival et al., 2013). Large, open patches of tailings, ideally at least 10 m by 10 m (the minimum pixel size of the Sentinel-2 images) were targeted, to try and avoid locations where the image pixel would be mixed with forest or other land cover types. Two types of samples were collected at each location. A surface sample from the top cm was collected using a shovel, and another of the top 10-15 cm depth (including the top cm) was collected using a hand auger. Neither stratigraphic sequence nor way-up were maintained in the latter 10-15 cm samples, which would later be mixed to obtain random subsamples. Samples were put in labelled bags and placed in a cooler until they could be stored in a freezer.

Surface samples were meant to represent the material that is being directly observed by Sentinel-2's sensors, which cannot penetrate the sediment. Bulk samples were collected to investigate the correlation between the surface and underlying tailings and show that material composition observed by the satellite is not restricted to the immediate top layer when sediment is relatively homogenous. The shovel and hand auger were rinsed with distilled water

and wiped clean between each sample. We collected 16 paired samples (32 total), with six pairs at Oldham and four at Waverley on September 15th, 2020, and six at Montague on October 20th, 2020. Photos of tailings were taken at sample sites to record colour, the general level of vegetation and other environmental conditions. Coordinates were obtained by taking the mean of three points at each sample location with a consumer-grade GPS.

Soil samples were kept in a cooler in the field and brought directly to Saint Mary's University, where they were stored in a freezer. They were later thawed, placed in foil-lined glass dishes, dried in an oven at 50°C, checked daily, and removed when dry (roughly one to two days). It is worth noting that drying at this temperature may have led to a loss of Hg of approximately 4% (Smeds et al., 2022). Dried samples were shipped to Bureau Veritas Commodities Canada Ltd., in Vancouver, Canada. Samples were pulverized via mortar and pestle and processed by dissolution in aqua regia and analyzed by ICP-MS for 37 elements, including As, Hg, and iron (Fe).

2.2.2.2. Scanning Electron Microscope (SEM) Analysis

A subsample of each of the 16 surface samples was analyzed using a TESCAN Mira3 LMU SEM, equipped with an Oxford Instruments INCA X-max 80 mm² Energy Dispersive Spectroscopy (EDS) system at Saint Mary's University. Silt to sand-sized tailings grains were set in resin pucks, polished, and coated in carbon for analysis. Iron-bearing grains, specifically arsenopyrite, were easy to locate within each sample, as they were comparatively bright when using the backscattered electron (BSE) detector and could be further characterized by texture and habit (general shape of natural crystals). When bright minerals resembling target minerals

(sulphide and iron oxide minerals) were discovered, an image was saved, and the grain was further analyzed via EDS to obtain its composition. As hydrogen cannot be detected by EDS, identification of hydroxides was not possible, but certain sulphide and iron oxide minerals were identified.

2.2.3. Image Sampling for Training and Classification

2.2.3.1. Remote-Sensing Image Sample Design

To classify pixels in an image, a supervised classifier must first be trained using reference data labelled with the appropriate land-cover class. Our image sampling procedure follows recommendations by Stehman and Foody (2019). This process is simplified when using a binary classifier, where reference data need only be labelled as either belonging or not belonging to the target class, e.g., tailings, or non-tailings. The non-tailings class included all land cover, including bare sediment or soil, that was not mapped as tailings in the NSMTD or masked out using the vegetation and water masks described above. Relative to non-tailings pixels, tailings pixels were a very small class. Having a rare target class has implications on both sampling for training and accuracy assessment (Genuer et al., 2010), and as such slightly different sampling approaches were taken to sample the tailings and non-tailings classes. Tailings were sampled from areas labelled in the NSMTD that were not masked out. Non-tailings were sampled from throughout the entire image. These two training point sets were then combined to train the binary classifier.

2.2.3.2. Non-Tailings Sampling Using Stratified Random Sampling

To ensure that all land cover classes were sampled sufficiently in the non-tailings class, a stratified random sample design was implemented. Stratified random sampling was used on the scene classification map band automatically generated and attached to the Sentinel-2 Tier-2A image to provide spectral data for a variety of non-tailings land cover. The area of each of these classes was determined, and sample quantities per class were distributed according to their area proportion. The exact number of samples would vary for each image, but an example, as well as the landcover types, is given in Table 2. Scene classification map classes two to nine were used for stratification (Table 1). The number of pixels in each class was divided by the sum of pixels in the training area to obtain class area proportion. The total number of sample points was set at 7500, and this number was multiplied by each class proportion to reach the desired number of samples per class. After proportions were determined, 25 samples were added to each class to ensure that rare classes were still captured.

2.2.3.3. Sampling Tailings Areas in Sentinel-2 Images

Mapped tailings are present only around the 64 historic mine districts, and these districts were chosen as the minimum mapping unit (Olofsson et al., 2014) for the classification and training of the tailings class. Tailings were randomly sampled from all districts but the test districts, including those districts that were disqualified from the training/testing selection for having too few tailings pixels. We randomly selected 1/3 of the pixels and labelled them as tailings for the classifier trainer. Once non-tailings and tailings samples were collected, the two were merged into one feature collection and used as the training data for the classifier.

2.2.3.4. Splitting Training and Test Areas for Cross-Validation

The pixel-wise classifier was tested in two ways. In the first, only the Montague and Goldenville districts were used. In the second, Monte-Carlo cross-validation was used, where all districts in a Sentinel-2 image were split repeatedly into testing and training sets. By removing control over which districts were used, this method provided some insight into the difficulties of classifying districts that were not as well-documented as Montague or Goldenville. In each split, a random number was generated for each district, districts were ranked according to this number, and the top 1/3 of districts were set aside for testing. Training data was collected from the remaining 2/3 districts. Sample points were generated using the same procedure as in the Montague and Goldenville tests.

2.2.4. Classification

2.2.4.1. Random Forest Classifier

Once sample points for the target and non-target classes were collected, the classifier was trained and implemented. A random forest (RF) classifier was chosen – specifically, the Statistical Machine Intelligence and Learning Engine (SMILE) random forest (RF) classifier (Li, 2014), which is available within GEE. RF classifiers are ensemble tree classifiers that pass data through a series of nodes, randomly selecting variables and voting on their class membership. The majority of votes determines the input data's class label. These classifiers are popular in remote sensing because they are capable of high accuracy, even with large data sets and large amounts of input variables. The SMILE RF also has the advantage of automatically producing a variable importance value, which was used during classification to obtain an optimized set of

variables.

2.2.4.2. Accuracy Assessment: F-Score

Before variables could be optimized and classification could be performed, a method was established to test the accuracy of the model. There are many classification accuracy assessment metrics, including overall accuracy, producer's accuracy, and consumer's accuracy. These are poor choices, however, when the target class is rare compared to the non-target class (or classes) – a common scenario in binary classifiers (Branco et al., 2015). If every pixel in an image or mapping unit is being assessed, accuracy may be high even when the target class is not classified at all. Mine district areas with a radius of 2.5 km have about 50 thousand total pixels at 20 m resolution and in some cases 10 or fewer pixels of tailings unobstructed by vegetation or water. Using overall accuracy, a classifier that completely ignores the target class (e.g., all pixels labelled non-tailings) in this case would be considered about 99.8% accurate (10 errors out of 50 000 classified pixels), despite not attempting to classify the target. Other accuracy metrics have been developed to better address imbalanced target class distributions. The metric chosen in this study was the F-score, or more specifically, the F-Beta score, F_{β} , which is the weighted harmonic mean between recall and precision (Van Rijsbergen, 1979). The variable β can be adjusted to weigh either metric above the other. We calculate F_{β} as:

$$F_{\beta} = (1 + \beta^2) * \frac{\text{precision} * \text{recall}}{(\beta^2 + \text{recall})} \quad (3)$$

Where:

$$precision = \frac{true\ positive\ predictions}{true\ positive\ predictions + false\ positive\ predictions} \quad (4)$$

$$recall = \frac{true\ positive\ predictions}{true\ positive\ predictions + false\ negative\ predictions} \quad (5)$$

True positives are determined by the classifier labelling a pixel as tailings that is also labelled tailings in the reference data. False positives are labelled tailings by the classifier but non-tailings in the reference data. False negatives were not labelled tailings by the classifier but are labelled as such in the reference data. Note that true negative predictions do not contribute to F-Score at all. To put these metrics in other terms, precision measures the number of correctly classified tailings pixels out of total classified tailings and recall measures correctly classified tailings pixels out of total reference tailings. With β set to 1, $F\beta$ becomes F1-score or the balanced F-score. This is the most common configuration of the F-Score, and β was set to 1 for accuracy testing in this study, though it can be adjusted within the model to prioritize recall or precision during training, in theory changing how conservative the model is when predicting new tailings areas.

2.2.4.3. Variable Importance and Selection

Variable importance (VI) is a measure of how much any one variable affects accuracy in a classifier node. The method of calculation for VI varies based on the classifier used. The SMILE random forest model, which was used in this study, measures variable importance based on the Gini impurity index. The Gini index measures the probability that a randomly selected sample would be misclassified if it were assigned a random class label based on class distribution (Joshi, 2023). Each node in the classifier splits data according to model parameters, leading to a

decrease in impurity. In this case, VI was measured as the sum of the decrease in impurity for a variable across all nodes. The higher the VI, the greater impact a variable has on impurity.

Once variable importance was collected for the full set of input variables, an optimization or calibration stage was initiated to attempt to reduce unimportant or redundant variables. This optimization was performed using these steps:

- 1) Train a random forest classifier using previously obtained training points. Retrieve variable importance for each variable and out-of-bag (OOB) error for the classifier.
- 2) Remove the variable with the lowest VI and obtain the OOB error again. If the OOB error increases or stays the same, discard the variable. If it decreases, keep the variable.
- 3) Move through each variable, repeating the OOB error test.

This is non-recursive feature elimination (NRFE) (Díaz-Uriarte and Alvarez de Andrés, 2006; Gregorutti et al., 2017; Svetnik et al., 2004). It is contrasted by recursive feature-elimination (RFE), which recalculates variable importance each time a variable is removed. Though RFE is generally considered superior to NRFE (Genuer et al., 2010; Gregorutti et al., 2017; Svetnik et al., 2004), GEE does not handle recursive methods well due to the way it performs parallel processing on the cloud, and NRFE was selected.

OOB error is obtained via bootstrapping, where a subset of the training data is set aside, and the accuracy of the classifier is tested on this subset. This allows the classifier to test its accuracy internally, without having to explicitly assign testing data. Bias is reduced by separating training and testing data, although spatial autocorrelation may still have been a factor. The districts used to test variable importance were kept constant, to control for the variability of accuracy between them. Tests were run on Montague and Goldenville (Figure 7).

Reducing the number of variables provides two advantages. First, it reduces the computational cost by removing input data. This may not be an important factor when using random forest, which easily handles very large variable inputs. This step could, however, be used before switching to a classifier such as support vector machines, which is very sensitive to the number of input variables (Mountrakis et al., 2011). The second, more important, advantage is that this cleanup removed some correlated variables, which would have introduced noise, reduced performance, and made it harder to explain results. For example, if iron feature depth and ferric iron index were included in the input, both would likely score high VI values because they are good at defining the tailings class. However, these indices are very similar, and one is not providing much new information over the other. A classifier based only on these two inputs would perform poorly. In the case of random forest nodes, which select a set number of variables randomly, if a node were to select both variables, they may be “taking up space” that would be better held for an uncorrelated variable. An individual variable’s impact can be described by VI, but this metric alone does not always lead to the best variable set.

An alternative option to using OOB error would be to optimize using F-Score on the test district(s). F-Score has the added ability to change weight between recall and precision, potentially allowing optimization of one parameter over the other. This would introduce bias, however, since it only works if we have *a priori* knowledge of the site. It may be useful if only some tailings were known at a site and the goal of classification was to find other similar, nearby tailings. Training parameters could easily be changed, based on the context and the area being analyzed.

2.2.4.4. Pixel-Wise Classification of Test Areas

Once variables were optimized, the classifier was used on the districts set aside for testing. Every pixel in the district was classified, based on its reflectance and index values, as either tailings or non-tailings. Accuracy assessment was performed in each district. Two types of tests were performed. One used only the Montague and Goldenville districts as test sites. The other used all districts within the boundary of the selected Sentinel-2 image, randomly assigning a subset for testing and using the rest for training.

2.2.5. Object-Based Classification

In addition to the pixel-wise classification, three object-based methods were tested. In object-based classification, rather than classifying each pixel individually, steps are taken to first segment an image by clustering pixels that are spectrally alike and/or near one another. These groups of pixels are then treated as one object or superpixel (Achanta and Ssstrunk, 2017; Kamal and Phinn, 2011) by aggregating values across all individual pixels and applying it to the group (e.g., assigning the mean value of each band across all pixels to the object). Incorporating surrounding pixels acknowledges the autocorrelation of classes of land cover. Object-based methods are well suited for the sites observed in this study, as tailings are not randomly distributed across the landscape (either at the district or regional scale) and tend to exist in patches.

There are numerous methods and algorithms for clustering pixels into objects. In this study, the simple non-iterative clustering (SNIC) algorithm was used, which is available in GEE (Achanta and Ssstrunk, 2017). This algorithm takes a grid of points and grows these points

according to a distance measure that incorporates spatial and colour distance (proximity and spectral similarity). As objects grow, every pixel will eventually be added to the connected object with the lowest distance value. The user has control of several parameters to adjust compactness (how square the objects are) and whether pixels are connected orthogonally (4 connected pixels) or in all directions (8 connected pixels).

A potential downside of SNIC is that the objects it produces are highly dependent on the original starting points. A random grid may not place sufficient starting points on tailings, which at the largest only tend to be 10 or so pixels across. Due to its non-iterative nature, SNIC cannot subdivide objects once they are created, unlike other clustering algorithms (e.g., ISODATA. [Tou, 1974]). Increasing the density of the starting grid will create more objects, until eventually, the grid matches the image resolution, restricting space for objects to grow and producing objects which contain only one pixel each. Three different starting grids were tested, with increasing levels of user involvement.

Rather than the regular grid recommended for use with SNIC, the first test was the “pure random seeds” experiment, which tested the use of random points distributed across the test districts. The model generated 500 randomly distributed points and converted them to a raster to be used as input to the SNIC segmentation function. The origin point for the regular seed grids is always the same, so if a land cover feature is missed once, it would always be missed at the same point density. Using random points should compensate for situations where land cover patterns exist and are missed by the regular grid points (Stehman, 2009).

The second experiment was “classified pixels as seeds”, where 200 points were randomly sampled from the pixels labelled as tailings by the pixel-wise random forest classifier.

An additional 1000 non-tailings points were sampled. Objects were grown using SNIC using all 1200 points. Non-tailings starting points were required because SNIC does not produce a background class. If only tailings were used to create SNIC objects, these objects would likely grow until they filled the entire test area. By sampling non-tailings as well as tailings pixels to create objects, we introduce bounds on the tailings objects. The accuracy of this method was tested per district by F-Score, recall, and precision.

The third experiment, the “user-generated seeds”, had the highest degree of user interaction. Objects were grown from points dropped on the map. These points were on well-documented tailings based on mineralogy and bulk chemistry datasets. Four points were created at Montague, based on locations sampled in this study. Five points were created at Goldenville, using locations sampled in Parsons et al. (2012). We also sampled 500 random points, distributed throughout the target districts, to provide background objects. By inputting a small number of collected samples or relying on high-quality datasets to verify tailings are present, a user could input their locations and use this model to estimate its extent.

2.3. Results

2.3.1. Physical Analysis of Tailings

2.3.1.1. Mineralogy and bulk geochemistry

Out of the 16 paired samples for 3 historic tailings sites (Table 3) As was highest at Montague (Figure 5a), with a mean surface concentration of 9868 ppm As, a mean bulk sample concentration of 5692 ppm As, and the highest concentration of any sample 16,300 ppm As (MO02 surface sample). Waverley (Muddy Pond) had the next highest As concentrations (Figure

5b), with a mean value at the surface of 1921 ppm As, and a mean bulk sample value of 4364 ppm As, with the highest value at 6143 ppm As (WV01 bulk sample). In addition, Waverley was the only site of the three in which bulk samples had a higher As concentration than surface samples. Oldham had the lowest As concentrations of the three sites, with a mean surface value of 999 ppm As, and a bulk sample mean of 635 ppm As (Figure 5c). The highest As concentration at Oldham was 2362 ppm As (OH06 surface). All samples exceeded the CCME guidelines of 12 ppm As, which is consistent with previous studies of historical gold tailings at other sites in Nova Scotia (Parsons et al., 2012).

2.3.1.2. SEM Results

We examined the 16 resin pucks via SEM, each of which contained a random sample of material from shallow tailings at each site. Potential sulphides, iron oxides, arsenates, and iron oxyhydroxides were targeted in the 16 resin pucks containing sub-sample of the surface samples using backscatter and EDS. Sulphide mineral grains (arsenopyrite or, more rarely, pyrite) were commonly weathered around the rim, where iron oxide minerals were identified (Figure 8), which corresponds with established documentation of sulphide minerals with weathered edges overgrown with secondary phases (DeSisto et al., 2016; Swayze et al., 2000). The presence of these weathered rims was considered evidence that a sample comprised tailings and not naturally-occurring sediment.

2.3.2. Vegetation and Water Masks

The NDVI threshold was tested first, using values of 0.2, 0.4, 0.6, 0.8, and 1.0, with the water threshold set to 0.0 (Figure 3). The interquartile range within each threshold was

generally low, except for 0.2 NDVI. Mean precision increased until reaching 0.64 at 0.6 NDVI, then it began to decline. An NDVI threshold of 1.0 (i.e., no vegetation mask) had the lowest mean precision, at 0.39, as it included all vegetated pixels in the training data. Based on those results, 0.6 was chosen as the optimized NDVI threshold for its high precision and small interquartile range, as all dense canopy cover in treed areas and thick grass patches were reduced. Just as importantly, this value of 0.6 did not filter out sparse vegetation that sometimes encroached on tailings areas, which allowed mixed pixels that were still dominated by tailings to remain in the training set. A more precise threshold value may have been identified by using a step size finer than 0.2, though this may have been less generalizable when expanding to all sites. More robust threshold detection methods (e.g., Otsu's method, Otsu, 1979) could potentially provide an optimized threshold for each site on the fly, though methods that require recursive iteration may be difficult to implement in GEE. The histogram for MNDWI showed a bimodal distribution with peaks around 0.0 and 0.35, likely corresponding to dry land and shallow water, respectively. Deep water pixels appear to have more noise and values were distributed evenly across the 0.35-1.0 range. The right peak was not as well-defined as the peak around 0.0 and was slightly positively skewed. A narrow area existed around most waterbodies that was not successfully masked using this threshold. Lowering the threshold (making it more restrictive) started to remove tailings pixels as well. An MNDWI threshold value of 0.0 was selected which captured shallow ponds and larger waterbodies, except for the area at their shores.

Water thresholds were tested at values of -0.4, -0.2, 0.0, 0.2, and 0.4, with the vegetation threshold set at 0.6 (Figure 4). The water threshold value results showed much less

variation than the vegetation threshold values. Though -0.4 had the highest precision by a small margin, visual inspection of the image showed that such a low threshold would remove areas of tailings that could not be confirmed as wet or dry. A value of 0.0 was chosen, as a balance between avoiding possibly dry tailings while still removing most areas of open water. Pixels below thresholds were included in the mask. The result was a single image where pixels in the mask indicated an “unvegetated and dry” surface. This filtered image was used to train the classifier.

2.3.3. Variable Optimization

Potential variable sets were determined via the non-iterative feature elimination process previously described, then target districts were classified 25 times using each optimized set (Figure 7). All model parameters were kept constant, including the vegetation and water threshold values, which were set at 0.6 and 0.0, respectively. Only one district was tested at a time, and five optimized sets were generated per district. Montague and Goldenville were used as the target districts, with the other districts present in their respective Sentinel-2 image boundaries used as training districts (Figure 2). A total of 250 iterations were tested, and summary statistics of each variable set are displayed in Figure 7. The set [Band 3 (green), Band 6 (vegetation red edge), Band 7 (vegetation red edge), Band 8A (NIR), Band 12 (SWIR), NDVI, MNDWI] was selected based on its high mean F1-Score and low variance. The inclusion of two red edge bands may be redundant. On the other hand, the exclusion of the two iron indices was surprising. Indices do not actually provide new data, however, as they are just combinations of existing data that can reduce noise and highlight features. It is possible that these were also determined by the model to be redundant, and so they were removed.

2.3.4. Pixel-Wise Classification

2.3.4.1. Montague and Goldenville Districts

Once threshold values were chosen and variable sets were generated, classification was performed again. First, Montague and Goldenville were classified, using all other districts in their respective images for training. Accuracy (F1-Score) was collected in the test district for each iteration. The model was run 50 times per district, and summary statistics were obtained. Results are visualized in Figure 9a and 9b, based on the frequency of positive classification per pixel. Where the background (satellite image) is visible, this indicates the pixel was never labelled as tailings.

2.3.4.2. All Districts Using Random Testing and Training Subsets

Finally, all districts within the two Sentinel-2 images were tested using a Monte Carlo cross-validation technique (Lyons et al., 2018). The classifier was run 100 times, each time randomly selecting two test districts and using the remainder for training. This captures a range of accuracy across iterations, each of which uses different combinations of testing and training districts, as well as different randomly selected training points and random forest outcomes. F1-Score was collected for all test districts and is displayed in Figure 10a and 10b. Note that Caribou is present in both the Montague and Goldenville regions, as there is a slight overlap in Sentinel-2 images (Figure 2).

2.3.5. Object-Based Classification

Three methods were tested to classify tailings from segmented images, using the object-based methods. The same sample points were used to train these classifiers as from the pixel-

wise classification. Results from Montague and Goldenville are shown here, as these sites were the only ones tested using the “objects grown from samples” method.

The pure random seeds experiment did not outperform pixel-wise classification. At its best, it came close to the F1-Score of the pixel-wise classification. Results were good at Goldenville but very poor at Montague, which had a median of just over 0.5 but a high variance and many results with no tailings classified at all (Figure 11).

The classified pixels as seeds results showed an improvement over the random points but this experiment still failed to outperform the pixel-wise classification (Figure 12). It did have the advantage of cleaning up some of the scattered false positives that were often present as single, isolated pixels. Median F1-Score increased for both sites, and Montague had at least some classified pixels in all iterations. The mean recall was consistently higher than both the median F1-Score and mean precision.

The final experiment was creating objects from user-generated seeds. Locations of physical tailings sample sites were manually entered. For Montague, the locations of samples collected in this study were used (Figure 5a). At Goldenville, locations were taken from Parsons et al. (2012). Four points were used for Montague and five for Goldenville. These manually entered points existed in addition to the random points used in the previous iterations. This method was like previous ones but allowed a more guided object generation when information was available. Goldenville has a slightly lower median F1-Score than in the previous method and a much larger interquartile range that is highly negatively skewed (Figure 13). The mean precision for Goldenville is much higher than the mean recall. Results at Montague were better using this method than the previous methods. Median F1-Score is slightly higher, and the

variance is lower.

2.4. Discussion

2.4.1. Data Sources for Training and Validation

Studying sites that have been known to historical surveyors and modern researchers for such a long time means that a wealth of data is available that can potentially be used for the training and validation of models. These historic gold mine sites are ideal in many ways as a workshop and testing ground for big data analytical methods. The use of existing data, however, has advantages and disadvantages. Using existing data significantly reduced the cost of this study, and the amount of time spent in the field. Data was also available from a much greater spatial range than what would have been practical to collect on our own, in the available timeframe. Time restrictions were especially important, as the scheduled field sample season was impacted by safety restrictions put in place during the Covid-19 pandemic. Without using existing data, the number of sites included in this study would likely have been restricted to just two or three.

Using existing data was not as simple as putting everything in a spatial format and feeding it into the model. There were limitations in the data that had to be considered when training and validating, and that must be accounted for when interpreting results. The age of the data ranged from very recent (i.e., the Nova Scotia Mine Tailings Database, [Hennick and Poole, 2020]) to a century old (Faribault, 1900). Even the oldest data can help to provide an idea of the location and possibly the spatial extent of tailings, but it does not provide a reliable description of the current tailings extent, much less the detailed modern mineralogy. While

gold mine tailings may reach an equilibrium point where mineralogy can become relatively stable in the medium-long term (Roussel et al., 2000; von der Heyden and Roychoudhury, 2015), shifts in pH, bacterial activity, or water-level changes may cause rapid dissolution or more gradual remineralization (Riaza and Müller, 2010; Seal and Hammarstrom, 2003), changing the minerals present and thus the spectral signature of the aggregate tailings. For this reason, it is generally better for most remote sensing methods to use data from samples collected as close as possible to the date of satellite image acquisition. The large time range of data used in this study would have made spectral-matching techniques such as spectral mixture analysis difficult and likely inappropriate, as validation would require up-to-date mineralogical data. We addressed this problem by using the data to define only the areal extent of tailings and collecting training data directly from the images. In theory, this method captures mineralogical changes that have occurred between physical sampling and image classification, allowing for discrimination of tailings and non-tailings, as long as reflectance of tailings differs from that of surrounding sediment.

When using existing data, there may be varied definitions of tailings between studies. Previous surveys that physically sampled tailings typically sought to discover and describe tailings whether they were under vegetation, non-tailings sediment or soil, or under water. In the context of optical remote sensing, only tailings that are exposed at the surface are useful for training and validating a classification model. If, for instance, the entire Nova Scotia Mine Tailings Database were used to train a model, it would have included many pixels labelled as tailings that were obscured in the satellite imagery. This would have introduced non-tailings sample points to the tailings training data, reducing the model's ability to discriminate between

these two land cover types. This is also related to the time range of data collection, especially concerning vegetation. Data collected even a few years ago may indicate exposed tailings in a particular pixel that may have become overgrown. This was addressed using the vegetation and water masks derived from image band values to remove some tailings pixels before training the model. As a test, the model was run without filtering tailings pixels for vegetation, and it performed as expected – vastly overestimating tailings regions (Figure 14) due to incorporating pixels with vegetation into the tailings class. The NDVI threshold test showed a similar result when a value of 0.2 was used (Figure 3).

Setting the vegetation and water thresholds was the fastest and simplest way to remove large areas of incompatible training data and these data layers consistently ranked high in variable importance. In regions with ample forest cover, tailings often remain unvegetated, allowing easy discrimination via NDVI. This index alone would not necessarily help in distinguishing non-tailings sediment or soil from tailings, since pure pixels of either of these classes should have values near zero for either index, but they provide enough information to the classifier that it was able to focus on bare, dry sediment. Water masking via MNDWI was not as effective as vegetation masking but still helped to remove some areas from the Nova Scotia Mine Tailings Database layers which, for our purposes, should not be considered tailings. Initially, the same vegetation and water masks were applied to classifier results that were applied in pre-processing the training data, but it made very little difference in the total number of pixels classified. The random forest model was able to decide on its own to prioritize these indexes when classifying.

2.4.2. Variable Importance

Feature reduction is an important step in hyperspectral image analysis, where a large number of bands can lead to problems of correlation while also being computationally expensive to process (Gregorutti et al., 2017), but it is not commonly used with multispectral data. Sentinel-2 bands are spaced apart, reducing correlation, and there are fewer of them, reducing the computational cost. Even with a small number of bands, feature elimination methods may identify redundant bands which do not effectively increase accuracy, but it seems to have had a limited effect in this study. The random forest classifier performs an internal variable selection process repeatedly as it runs by randomly selecting a subset of variables at its nodes and testing accuracy on a subset of training data (Breiman, 2001; Genuer et al., 2010). With only 10 spectral bands used and four indices to start with, though it showed a slight benefit, F1-Scores across the tested variable sets did not vary by a large degree and the slight reduction in the quantity of input variables had little to no impact on model performance (Figure 7). The optimization step could likely have been omitted with little effect.

2.4.3. Pixel-Wise Classification

Accuracy, measured in F1-score, was high for most sites for the pixel-wise classification. This shows that it is possible to train a classifier to differentiate exposed tailings from non-tailings using only multispectral bands. The analysis was largely made possible by the existence of good-quality training data captured over a large region. It does not appear that the large distance separating the sites is hindering the model's performance. An advantage of the sites used in this study is that they all exist in the same geological terrane, spanning only a few different formations. While many conditions may vary at the surface of these sites, bedrock and the ore extracted during mining are similar, providing a relatively consistent background signal

(Figure 15).

Waverley and Lake Catcha had the lowest median F1-scores, and variance was high at Lake Catcha. These sites both consist of partial wetlands, and large shoreline areas, both land cover types which appear to confuse the classifier.

The average reflectance of tailings was recorded at all sites that exceeded the minimum pixel count threshold (Figure 15). Mean spectra plots are divided between the sites around Montague and the sites around Goldenville, for a total of 12 spectra (Caribou is included in both regions and only counted once). Some absorption can be observed for band 8 at many of the districts which could be attributed to the iron absorption feature of various iron-bearing minerals present in tailings that may not be present in background sediments or soils. Band 8 was not used in the classification, however, due to its overlap with band 8A. Band 8A was chosen over band 8 to reduce band correlation, and based on the assumption that its narrower bandwidth would help target iron absorption in minerals. Since absorption can be observed in band 8 but not band 8A, any absorption due to iron-bearing minerals was likely in band 8's range below band 8A's range (i.e., approximately 780 to 845 nm, Table 1).

Moosehead, Fifteen Mile Stream, Lawrencetown, and East Rawdon are outliers in spectral shape, magnitude, or both. Exposed? Tailings areas at these sites are small, especially after filtering for vegetation. Several are just over the pixel count threshold for eliminating the sites, and there are fewer pixels to sample. The smaller areas may also lead to more mixed pixels at the edges of tailings. The tailings polygons for Moosehead and Lawrencetown from the Nova Scotia Mine Tailings Database appear to show deposition directly into the ocean. This may be observed in the relatively flat, low-reflectance spectra for these sites, which suggest that the

pixels are indicating water rather than tailings, or at least wet sediment (Lekner and Dorf, 1988; Nolet et al., 2014). The use of a more reliable method for removing wet pixels would likely shift the outlying spectra closer to the mean, providing better training data for the classifier. Some of the districts would be removed from the analysis entirely. Changing the MNDWI threshold would likely not suffice on its own. Setting the water threshold value aggressively began to remove tailings, and setting it conservatively failed to remove wetlands and pixels that seemed to contain turbid water.

Many false positives were observed along shorelines, possibly resulting from the broad definition of tailings in the tailings data. It is difficult to determine whether the confusion was caused by a mixed-pixel effect at the boundary of water and land, or if the problem is the saturation of the shoreline sediment. If it was the former, sub-pixel identification could help improve results here. If it was the latter and the pore space of shoreline sediments is saturated, unmixing would be more difficult. It is possible that a classifier, trained on wet non-tailings sediment, could differentiate dry tailings from wet non-tailings, though it may require greater spectral resolution. This question is further explored in chapter two.

Roads, and to a lesser extent other built-up areas like houses, were sometimes erroneously labelled as tailings by the classifier. Looking at Figure 9a and 9b, it does appear that there are trends along roads or in residential areas, with incorrect labels appearing throughout but in low frequencies. Urban and built-up land cover have similar spectra to tailings (Figure 16), but the model appeared to be able to differentiate the two most of the time and false positives can likely be attributed to noise.

2.4.4. Object-Based Classifier

Object-based classification using the SNIC algorithm shows some promise in removing false positives, especially lone pixels erroneously classified as tailings. The downside is that it sometimes misses tailings areas and missing these tailings objects contributes to greater omission error than missing an individual pixel. Growing objects from random points didn't yield better results than the pixel-wise classification, performing very poorly at most sites. This may be because the boundary of tailings at most sites is not as well-defined as at Goldenville or Montague, making it harder for the algorithm to know where one object should stop, and another begin. On the other hand, when objects are grown from seeds which are placed on tailings, they seem to be more successful in classifying mixed pixels at the edges where vegetation or water begins.

The user-generated seeds test was much more accurate and showed that expert input and geochemical testing of a limited number of physical samples can guide the classification process. The SNIC procedure allows for interactive and intuitive guidance of segmentation and subsequent classification. By using this method, tailings maps could be generated based only on a few well-defined samples. This could be applied after physical sampling has been performed, or beforehand to help predict tailings extent and guide sampling procedures. Combining this method with the collection of field spectra could allow for the prediction of an interpolated tailings area using a limited number of high spatial and/or spectral resolution measurements. Field spectra were not used in this study, as it would take many data points to train a random forest model, and we instead opted to use the large Nova Scotia Mine Tailings Database. Testing a classifier that has been trained on the large database and applied to higher resolution field spectra could be a valuable future study.

2.5. Conclusion

The primary goal of this study was to determine if multispectral data from the Sentinel-2 satellite mission provided sufficient data to train a random forest classifier to differentiate tailings from non-tailings. An optimization step was used to determine which spectral bands and computed indexes provided the best results. This step showed that some Sentinel-2 bands are not necessary or may even be detrimental, however, results did not vary greatly across different sets of variables. This can probably be attributed to the efficiency of random forest classifiers, which internally select variables based on an importance score. Two indexes, ferric iron index and iron feature depth, were computed that were meant to target the iron absorption feature suspected to be present in tailings. Neither of these indexes were included in the variable sets with the highest F1-Score and were not used in the final classification. This may have been because tailings did not display as clear an iron absorption feature as expected, or the iron absorption feature may have been captured adequately by the narrow NIR band – band 8A.

Accuracy, as measured by F1-Score, varied greatly across the districts. Not surprisingly, the larger sites with clearly visible tailings were classified with much higher accuracy than small sites with vegetation or, especially, water and wetlands. If viability of tailings detection is a function of tailings area, a more sophisticated method of eliminating sites should be explored. In this study sites were eliminated as potential targets based on pixel count alone, under the assumption that tailings of a certain size were more likely to contain more “pure” tailings pixels. In other words, small sites would have more edge pixels and therefore more mixed spectra. This method did not consider the possibility that a large site may be narrow (i.e., fewer than 3

pixels across) and would still contain a large proportion of edge pixels.

Tailings that are covered by vegetation cannot be identified via optical remote sensing, though it is possible that using multiple classes of tailings could increase accuracy in wetlands. Tailings were often deposited in wetlands at these historic mines, and if tailings in shallow water could be indicated it would greatly increase the applicability of these methods.

Testing of variable importance often prioritized NDVI, indicating that the absence of vegetation was one of the most important factors in identifying tailings areas. It is important to note that this study took place in an area with a temperate climate and extensive forest cover. In an arid setting, NDVI would not have been as important a factor, though it is not clear how this would impact overall accuracy. There were enough bare ground pixels in the images that were correctly labelled as non-tailings that it seems the classifier was capable of discerning bare sediment from tailings, but it would be interesting to see the same model applied in a desert setting where NDVI would not be important at all.

The single most important contributing factor to the accuracy of this model was the extensive database produced by the Nova Scotian government. This data provided a diverse training set and allowed for automated training and validation data collection for historic mine sites almost anywhere in the province. By using computed indices from the Sentinel-2 images, this data could be cleaned up to train the classifier and used across different dates and locations. Considering this, perhaps the greatest hindrance to improving the performance of the model was the inability to fully remove pixels representing saturated sediment from the training data. This is potentially what led to the consistent classification of shorelines as tailings.

The results of this study show that tailings data from diverse sources, even spanning a

large time range, can be used to train an accurate classifier, as long as the data is processed to match remote sensing constraints. When using a binary classifier, multispectral data provided by Sentinel-2 appears to be sufficient to discern tailings from non-tailings, at least in non-vegetated areas where bedrock is relatively homogenous between target sites. Further research may explore the use of hyperspectral data to determine whether tailings could be separated into sub-classes, which would provide more information on mineralogy and the risk of contaminants. These sub-classes could represent mineral groups, vegetation types (e.g., grasses vs. lichens), or they could separate dry, wet, and shoreline tailings pixels. Space-based hyperspectral platforms typically produce images with pixel sizes greater than those of Sentinel-2, so it is possible that the higher spectral resolution would not be sufficient to compensate for the mixed pixel effect. Field-based spectrometers produce data for a very small (and adjustable) region on the ground, largely removing the impact of mixed spectra. As the model described in this paper relied on a large number of training points, the use of a handheld spectrometer may not be practical, however, future work could determine the minimum number of points needed to train a classifier that could then be applied to a region (whether an area the size of a Sentinel-2 image, or a single tailings site).

2.6. Figures

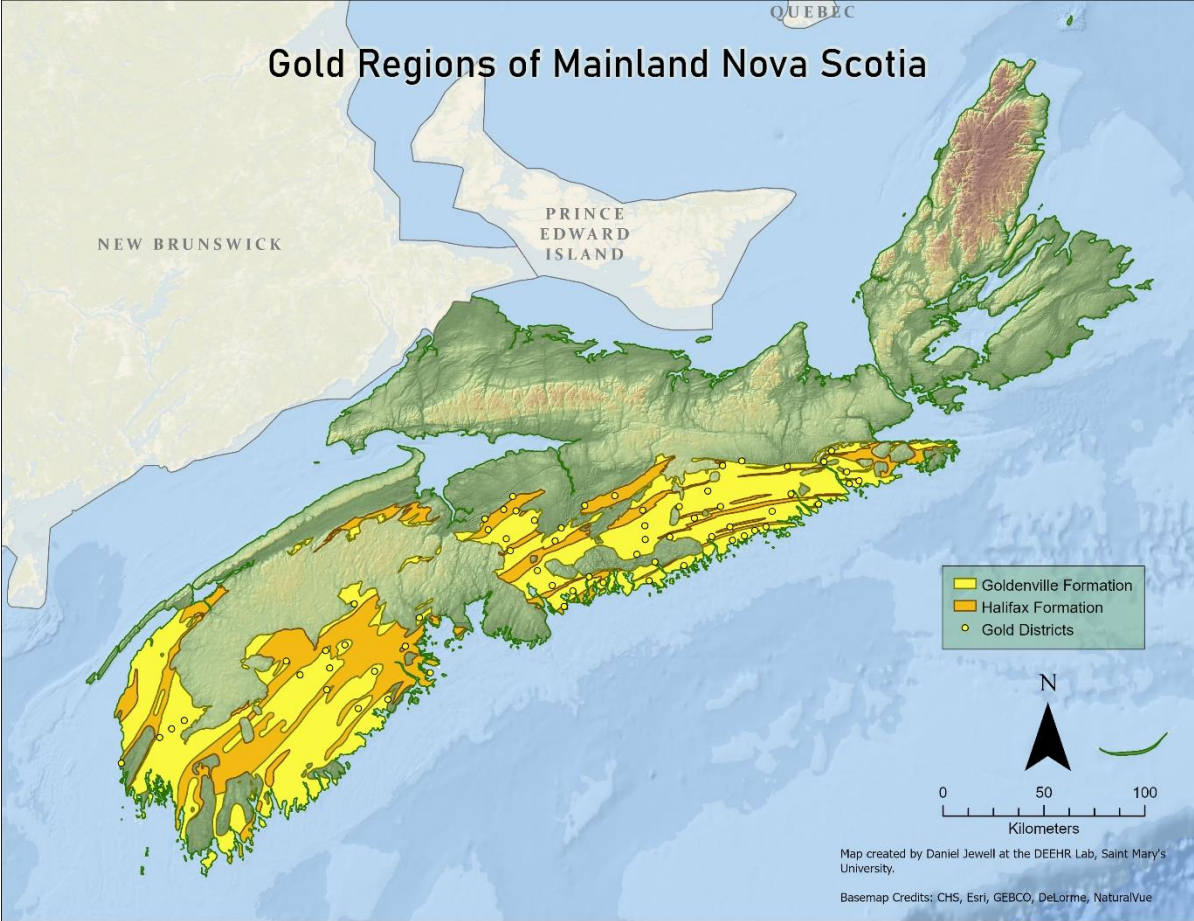


Figure 1. A map of gold-bearing geological formations in Nova Scotia. The province's 64 historic gold mining districts are located in these areas.

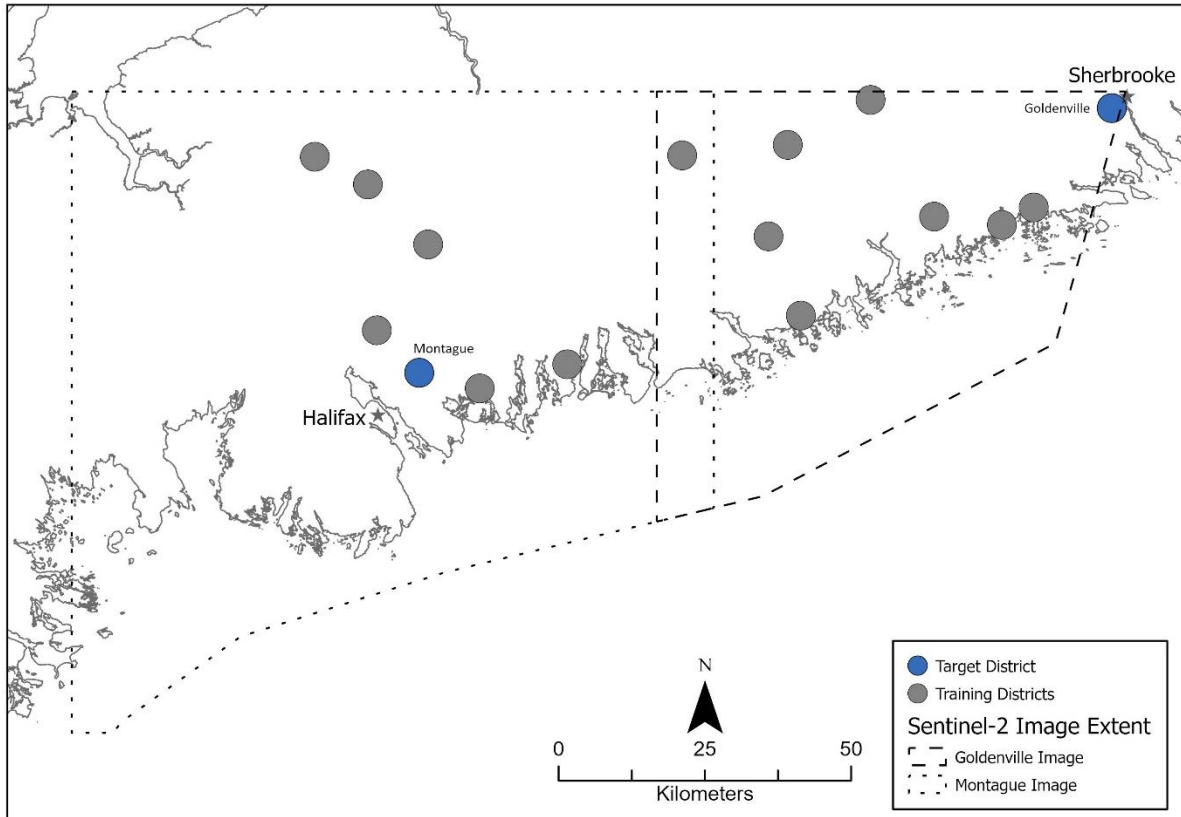


Figure 2. The extent of the two Sentinel-2 images (left: Montague region. Right: Goldenville region. Both images were captured on August 2nd, 2019), and the location of various historic gold mine districts within each image. The “training districts” provided the pixels in each image were used to train and validate the classification model using a Random Forest Classification approach. The “target districts”, Montague and Goldenville, were used for the final model assessment, as there is more data available for those sites.

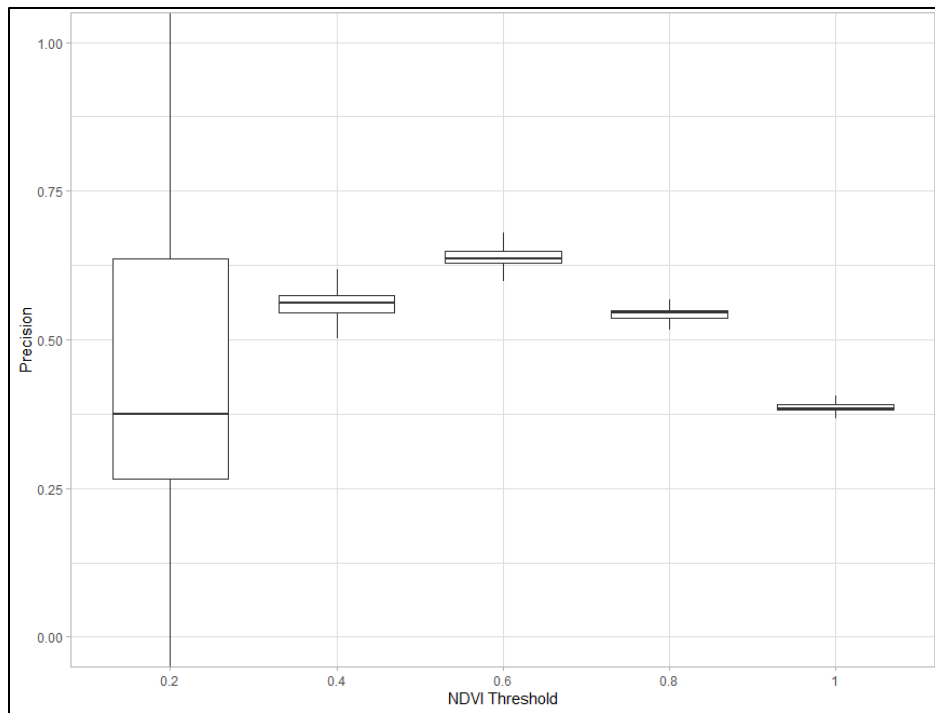


Figure 3. Box and whisker plot comparing precision to the NDVI value used to mask training data. Center horizontal line shows median, and whiskers represent 1.5 times the interquartile range. Precision value was chosen by classifying tailings at Montague 25 times at each NDVI threshold. The precision of results was used to determine the most appropriate mask value. Precision rose between an NDVI of 0.2-0.6, then began to decline.

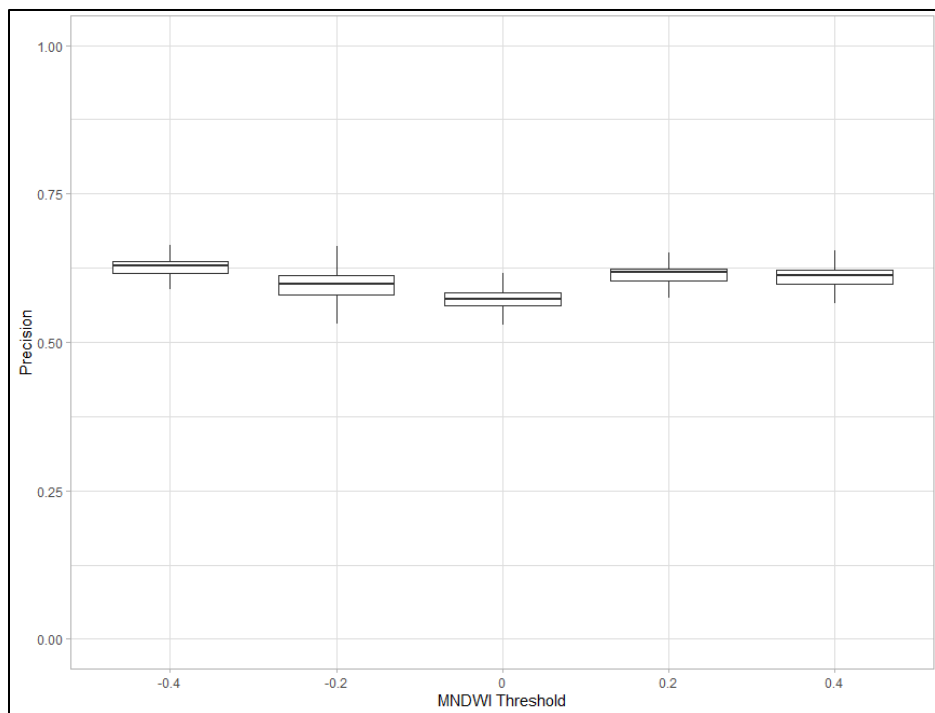


Figure 4. Box and whisker plot comparing modified normalized difference water index (MNDWI) value and precision. Center horizontal line shows median, and whiskers represent 1.5 times the interquartile range. The water mask was generated by testing values of the MNDWI. Precision was measured at each threshold value. There was little variation in precision between the MNDWI values.



Figure 5a. Locations of tailings samples at the Montague historic gold mine district over a satellite image of the site. Sample ID is shown, and colour represents the surface (top 1 cm) As concentrations (ppm dry weight). Basemap image credit: Maxar.



Figure 5b. Locations of tailings samples at the Waverley (Muddy Pond) historic gold mine district over a satellite image of the site. Sample ID is shown, and colour represents the surface (top 1 cm) As concentrations (ppm dry weight). Basemap image credit: Maxar.



Figure 5c. Locations of tailings samples at the Oldham historic gold mine district over a satellite image of the site. Sample ID is shown, and colour represents the surface (top 1 cm) As concentrations (ppm dry weight). Basemap image credit: Maxar.



Figure 6. Region map showing the location of Montague, Oldham, and Waverley gold districts. Key map shows Nova Scotia with point representing study area.

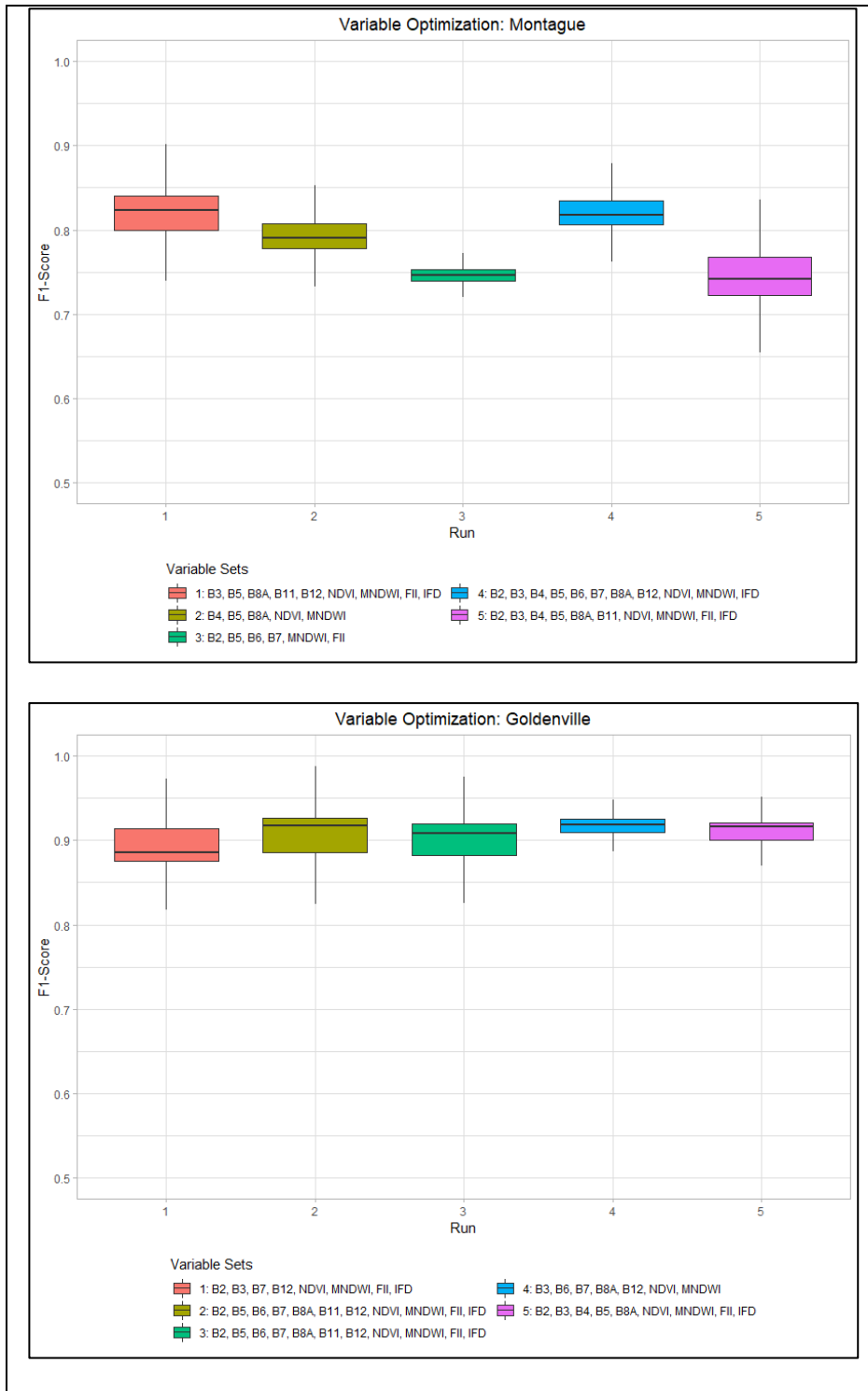


Figure 7. Box and whisker plot comparing accuracy, as measured by F1-Score, to multiple variable sets at Montague (top) and Goldenville (bottom). Center horizontal line shows median, and whiskers represent 1.5 times the interquartile range. The variable optimization process started with all Sentinel-2 bands, as well as 4 indices: NDVI, MNDWI, IFD, and FII. Variable importance was determined using the random forest classifier, measured by OOB error. A variable was kept if removing it increased out-of-bag error until each variable was tested, providing the final set. Five unique variable sets were generated for

Montague, and each was tested 25 times. The set with the highest overall F1-Score between this and the Montague tests (Goldenville set #4) was chosen as the “optimized” variable set for future analysis.

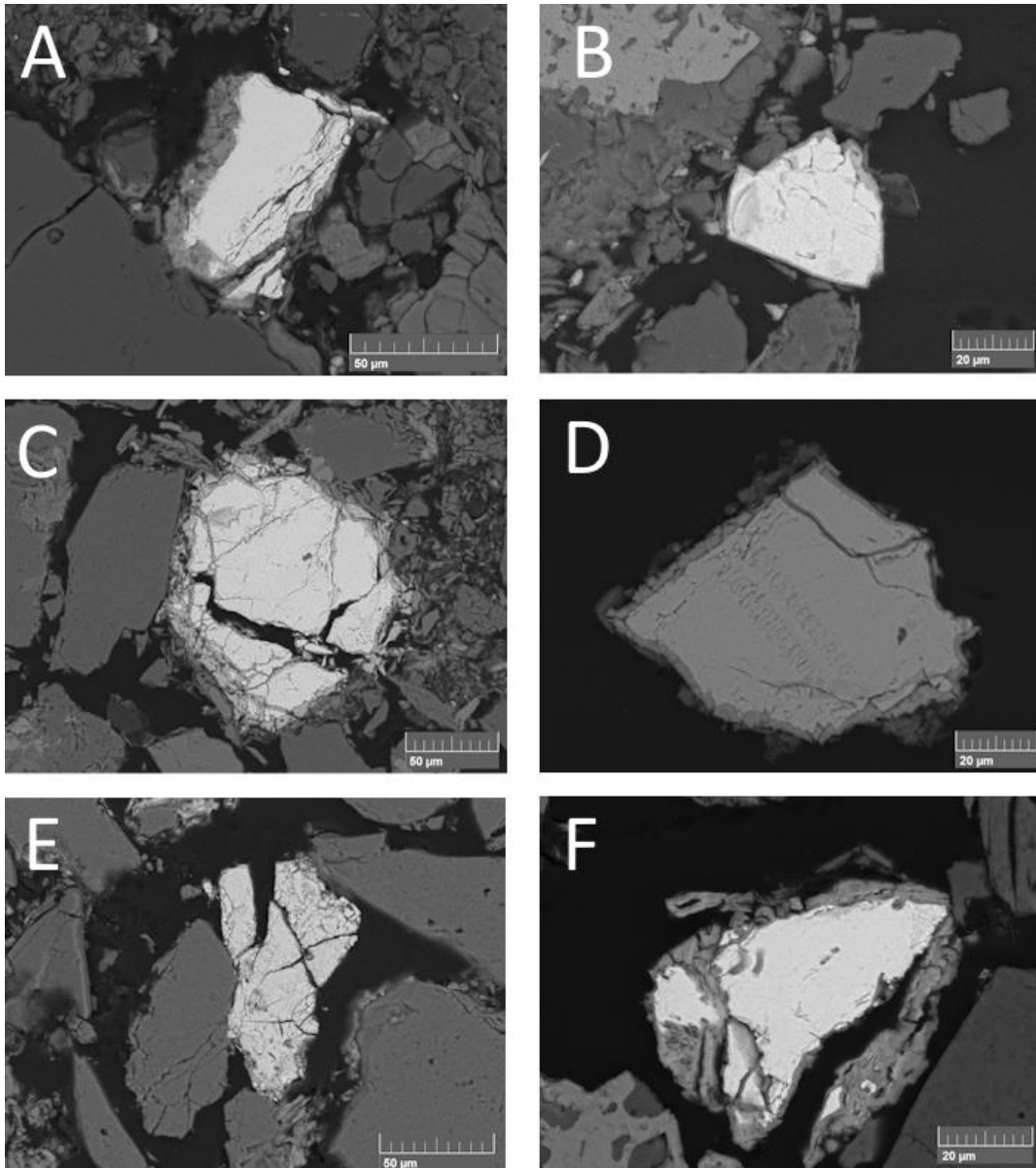


Figure 8. SEM images of arsenopyrite grains found in tailings samples. Images are from backscatter SEM, except for D, which is a secondary electron image to emphasize texture. Arsenopyrite grains have iron oxide, iron oxyhydroxide, or iron arsenate forming in cracks and along outer edges. These images correspond with the sampling locations in Figures 4a-c: A) MO_SM00, B) MO_SM03, C) OH_SM06, D) OH_SM06, E) WV_SM00, F) WV_SM01. Analyzed using TESCAN Mira3 LMU SEM, equipped with an Oxford Instruments INCA X-max 80 mm² Energy Dispersive Spectroscopy (EDS) system.

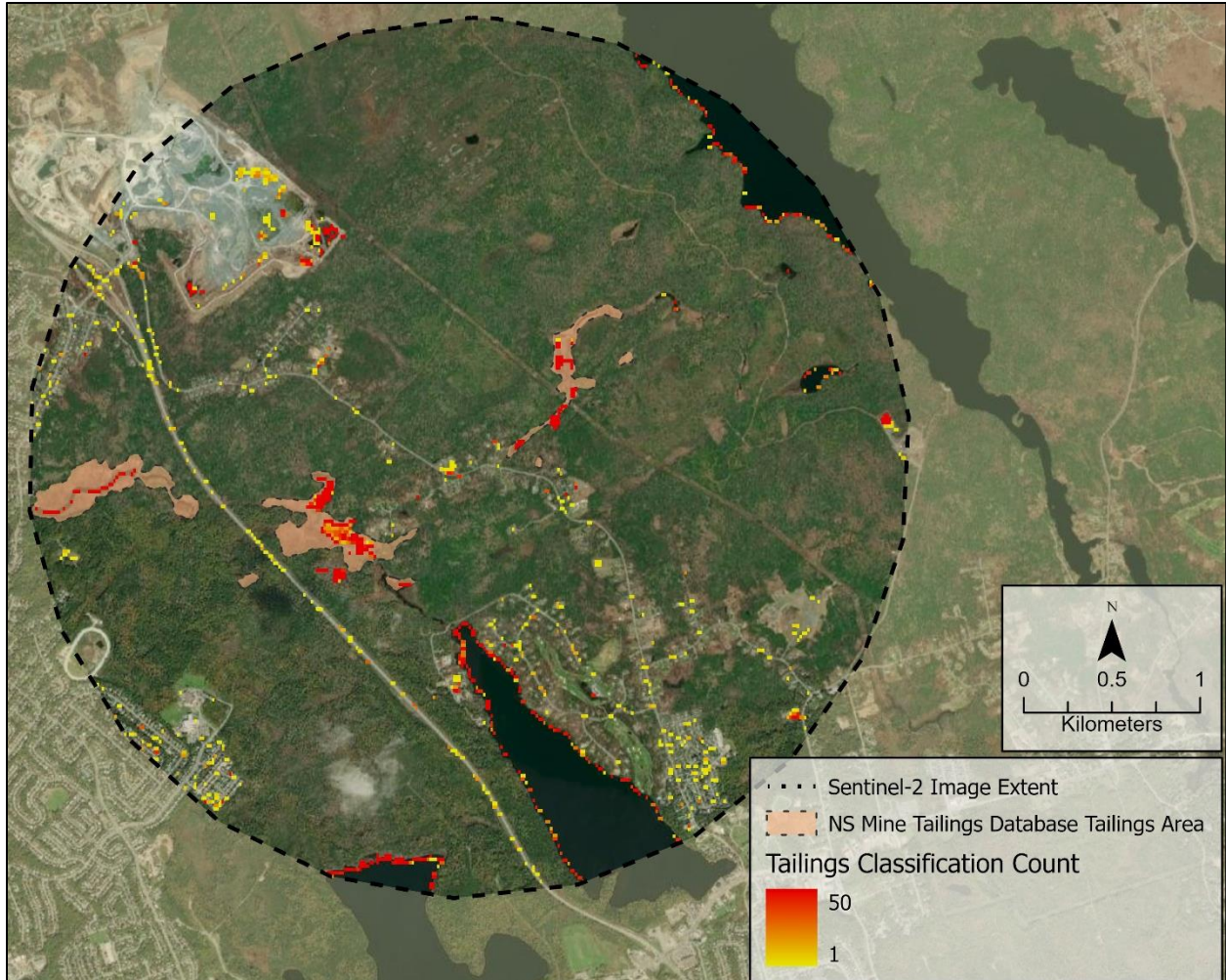


Figure 9a. Map showing areas classified as tailings by the model overlain on a satellite image. The Montague Gold District was classified 50 times and compared to ground-truth data from the NSMTD. Figure shows how many times each pixel was labelled as tailings. Background image (i.e., satellite basemap) indicates the pixel was never labelled as tailings. Satellite image credit: Maxar.

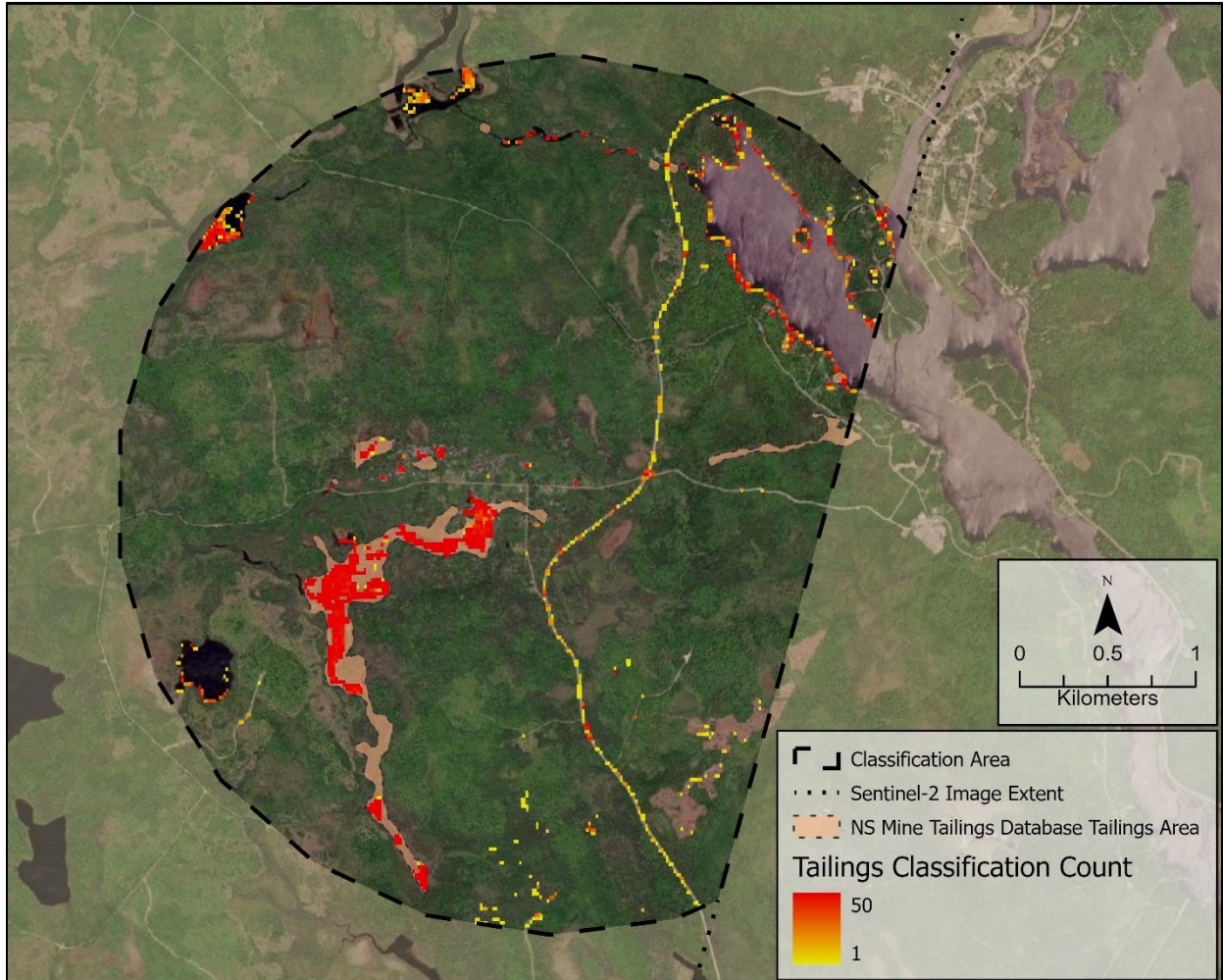


Figure 9b. Map showing areas classified as tailings by the model overlain on a satellite image. The Goldenville Gold Mine District was classified 50 times and compared to ground-truth data from the NSMTD. Figure shows how many times each pixel was labelled as tailings. Background image (i.e., satellite basemap) indicates the pixel was never labelled as tailings. Satellite image credit: Maxar.

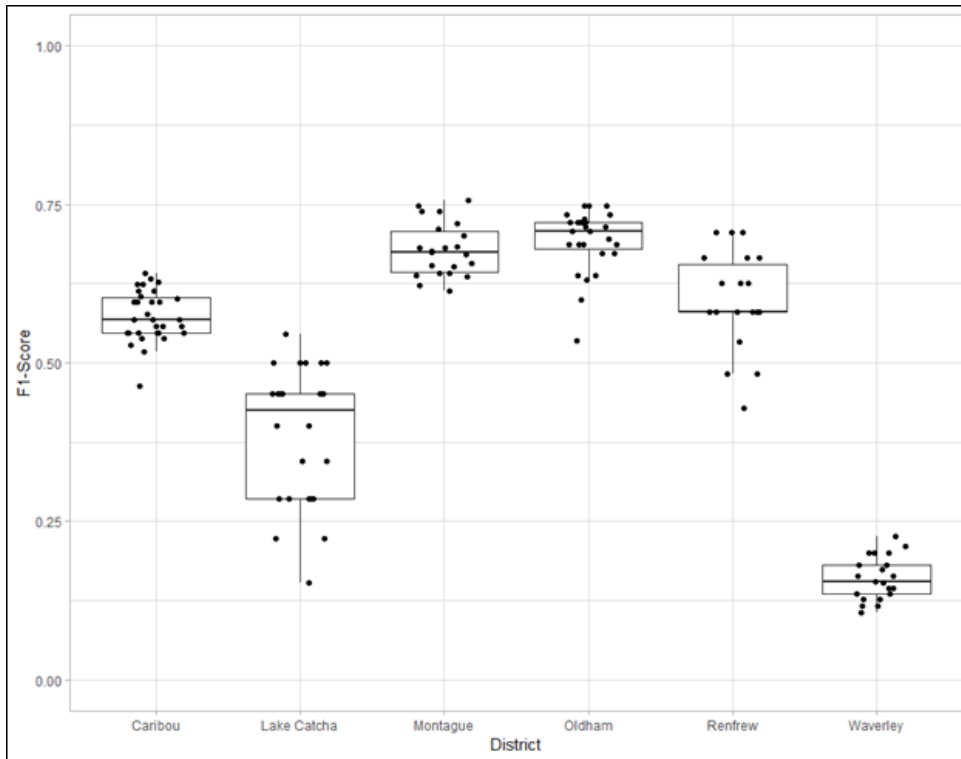


Figure 10a. Box and whisker plot displaying F1-Score of classification at multiple mine districts within the Sentinel-2 image intersecting Montague. Points are jittered along the x-axis to help show distribution.

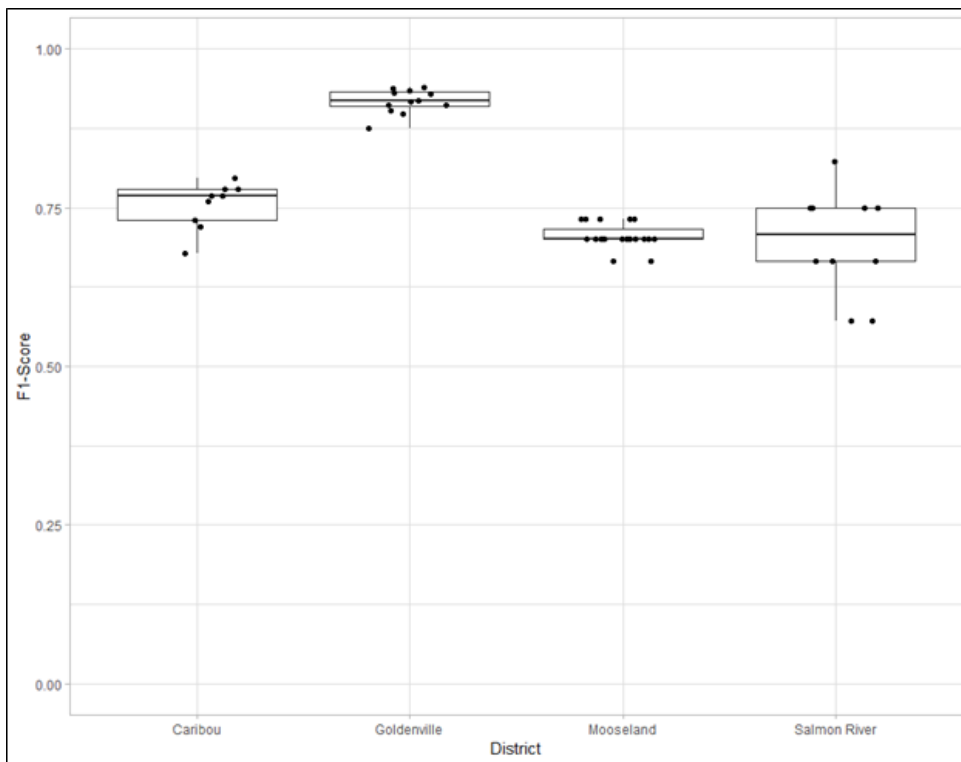


Figure 10b. Box and whisker plot displaying F1-Score of classification at multiple sites within the Sentinel-2 image intersecting Goldenville. Points are jittered along the x-axis to help show distribution.

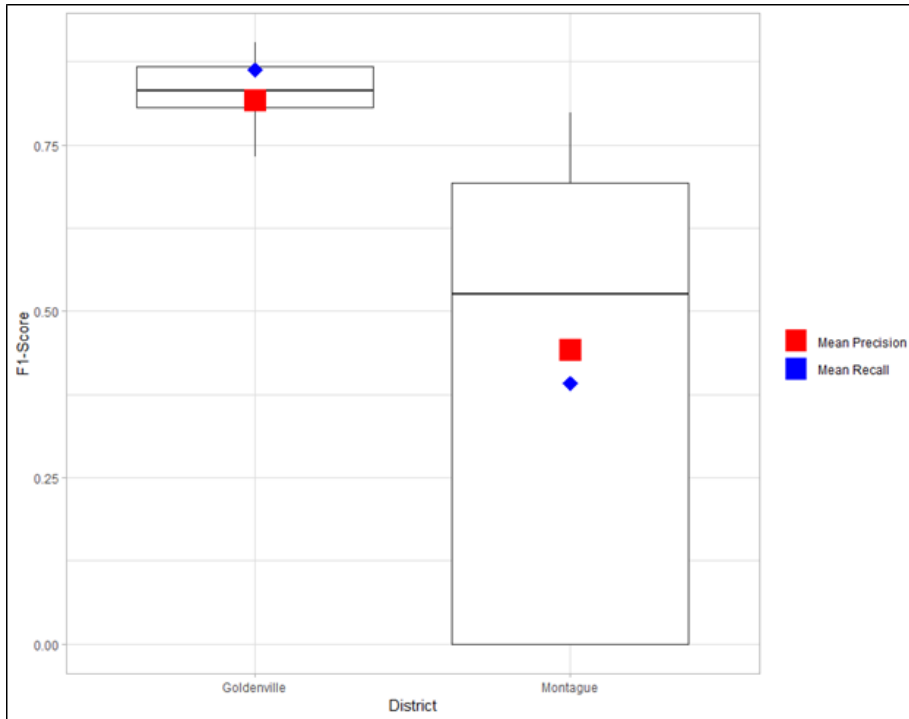


Figure 11. Box and whisker plot displaying the distribution of F1-Score for pure random seeds experiment. Points were scattered randomly throughout the target district, and the SNIC algorithm was used to grow objects from them. This method did not outperform the pixel-wise classification. This is especially evident at Montague, where in many cases no pixels were labelled as tailings.

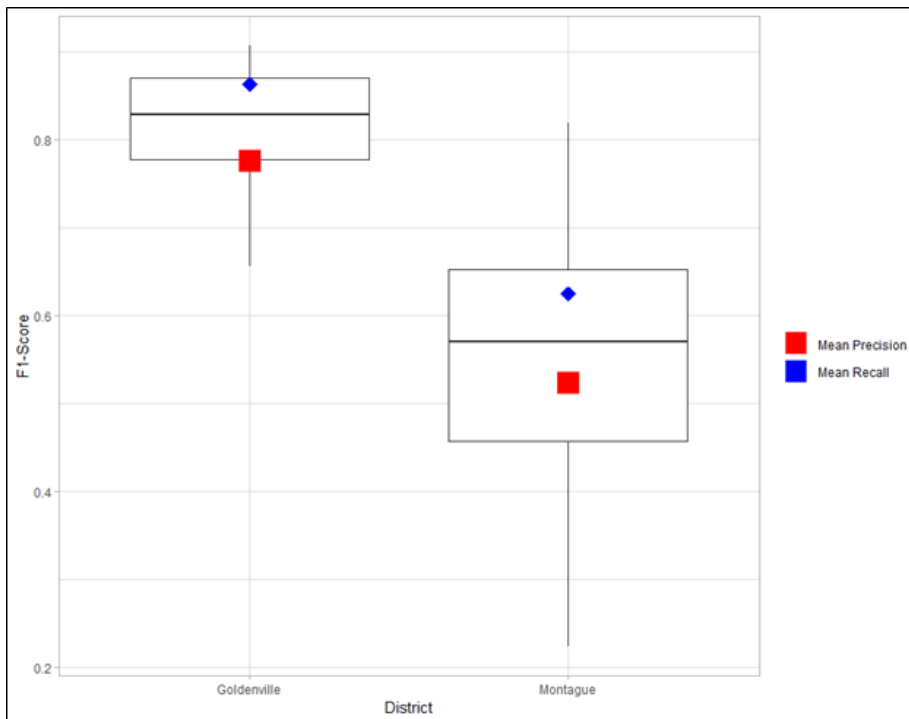


Figure 12. Box and whisker plot displaying F1-Score for “classified pixels as seeds” experiment. A stratified sample method was used in the target districts to create tailings and non-tailings seeds. The tailings seeds were placed in pixels labelled as tailings in the pixel-wise classification step. Though

improved from the pure random seeds test, results were only about as good or slightly lower than the pixel-wise classification.

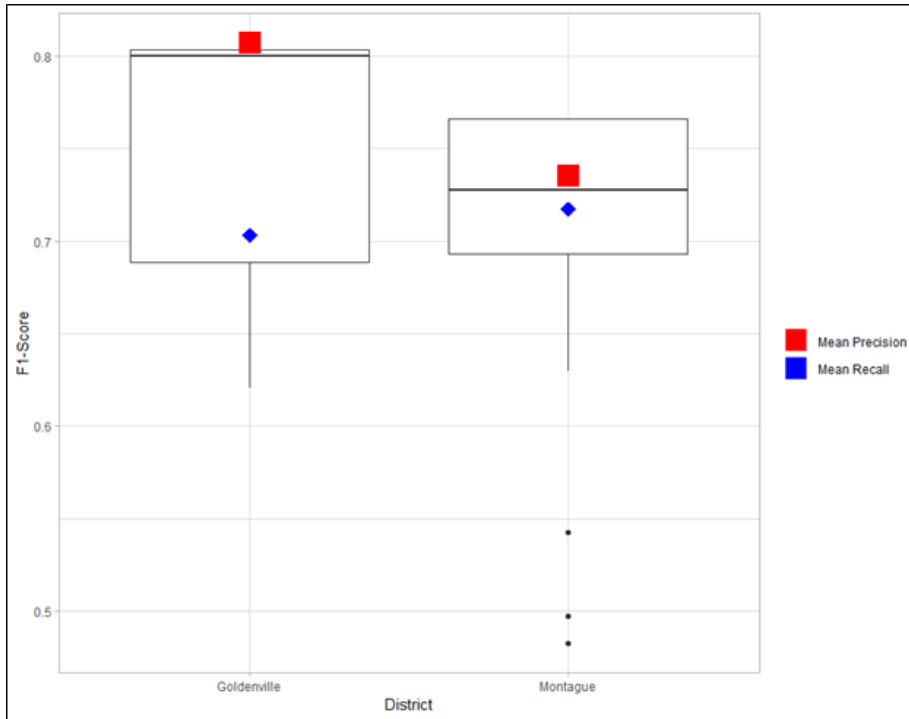


Figure 13. Box and whisker plot displaying F1-Score of “user-generated seeds” experiment. Physical sample locations were used to generate seed points for the SNIC algorithm. Four points were used each at Montague and Goldenville. These points coincide with sediment samples which have been analyzed and confirmed to consist of tailings. Results were much better than the two previous object-based experiments and had fewer false positives than the pixel-wise classification, as shown in the precision metric (Equation 4), which is especially high in this experiment.

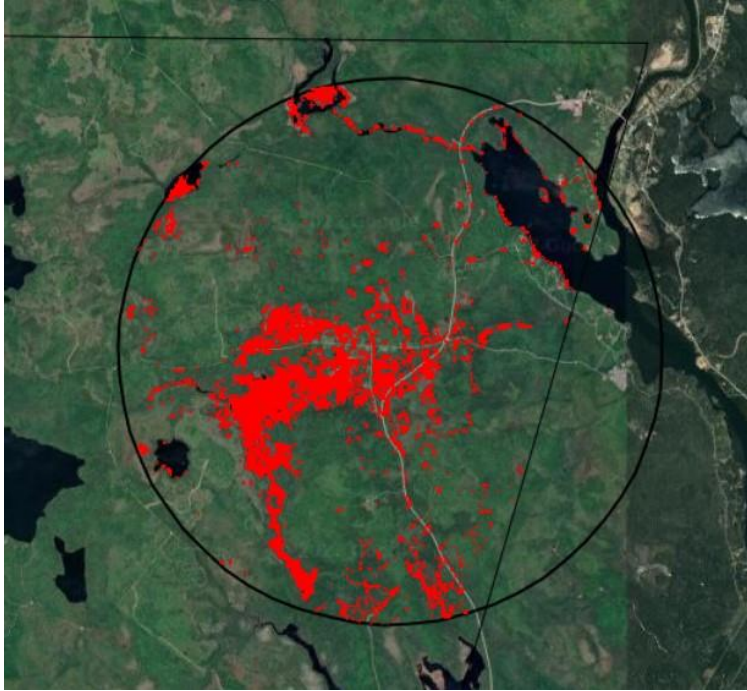


Figure 14. An image showing pixels classified as tailings overlain on a satellite of Goldenville. This is an example of running the pixel-wise classification without filtering out training data (Nova Scotia Mine Tailings Database layer) for vegetation at Goldenville. Pixels that are labelled as tailings in the training data, but which are obscured by vegetation in the Sentinel-2 image introduce vegetated pixels to the training set. The result is a weaker boundary between tailings and non-tailings, especially when tailings are surrounded by vegetation. Red pixels are 20m by 20m, and north is at the top of the image.

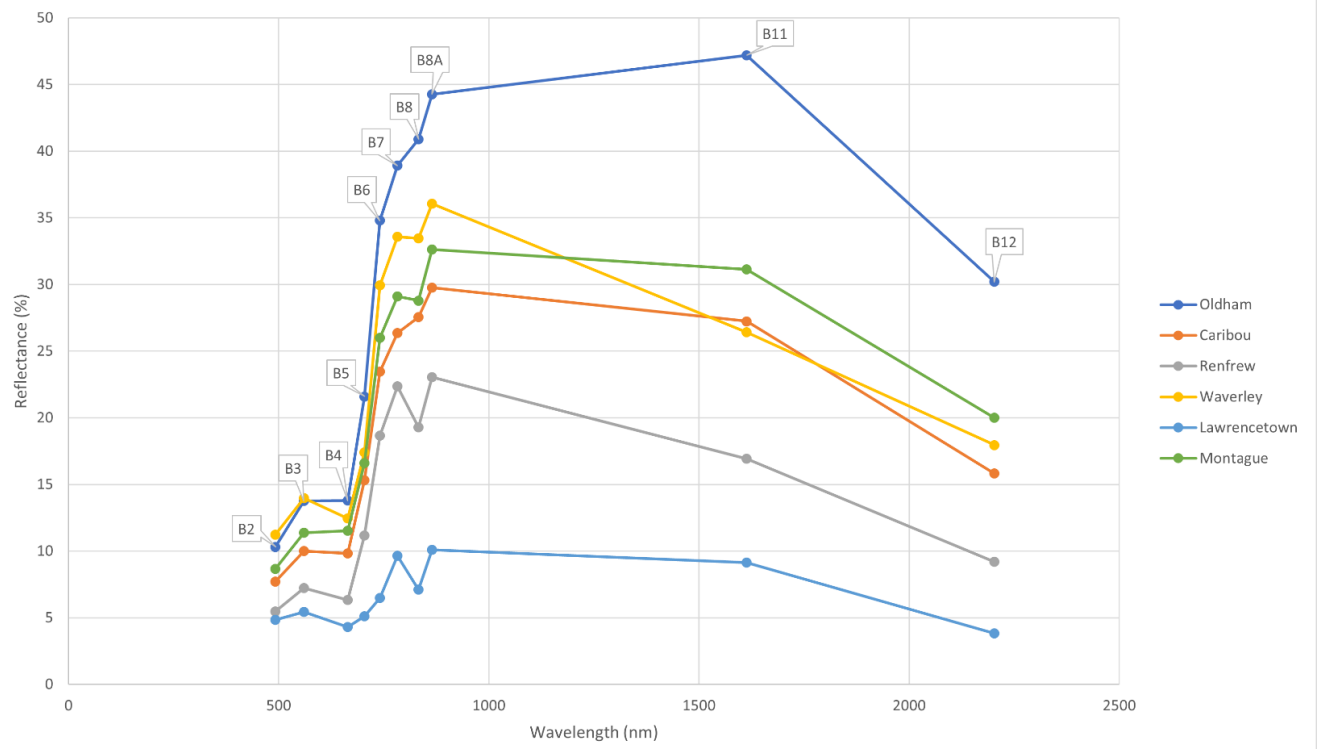
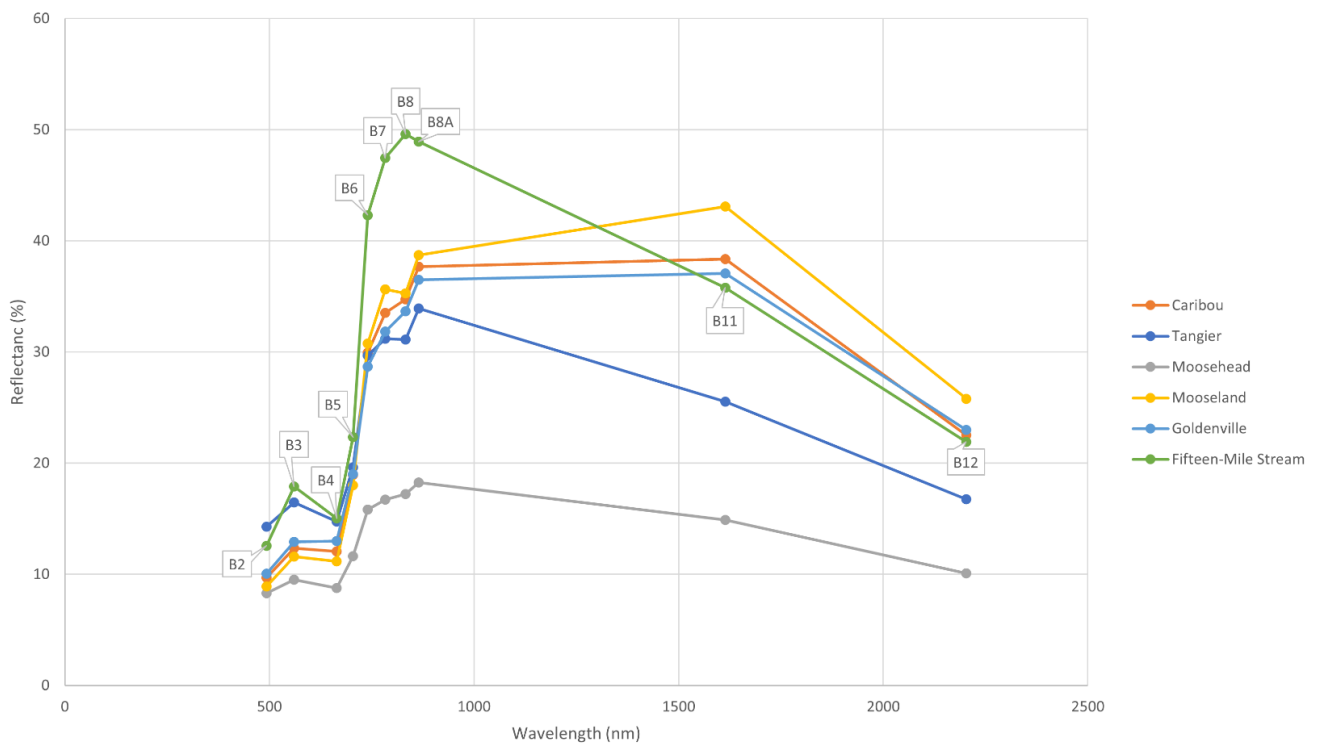


Figure 15. Line chart showing mean reflectance of tailings at districts in Sentinel-2 image intersecting Goldenville (top), and Montague (bottom). Points represent Sentinel-2 band centers. Lines between points are linearly interpolated, and may not represent real reflectance in that spectral region. One spectrum is labelled with band names in each plot, though all spectra share the same band names.

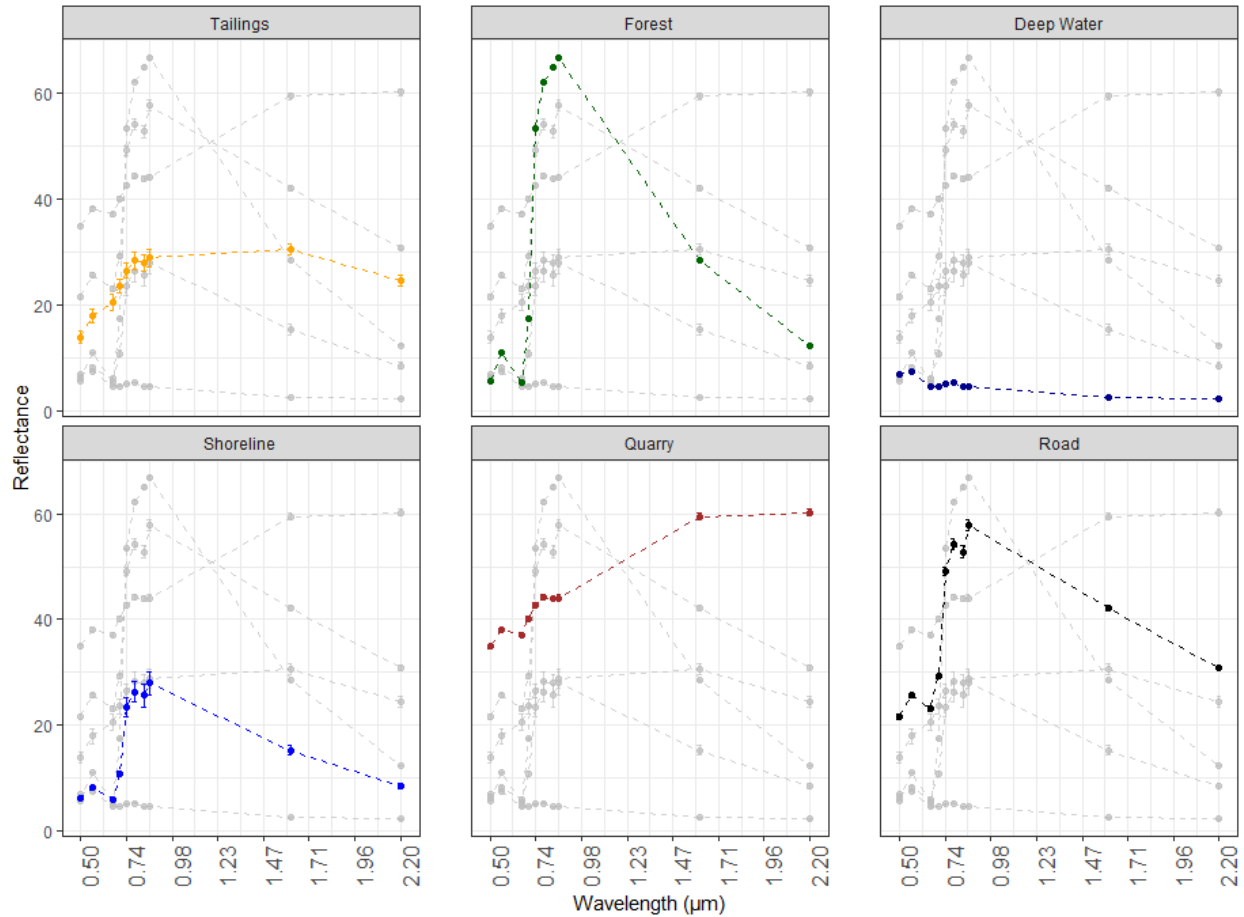


Figure 16. Faceted biplot of measured reflectance by wavelength at six land cover types. Points in plot denote Sentinel-2 band centers, while lines are a prediction of reflectance between bands based on linear interpolation. Land cover types were manually delineated and reflectance was measured via Sentinel-2 image. The tailings class was created at Montague.

2.7. Tables

Table 1. Sentinel-2 10 and 20 m bands, with bandwidth and band center. All bands were resampled to 20 m for analysis. Values are shown for Sentinel-2A – Sentinel-2B has very similar band values.

Band Name	Bandwidth (nm)	Band Center (nm)	Spatial Resolution (m)
B2 – Blue	66	492.4	10

B3 – Green	36	559.8	10
B4 – Red	31	664.6	10
B5 – Vegetation red edge	15	704.1	20
B6 – Vegetation red edge	15	740.5	20
B7 – Vegetation red edge	20	782.8	20
B8 – NIR	106	832.8	10
B8A – Narrow NIR	21	864.7	20
B11 – SWIR	91	1613.7	20
B12 - SWIR	175	2202.4	20

Table 2. Example of stratified samples used to collect non-tailings training points. These land cover classes are obtained from the Sentinel-2 Scene Classification Layer. Class integer corresponds to the default values of the Scene Classification Layer available with Sentinel-2 Level-2A images. Sample count is the number of points in each class.

Class	Sample Count
2 – Dark Area Pixels	80
3 – Cloud Shadows	26
4 – Vegetation	4893
5 – Bare Soils	97
6 – Water	2496
7 – Clouds Low Probability/Unclassified	52
8 – Clouds Medium Probability	26
9 – Clouds High Probability	26
Sum	7696

Table 3. Statistical summary of arsenic across all 32 sample points at three tailings sites

Site	Min Arsenic (ppm)	Max Arsenic (ppm)	Mean Arsenic (ppm)	Median Arsenic (ppm)
Waverley	902.9	6142.6	3142.475	2513.35
Oldham	160.7	2362.2	817.3083	680.6
Montague	2085	16300	7780.333	6122.55

2.8. References

Achanta, R., Ssstrunk, S., 2017. Superpixels and Polygons Using Simple Non-iterative Clustering, in: 2017 IEEE Conference on Computer Vision and Pattern Recognition (CVPR). pp. 4895–4904.

<https://doi.org/10.1109/CVPR.2017.520>

Azizur Rahman, M., Hasegawa, H., 2012. Arsenic in freshwater systems: Influence of eutrophication on occurrence, distribution, speciation, and bioaccumulation. *Appl. Geochem.* 27, 304–314.

<https://doi.org/10.1016/j.apgeochem.2011.09.020>

Bates, J.L.E., 1987. Gold in Nova Scotia, Canadian Cataloguing in Publication Data. Nova Scotia Dept. of Mines and Energy, Halifax.

Branco, P., Torgo, L., Ribeiro, R., 2015. A Survey of Predictive Modelling under Imbalanced Distributions. ArXiv150501658 Cs.

Breiman, L., 2001. Random Forests. *Mach. Learn.* 45, 5–32. <https://doi.org/10.1023/A:1010933404324>

CCME, 1997. Canadian Soil Quality Guidelines for the Protection of Environmental and Human Health - Arsenic (Inorganic). *Can. Environ. Qual. Guidel.* 7.

Clark, A.J., Labaj, A.L., Smol, J.P., Campbell, L.M., Kurek, J., 2021. Arsenic and mercury contamination and complex aquatic bioindicator responses to historical gold mining and modern watershed stressors in

urban Nova Scotia, Canada. *Sci. Total Environ.* 787, 147374.

<https://doi.org/10.1016/j.scitotenv.2021.147374>

Clark, R.N., Lucey, P.G., 1984. Spectral properties of ice-particulate mixtures and implications for remote sensing: 1. Intimate mixtures. *J. Geophys. Res. Solid Earth* 89, 6341–6348.

<https://doi.org/10.1029/JB089iB07p06341>

Clark, R.N., Roush, T.L., 1984. Reflectance spectroscopy: Quantitative analysis techniques for remote sensing applications. *J. Geophys. Res. Solid Earth* 89, 6329–6340.

<https://doi.org/10.1029/JB089iB07p06329>

Clark, R.N., Swayze, G.A., Livo, K.E., Kokaly, R.F., Sutley, S.J., Dalton, J.B., McDougal, R.R., Gent, C.A., 2003. Imaging spectroscopy: Earth and planetary remote sensing with the USGS Tetracorder and expert systems. *J. Geophys. Res. - Planets* 108, 5131-n/a. <https://doi.org/10.1029/2002JE001847>

Cleaver, A.E., Jamieson, H.E., Rickwood, C.J., Huntsman, P., 2021. Tailings dust characterization and impacts on surface water chemistry at an abandoned Zn-Pb-Cu-Au-Ag deposit. *Appl. Geochem.* 128, 104927. <https://doi.org/10.1016/j.apgeochem.2021.104927>

Corriveau, M.C., Jamieson, H.E., Parsons, M.B., Hall, G.E.M., 2011. Mineralogical characterization of arsenic in gold mine tailings from three sites in Nova Scotia. *Geochem. Explor. Environ. Anal.* 11, 179–192. <https://doi.org/10.1144/1467-7873/09-246>

DeSisto, S.L., Jamieson, H.E., Parsons, M.B., 2017. Arsenic mobility in weathered gold mine tailings under a low-organic soil cover. *Environ. Earth Sci.* 76, 773. <https://doi.org/10.1007/s12665-017-7041-7>

DeSisto, S.L., Jamieson, H.E., Parsons, M.B., 2016. Subsurface variations in arsenic mineralogy and geochemistry following long-term weathering of gold mine tailings. *Appl. Geochem.* 73, 81–97.

<https://doi.org/10.1016/j.apgeochem.2016.07.013>

DeSisto, S.L., Jamieson, H.E., Parsons, M.B., 2011. Influence of hardpan layers on arsenic mobility in historical gold mine tailings. *Appl. Geochem.* 26, 2004–2018.

<https://doi.org/10.1016/j.apgeochem.2011.06.030>

Díaz-Uriarte, R., Alvarez de Andrés, S., 2006. Gene selection and classification of microarray data using random forest. *BMC Bioinformatics* 7, 3. <https://doi.org/10.1186/1471-2105-7-3>

Drage, J., 2015. Review of the Environmental Impacts of Historical Gold Mine Tailings in Nova Scotia. Open File Rep. ME 2015-004 15.

Du, Y., Zhang, Y., Ling, F., Wang, Q., Li, W., Li, X., 2016. Water Bodies' Mapping from Sentinel-2 Imagery with Modified Normalized Difference Water Index at 10-m Spatial Resolution Produced by Sharpening the SWIR Band. *Remote Sens.* 8, 354. <https://doi.org/10.3390/rs8040354>

European Space Agency, 2015. Sentinel-2 User Handbook 64.

Faribault, E.R., 1900. The gold measures of Nova Scotia and deep mining / by E.R. Faribault. Together with other papers bearing upon Nova Scotia gold mines. Mining Society of Nova Scotia, Halifax, N.S.

Genuer, R., Poggi, J.-M., Tuleau-Malot, C., 2010. Variable selection using random forests. *Pattern Recognit. Lett.* 31, 2225–2236. <https://doi.org/10.1016/j.patrec.2010.03.014>

Goetz, A.F.H., Curtiss, B., Shiley, D.A., 2009. Rapid gangue mineral concentration measurement over conveyors by NIR reflectance spectroscopy. *Miner. Eng.* 22, 490–499.

<https://doi.org/10.1016/j.mineng.2008.12.013>

Gorelick, N., Hancher, M., Dixon, M., Ilyushchenko, S., Thau, D., Moore, R., 2017. Google Earth Engine: Planetary-scale geospatial analysis for everyone. *Remote Sens. Environ.* 202, 18–27.

<https://doi.org/10.1016/j.rse.2017.06.031>

Gregorutti, B., Michel, B., Saint-Pierre, P., 2017. Correlation and variable importance in random forests. *Stat. Comput.* 27, 659–678. <https://doi.org/10.1007/s11222-016-9646-1>

Groves, D.I., Goldfarb, R.J., Gebre-Mariam, M., Hagemann, S.G., Robert, F., 1998. Orogenic gold deposits: A proposed classification in the context of their crustal distribution and relationship to other gold deposit types. *Ore Geol. Rev.* 13, 7–27. [https://doi.org/10.1016/S0169-1368\(97\)00012-7](https://doi.org/10.1016/S0169-1368(97)00012-7)

Guha, A., 2020. Mineral exploration using hyperspectral data, in: Pandey, P.C., Srivastava, P.K., Balzter, H., Bhattacharya, B., Petropoulos, G.P. (Eds.), *Hyperspectral Remote Sensing, Earth Observation*. Elsevier, pp. 293–318. <https://doi.org/10.1016/B978-0-08-102894-0.00012-7>

Hartlen, J., 1988. *Gold! The Wealth of Waverley*. Lancelot Press, Hantsport, Nova Scotia.

Hennick, E.W., Poole, J.C., 2020. Nova Scotia Mine Tailings Database.

Hindmarsh, J., McLetchle, O.R., Heffernan, L., Hayne, O., Ellenberger, H.A., Mccurdy, R., Thiébaux, H.J., 1977. Electromyographic Abnormalities in Chronic Environmental Arsenicalism. <https://doi.org/10.1093/JAT/1.6.270>

Homem Antunes, M.A., Bolpato, I.F., 2018. Atmospheric Correction and Cirrus Clouds Removal from MSI Sentinel 2A Images, in: *IGARSS 2018 - 2018 IEEE International Geoscience and Remote Sensing Symposium*. Presented at the IGARSS 2018 - 2018 IEEE International Geoscience and Remote Sensing Symposium, IEEE, Valencia, pp. 9145–9148. <https://doi.org/10.1109/IGARSS.2018.8518824>

Intrinsik Corp, EcoMetrix, Crippen Berger, K., Wood, 2020. Human Health Risk Assessment of Sediment, Surface Water, and Fish from Barry’s Run, Halifax Regional Municipality.

Intrinsik Corp, EcoMetrix, Crippen Berger, K., Wood, 2019a. Conceptual Closure Plan For The Historic Goldenville Tailings Areas Goldenville, Nova Scotia Final Report (Consulting).

Intrinsic Corp, EcoMetrix, Crippen Berger, K., Wood, 2019b. Conceptual Closure Study For The Historic Montague Mines Tailings Areas. Halifax, Nova Scotia. Final Report (Consulting). NS Lands Inc.

Jamieson, H.E., Walker, S.R., Parsons, M.B., 2015. Mineralogical characterization of mine waste. *Appl. Geochem.*, *Environmental Geochemistry of Modern Mining* 57, 85–105.

<https://doi.org/10.1016/j.apgeochem.2014.12.014>

Jewell, D.A., 2021. Tailings Classification NS Repository. <https://doi.org/10.5281/zenodo.8273117>

Joshi, A.V., 2023. Decision Trees, in: Joshi, A.V. (Ed.), *Machine Learning and Artificial Intelligence*. Springer International Publishing, Cham, pp. 73–87. https://doi.org/10.1007/978-3-031-12282-8_7

Kamal, M., Phinn, S., 2011. Hyperspectral Data for Mangrove Species Mapping: A Comparison of Pixel-Based and Object-Based Approach. *Remote Sens.* 3, 2222–2242. <https://doi.org/10.3390/rs3102222>

Koch, I., McPherson, K., Smith, P., Easton, L., Doe, K.G., Reimer, K.J., 2007. Arsenic bioaccessibility and speciation in clams and seaweed from a contaminated marine environment. *Mar. Pollut. Bull.* 54, 586–594. <https://doi.org/10.1016/j.marpolbul.2006.12.004>

Kokaly, R.F., Clark, R.N., Swayze, G.A., Livo, K.E., Hoefen, T.M., Pearson, N.C., Wise, R.A., Benzel, W.M., Lowers, H.A., Driscoll, R.L., Klein, A.J., 2017. USGS Spectral Library Version 7: U.S. Geological Survey Data Series 1035. *US Geol. Surv. Data Ser., Data Series 1035*, 61. <https://doi.org/10.3133/ds1035>

Kontak, D.J., Jackson, S.J., 1999. Documentation of variable trace- and rare-earth-element abundances in carbonates from auriferous quartz veins in Meguma lode gold deposits, Nova Scotia. *Can. Mineral.* 37, 469–488.

Lane, P.A., Pett, Robert J., Crowell, M. J., MacKinnon, D. S., Graves, Milton C., 1989. Further studies on the distribution and fate of arsenic and mercury at a site contaminated by abandoned gold mine tailings. *CANMET Spec. Publ.* 89–9, 77–107.

LeBlanc, M.E., Parsons, M.B., Chapman, E.E.V., Campbell, L.M., 2020. Review of ecological mercury and arsenic bioaccumulation within historical gold mining districts of Nova Scotia. *Environ. Rev.* 28, 187–198.

<https://doi.org/10.1139/er-2019-0042>

Lekner, J., Dorf, M., 1988. Why some things are darker when wet. *Appl. Opt.* 27, 1278–80.

<https://doi.org/10.1364/AO.27.001278>

Li, H., 2014. Smile.

Little, M.E., Parsons, M.B., Law, B.A., Milligan, T.G., Smith, J.N., 2015. Impact of historical gold mining activities on marine sediments in Wine Harbour, Nova Scotia, Canada. *Atl. Geol.* 51, 344.

<https://doi.org/10.4138/atlgeol.2015.016>

Lyons, M.B., Keith, D.A., Phinn, S.R., Mason, T.J., Elith, J., 2018. A comparison of resampling methods for remote sensing classification and accuracy assessment. *Remote Sens. Environ.* 208, 145–153.

<https://doi.org/10.1016/j.rse.2018.02.026>

Mielke, C., Muedi, T., Papenfuss, A., Boesche, N.K., Rogass, C., Gauert, C.D.K., Altenberger, U., de Wit, M.J., 2016. Multi- and hyperspectral spaceborne remote sensing of the Aggeneys base metal sulphide mineral deposit sites in the Lower Orange River region, South Africa. *South Afr. J. Geol.* 119, 63–76.

<https://doi.org/10.2113/gssajg.119.1.63>

Montero, I.C., Brimhall, G.H., Alpers, C.N., Swayze, G.A., 2005. Characterization of waste rock associated with acid drainage at the Penn Mine, California, by ground-based visible to short-wave infrared reflectance spectroscopy assisted by digital mapping. *Chem. Geol., Geochemistry of Sulfate Minerals: A*

tribute to Robert O. Rye 215, 453–472. <https://doi.org/10.1016/j.chemgeo.2004.06.045>

Mountrakis, G., Im, J., Ogole, C., 2011. Support vector machines in remote sensing: A review. *ISPRS J.*

Photogramm. Remote Sens. 66, 247–259. <https://doi.org/10.1016/j.isprsjprs.2010.11.001>

Mudroch, A., Clair, T.A., 1986. Transport of arsenic and mercury from gold mining activities through an aquatic system. *Sci. Total Environ.* 57, 205–216. [https://doi.org/10.1016/0048-9697\(86\)90024-0](https://doi.org/10.1016/0048-9697(86)90024-0)

Ngole-Jeme, V.M., Fantke, P., 2017. Ecological and human health risks associated with abandoned gold mine tailings contaminated soil. *PLOS ONE* 12, e0172517.
<https://doi.org/10.1371/journal.pone.0172517>

Nolet, C., Poortinga, A., Roosjen, P., Bartholomeus, H., Ruessink, G., 2014. Measuring and Modeling the Effect of Surface Moisture on the Spectral Reflectance of Coastal Beach Sand. *PLoS ONE* 9, e112151.
<https://doi.org/10.1371/journal.pone.0112151>

Olofsson, P., Foody, G.M., Herold, M., Stehman, S.V., Woodcock, C.E., Wulder, M.A., 2014. Good practices for estimating area and assessing accuracy of land change. *Remote Sens. Environ.* 148, 42–57.
<https://doi.org/10.1016/j.rse.2014.02.015>

Otsu, N., 1979. A Threshold Selection Method from Gray-Level Histograms. *IEEE Trans. Syst. Man Cybern.* 9, 62–66. <https://doi.org/10.1109/TSMC.1979.4310076>

Parsons, M.B., LeBlanc, K.W.G., Hall, G.E.M., Sangster, A.L., Vaive, J.E., Pelchat, P., 2012. Environmental geochemistry of tailings, sediments and surface waters collected from 14 historical gold mining districts in Nova Scotia (No. 7150). <https://doi.org/10.4095/291923>

Parsons, M.B., Little, M.E., 2015. Establishing geochemical baselines in forest soils for environmental risk assessment in the Montague and Goldenville gold districts, Nova Scotia, Canada. *Atl. Geol.* 51, 364.
<https://doi.org/10.4138/atlgeol.2015.017>

Percival, J.B., White, H.P., Goodwin, T.A., Parsons, M.B., Smith, P.K., 2013. Mineralogy and spectral reflectance of soils and tailings from historical gold mines, Nova Scotia. *Geochem. Explor. Environ. Anal.* Vol. 14, 3–16. <http://dx.doi.org/10.1144/geochem2011-071>

Riaza, A., Müller, A., 2010. Hyperspectral remote sensing monitoring of pyrite mine wastes: a record of climate variability (Pyrite Belt, Spain). *Environ. Earth Sci.* 61, 575–594. <https://doi.org/10.1007/s12665-009-0368-y>

Richards, J.A., 2013. *Remote Sensing Digital Image Analysis*. Springer Berlin Heidelberg, Berlin, Heidelberg. <https://doi.org/10.1007/978-3-642-30062-2>

Roussel, C., Néel, C., Bril, H., 2000. Minerals controlling arsenic and lead solubility in an abandoned gold mine tailings. *Sci. Total Environ.* 263, 209–219. [https://doi.org/10.1016/S0048-9697\(00\)00707-5](https://doi.org/10.1016/S0048-9697(00)00707-5)

Sangster, A.L., Smith, P.K., Goodfellow, W.D., 2007. *Metallogenic Summary of the Meguma Gold Deposits, Nova Scotia (Special Publication No. 5), Mineral Deposits of Canada: A Synthesis of Major Deposit-Types, District Metallogeny, the Evolution of Geological Provinces, and Exploration Methods*. Geological Association of Canada, Nova Scotia.

Sasaki, Y., 2007. The truth of the F-measure. *Conf. Pap.*

Schowengerdt, R.A., 2007. *Remote Sensing : Models and Methods for Image Processing*, 3rd ed. Academic Press, Burlington, MA.

Seal, R.R., Hammarstrom, J.M., 2003. *Geoenvironmental Models of Mineral Deposits: Examples from Massive Sulfide and Gold Deposits*, in: *Environmental Aspects of Mine Waste, Short Course Series*. Mineralogical Association of Canada, pp. 11–50.

Smeds, J., Mats & Ouml, quist, Nilsson, M.B., Bishop, K., 2022. A Simplified Drying Procedure for Analysing Hg Concentrations. *Water Air Amp Soil Pollut.* 233, NA-NA. <https://doi.org/10.1007/s11270-022-05678-7>

Stehman, S.V., 2009. Sampling designs for accuracy assessment of land cover. *Int. J. Remote Sens.* 30, 5243–5272. <https://doi.org/10.1080/01431160903131000>

- Stehman, S.V., Foody, G.M., 2019. Key issues in rigorous accuracy assessment of land cover products. *Remote Sens. Environ.* 231, 111199. <https://doi.org/10.1016/j.rse.2019.05.018>
- Svetnik, V., Liaw, A., Tong, C., Wang, T., 2004. Application of Breiman's Random Forest to Modeling Structure-Activity Relationships of Pharmaceutical Molecules, in: Roli, F., Kittler, J., Windeatt, T. (Eds.), *Multiple Classifier Systems, Lecture Notes in Computer Science*. Springer Berlin Heidelberg, Berlin, Heidelberg, pp. 334–343. https://doi.org/10.1007/978-3-540-25966-4_33
- Swayze, G.A., Clark, R.N., Goetz, A.F.H., Livo, K.E., Breit, G.N., Kruse, F.A., Sutley, S.J., Snee, L.W., Lowers, H.A., Post, J.L., Stoffregen, R.E., Ashley, R.P., 2014. Mapping Advanced Argillic Alteration at Cuprite, Nevada, Using Imaging Spectroscopy. *Econ. Geol.* 109, 1179–1221. <https://doi.org/10.2113/econgeo.109.5.1179>
- Swayze, G.A., Smith, K.S., Clark, R.N., Sutley, S.J., Pearson, R.M., Vance, J.S., Hageman, P.L., Briggs, P.H., Meier, A.L., Singleton, M.J., Roth, S., 2000. Using Imaging Spectroscopy To Map Acidic Mine Waste. *Environ. Sci. Technol.* 34, 47–54. <https://doi.org/10.1021/es990046w>
- Tou, J.T., 1974. *Pattern recognition principles, Applied mathematics and computation*, no. 7. Addison-Wesley Pub. Co., Reading, Mass.
- van der Meer, F., 2004. Analysis of spectral absorption features in hyperspectral imagery. *Int. J. Appl. Earth Obs. Geoinformation* 5, 55–68. <https://doi.org/10.1016/j.jag.2003.09.001>
- van der Meer, F.D., van der Werff, H.M.A., van Ruitenbeek, F.J.A., 2014. Potential of ESA's Sentinel-2 for geological applications. *Remote Sens. Environ.* 148, 124–133. <https://doi.org/10.1016/j.rse.2014.03.022>
- Van der Werff, H., Van der Meer, F., 2015. Sentinel-2 for Mapping Iron Absorption Feature Parameters. *Remote Sens.* 7, 12635–12653. <https://doi.org/10.3390/rs71012635>
- Van Rijsbergen, C.J., 1979. *Information retrieval*, 2d ed. ed. Butterworths, London ; Boston.

von der Heyden, B.P., Roychoudhury, A.N., 2015. Application, Chemical Interaction and Fate of Iron Minerals in Polluted Sediment and Soils. *Curr. Pollut. Rep.* 1, 265–279. <https://doi.org/10.1007/s40726-015-0020-2>

Walker, S.R., Parsons, M.B., Jamieson, H.E., Lanzirotti, A., 2009. ARSENIC MINERALOGY OF NEAR-SURFACE TAILINGS AND SOILS: INFLUENCES ON ARSENIC MOBILITY AND BIOACCESSIBILITY IN THE NOVA SCOTIA GOLD MINING DISTRICTS. *Can. Mineral.* 47, 533–556. <https://doi.org/10.3749/canmin.47.3.533>

Weisener, C.G., 2003. Novel Spectroscopic Techniques to Characterize Mine Waste, in: *Environmental Aspects of Mine Waste, Short Course Series*. Mineralogical Association of Canada, pp. 181–202.

Wilkin, R.T., Barnes, H.L., 1997. Formation processes of framboidal pyrite. *Geochim. Cosmochim. Acta* 61, 323–339. [https://doi.org/10.1016/S0016-7037\(96\)00320-1](https://doi.org/10.1016/S0016-7037(96)00320-1)

Willick, F., 2021. Cost estimate for cleanup of abandoned N.S. mines still “a few years” away. CBC.

Chapter 3: Exploring the Causes of False Positives from a Tailings Classifier

Mines operating in the 19th to mid-20th centuries throughout Nova Scotia, Canada have left behind tailings containing arsenic (As) and mercury (Hg). These sites have been identified as an ongoing source of contamination and a threat to human and ecosystem health since the 1970s when the first cases of As intoxication from mine-impacted drinking water were reported (Hindmarsh et al., 1977). Ongoing surveys at additional historic mine sites have revealed that at some sites, tailings have moved downstream from their original locations to be deposited in lakes, riverbanks, and estuaries (Koch et al., 2007; Parsons et al., 2012). Over 300 gold mines have operated in the province, organized into 64 gold mine districts. Before sites can be cleaned up, they must first be assessed to determine whether tailings are present, and where.

Remote sensing methods can provide a preliminary assessment of historic mine sites, quickly analyzing large areas to indicate where tailings may be present. We trained a random forest classifier using historical maps of tailings and multispectral Sentinel-2 images so that indicators of tailings could be mapped across multiple gold mine districts. Pixel-wise classification accuracy was tested by repeating classification and recording the distribution of results (Chapter 1). By separating the results by district, we determined that accuracy among them was inconsistent. The classifier performed poorly at sites with significant areas of standing water and shorelines, even after filtering satellite images to the driest season (July and August). In this study, we compare the spectra, as provided by Sentinel-2, of areas where the classifier provided false positives, as confirmed by lab analysis of sediment. We also present

scanning electron microscope (SEM) analysis and bulk geochemistry of sediment collected from coastal and wetland areas, which are commonly confused by the classifier with tailings, and compare these sediments to tailings.

3.1. Historic Gold Mining and Modern Secondary Minerals

Most of the gold in Nova Scotia has historically been mined in the Goldenville and Halifax formations of the Meguma Supergroup, which is exposed throughout the southern mainland of the province (Figure 1). The high-grade gold deposits that were the main target of historic mining are found in quartz veins in the hinges of east-west trending folds, where gold has been concentrated by hydrothermal activity (Parsons et al., 2012; Sangster et al., 2007). Sulphide minerals also present in these hinges have been the main source of arsenic (As) and acid rock drainage released by mining and processing, and present a threat to human and ecosystem health (Ngole-Jeme and Fantke, 2017; Walker et al., 2009). The most common sulphide mineral found at these mine sites is arsenopyrite (FeAsS), which has been observed to comprise up to 15% of gold-bearing quartz veins (Sangster et al., 2007). Generally, lode gold deposits like those found in Nova Scotia can be expected to contain up to three to five percent sulphide minerals (DeSisto et al., 2016; Groves et al., 1998).

Ore was mainly extracted from underground shafts and was then crushed in stamp mills. In many cases, particularly in the 19th century, mercury (Hg) was used to separate gold from crushed material in a process called mercury amalgamation (Bates, 1987; LeBlanc et al., 2020; Parsons et al., 2012). The leftover waste rock and sand to silt-sized sediment, called tailings, was deposited in streams, wetlands, or nearby depressions with little to no regard for potential environmental impacts (Drage, 2015; LeBlanc et al., 2020). In these tailings areas, sulphide

minerals have been exposed to oxygen and surface water, leading to oxidation and dissolution of As and metals (DeSisto et al., 2017). Fine particles in tailings are susceptible to aeolian and fluvial transportation, spreading As and Hg beyond tailings areas (Cleaver et al., 2021). For example, at Lower Seal Harbour a large tailings deposit was discovered over two kilometres downstream of the original tailings area (Parsons et al., 2012). An estimated three million tonnes of tailings were produced across all districts (Parsons et al., 2012), most of which have sat untouched since their deposition, except for offroad vehicle use at some sites.

3.1.1. Historical Gold Mine Tailings Mineralogy

Though no two sites have identical mineralogy, the historic gold mine sites of mainland Nova Scotia share similar bedrock geology and processing methods. Most mines targeted auriferous quartz veins present in quartzite, slate, and metasiltstone. Present in smaller amounts are chlorite, biotite, muscovite, and plagioclase, alongside carbonates and sulphides (Walker et al., 2009). Long-term storage of tailings was not regulated in this period, and tailings were routinely left unmanaged and exposed to the environment. Up to a century of oxidation, reduction, dissolution, and precipitation have been at work at these locations, altering original mineralogy and producing a suite of secondary minerals.

Tailings mineralogy fluctuates spatially, as well as at depth. Minerals and controls on precipitation are guided mainly by whether an environment is oxidizing or reducing, which is closely related to pH. Acidity varies widely within individual tailings sites, based on surface type (e.g., tailings, mining concentrates, hardpan). A study of pore and surface water at Montague showed a pH between 2.43 and 7.13 (DeSisto et al., 2011).

In oxidizing conditions, arsenopyrite will dissolve, releasing As into pore water and

lowering pH. Pore water As may be incorporated into Fe arsenates (commonly scorodite), arsenate sulphates, Fe oxyhydroxides, Mn oxides, and Ca(Fe) arsenates (DeSisto et al., 2016). It may also be adsorbed onto Fe oxyhydroxides and gangue minerals. The conditions for this dissolution and precipitation may only be present in microenvironments found throughout the tailings areas (DeSisto et al., 2011).

In reducing conditions typical of subsurface tailings, sulphides will be more stable. Arsenopyrite is less likely to be dissolved, and secondary sulphides may precipitate. In these conditions, Fe and Mn oxides will be unstable and may dissolve, releasing As (DeSisto et al., 2016).

Secondary minerals of particular interest are Fe oxides and hydroxides, which have formed in many cases as rims on sulphide minerals such as arsenopyrite. These rims were ubiquitous on arsenopyrite grains from the Montague, Oldham, and Muddy Pond historic gold mine districts, as observed by SEM. For ground-truthing, we will consider sandy sediment with elevated As and weathered sulphides with Fe oxide rims to have originated from mine sites.

3.2. Mapping Historical Mine Tailings Indicators Using Multispectral Remote Sensing

Optical remote sensing images represent the surface of the earth as pixels, combining the reflectance of all materials within that pixel to produce values at each band. Bands represent a discrete range of the electromagnetic spectrum, measured from one wavelength to another. Sentinel-2 surface-reflectance images were obtained in Google Earth Engine for this study. These images have been georeferenced and corrected for the scattering of photons as they pass through the atmosphere (i.e., converted from “top-of-atmosphere” data as seen from

space to represent the “bottom-of-atmosphere” surface reflectance). Though some optical satellites have spatial resolutions approaching or below one metre, this still pales in comparison to handheld or lab spectrometers, which can provide reflectance spectra for a very precise point on the ground or on a mineral hand sample. Sentinel-2 pixels cover an area of 20 by 20 m on the ground. These are small pixels in comparison to those in images captured by past multispectral missions (e.g., the Landsat mission at 30 m), but at this resolution, a pixel will still likely capture many different surface materials. When a pixel contains a spectrum representing a mixture of materials, it becomes harder to assess the cause of false positive classifications. We could not collect spectra of pure tailings from within a mixed pixel, and the reflectance of a material spatially correlated to tailings may have been inadvertently captured, influencing our training class. For example, tailings consist largely of crushed quartz, and its inclusion in training pixels was inevitable, though it occurs in abundance elsewhere. Vegetation, whether at the edge of tailings or growing sparsely within it, would also be included in tailings training data. Comparing the spectra of tailings to areas that contain physically similar or co-occurring materials may indicate whether these materials are causing false positive results.

Surface materials not spatially correlated to tailings may also be falsely classified as tailings based on their spectral similarity at the resolution of the Sentinel-2 sensors. As a multispectral sensor, spectral resolution is low. Each band covers a wide range, and the apparent reflectance is resampled, or convolved, from the continuous electromagnetic spectrum to the coarse resolution of the sensor. Materials may appear to have the same reflectance signature according to Sentinel-2 when a higher resolution sensor may have detected subtle differences. This may lead to false positives.

3.2.1. Collecting Training Data from Images

A strength of our classifier was that its training data was collected using modern images. The spectra on which the classifier was trained represented modern mineralogy and incorporated mineralogical changes that have taken place since tailings were first deposited. The downside of this approach was that we could not explicitly control what spectral information was used to train the classifier, except by selecting training areas. The original hypothesis was that tailings mineralogy would be sufficiently different from other sandy sediments that it could be distinguished spectrally, even using only multispectral images. This appears to have been valid when analyzing dry sediment. False positives may have emerged when areas were included in the training dataset that should not have been, or because something (e.g., water in sediment pore space) shifted the reflectance of the false positive pixels to resemble dry tailings.

If the former is true, analyzing the mineralogy and spectra of an area or land cover type in which there were many false positives may help to remove that area from the training dataset. If the latter, additional analysis steps could be performed in a future study to remove effects on spectra (e.g., continuum removal and normalization).

Aside from false positives, there appear to be few false negative classifications.

3.2.2. Spectrally Active Minerals

Predicting the presence of a mineral or land cover type by using the reflectance spectrum of a remote sensing image pixel requires that the spectral signature of a target material be distinguishable from the background or other targets. This requires that the target, or a component of the target if it is made up of mixed spectra, be spectrally active. A spectrally

active material contains one or more absorption features in the spectral range of interest (i.e., 400 to 2300 nm in this study). Absorption features are regions of the reflectance spectrum where incoming photons are absorbed, rather than reflected, producing local reflectance minima (Guha, 2020). When observing spectra of mixed materials, such as land cover classes (e.g., forest, urban, tailings), absorption features of constituent materials within the class may still be present. Therefore, if a material is consistently included in a land cover type, even if that land cover type consists of many materials, the absorption may still be detected. This is called a diagnostic absorption feature. A relevant example is the iron absorption feature, where photons in Fe-bearing minerals are absorbed between ~700 and 1000 nm (Van der Werff and Van der Meer, 2015)

Identification of absorption features is limited by the spectral resolution of the sensor used. In hyperspectral image analysis, the spectral resolution is sufficient in some cases that absorption features can be used to indicate mineral species or chemical composition (Clark et al., 2003; van der Meer, 2004). Multispectral data, as obtained from Sentinel-2, lack the resolution to identify the center of an absorption feature. Sentinel-2 has bands with bandwidths ranging from 15 to 185 nm, whereas hyperspectral sensors typically have bandwidths of around 10 to 15 nm or less for all bands. If an absorption feature is captured by a wide band at a pixel, the reflectance value for the entire band will be lowered for that pixel. In other words, absorptions may affect multispectral band values, but we cannot determine absorption shape, including central wavelength and depth. We relied on bands 8 and 8A (with bandwidths of 106 and 21 nm, respectively) to detect subtle absorptions which may indicate the iron absorption feature of Fe oxides and hydroxides. The question then was whether

multispectral data and specifically Sentinel-2 bands 8 and 8A would be able to differentiate tailings from naturally occurring sand that originated from the same, or at least similar, Meguma bedrock, based only on this subtle difference.

3.2.3. The Mine Tailings Classification Model

Our model used existing mine tailings data from several sources to provide training data, in the form of pixels from Sentinel-2 images to a random forest classifier (Jewell, 2021). This section briefly describes the data used to train the classifier as well as its parameters. For more details on data processing, including how points were sampled and how images were selected, refer to chapter one.

Historic mine districts in Nova Scotia are distributed across nearly the entire province, and many of them have been studied in detail. Documents, including surveys outlining tailings extent, date back to the early 1900s (Faribault, 1900). Since the first cases of acute As poisoning were reported in the 1970s, the effort to map tailings and quantify contaminants has increased (Drage, 2015). The focus of these studies varies between geochemistry and mineralogy (DeSisto et al., 2017; Parsons et al., 2012; Percival et al., 2013; Walker et al., 2009) and the risk to human and ecosystem health (Drage, 2015; LeBlanc et al., 2020). Of particular note are the Nova Scotia Mine Tailings Database (Hennick and Poole, 2020), which combines historical and modern tailings data into a spatial database, and Parsons et al. (2012), which provided detailed descriptions, mineralogy, and geochemistry for 14 mine districts. The breadth of knowledge, as well as the geographic area that is covered, helped us to determine which mine districts should be targeted for analysis with our model and to interpret the results.

Due to changing environmental conditions at mine sites, maps of tailings extent created

a century ago, or even a decade ago, may need to be confirmed and updated. Our model used the Nova Scotia Mine Tailings Database to indicate past tailings areas from which we could spectrally sample Sentinel-2 image pixels to train a classifier. Sentinel-2 is a satellite mission operated by the European Space Agency. It is comprised of two nearly identical satellites, launched in 2015 and 2017 (Sentinel-2A and Sentinel-2B, respectively). The mission has a revisit period of five days or less (depending on latitude), which is the frequency at which it captures an image at a given location on Earth.

Sentinel-2 has 13 bands in varying spatial resolutions and bandwidths. It differs in this way from hyperspectral sensors that contain up to several hundred contiguous bands at very narrow bandwidths (as small as two to five nm in the lower wavelength region of the EM spectrum). The 13 bands were chosen carefully to fulfill specific objectives and fine-tune placement based on experience gained from similar multispectral missions such as Landsat (van der Meer et al., 2014). In general, Sentinel-2's bands are narrower than Landsat's to avoid spectral absorption due to water vapour in the atmosphere. Sentinel-2's band 8A (a near-infrared band centred at 865 nm) was carefully placed to avoid water vapour, target peak NIR reflectance in vegetation, and be sensitive to Fe oxides in soil (European Space Agency, 2015; van der Meer et al., 2014; Van der Werff and Van der Meer, 2015). More accurate discernment of vegetation improved the ability of our model to filter out vegetation on the surface, and Fe oxides were an important indicator when classifying tailings.

The bands used as input are the values that are considered by the random forest classifier when labelling each pixel as tailings or non-tailings. We initially selected eight bands to use in our model. The three 60 m atmospheric bands were removed. Band 8 was also removed,

as it entirely overlaps the narrower band 8A and was assumed to be highly correlated. Four indexes were generated and also included: normalized difference vegetation index (NDVI), modified normalized difference water index (MNDWI), ferric iron index, and iron feature depth. An optimization step removed some bands and indexes to determine which variables provided the most discrimination power between tailings and non-tailings pixels. The final model used seven variables: band 3 (red), band 6 (vegetation red edge), band 7 (vegetation red edge), band 8A (narrow near-infrared), band 12 (shortwave infrared), NDVI, and MNDWI.

Finally, we created a tailings spectral class – an averaged spectrum that the classifier would use to compare against all pixels when applying labels. To create the tailings spectrum, we sampled a Sentinel-2 image in areas previously mapped as tailings in the Nova Scotia Mine Tailings Database. The tailings areas included in this database were based on maps from within the last few years, as well as historic data. As such, we had to ensure that the pixels we sampled had not become overgrown with vegetation, or that the mapped area was not depicting where tailings had been deposited into water bodies. Optical reflectance data only represents the top mm or less (depending on the material) of the surface (Clark and Roush, 1984), so the inclusion of any pixels in which the surface is covered would have introduced noise to our tailings spectrum. An NDVI layer was generated to create a vegetation mask, where pixels with values over 0.6 were excluded from tailings sampling. Similarly, MNDWI was generated to filter out pixels which appeared to contain water. A value of 0.0 was used for the water mask, though this mask did not appear to be as effective as the vegetation mask (chapter 1).

3.2.4. Google Earth Engine

Desktop analyses, including data pre-processing, image acquisition, image sampling,

classification, and accuracy assessment, were performed in Google Earth Engine (GEE), a cloud platform created by Google for remote sensing (Gorelick et al., 2017). GEE is available via web browsers or as a Python package. GEE allows the uploading of spatial data and imagery, though there are many datasets available in its built-in library. Sentinel-2 surface reflectance images are available within GEE within a few hours of the original top-of-atmosphere images, allowing for the easy selection of images with no need for further processing. In addition to image collections, GEE has a large selection of functions that can be implemented in its JavaScript and Python APIs. Computation performed in GEE is run on Google's cloud servers, allowing for the rapid processing of massive datasets.

3.3. Applying Remote Sensing Model to Historic Gold Mine Sites

Three historic mine districts, Montague, Oldham, and Waverley were physically sampled to obtain mineralogy and geochemistry of known tailings. These samples were used as reference material when analyzing sediment from non-tailings areas. Tailings areas at these sites are included in the Nova Scotia Mine Tailings Database, and their mean reflectance spectra were also recorded. Sulphide grains were located within samples via SEM to determine if Fe oxide rims were present. We compared the geochemistry, SEM images, and mean spectra at each site to those of coastal areas that are produced false positive results in the classifier.

3.3.1. Montague Gold Mine District

Montague Gold Mine District is located north of the city of Halifax, in central Nova Scotia (latitude: 44.714°, longitude: -63.521°). The first stamp mill was constructed here in 1865, and extraction continued in some capacity until 1940 (Parsons et al., 2012). Tailings were slurried

into nearby Mitchell Brook and surrounding wetlands. Tailings have been identified 2.5 km downstream in Lake Charles, which continues into the Shubenacadie Watershed (Clark et al., 2021; Mudroch and Clair, 1986). Over 120,000 tonnes of ore were crushed during mining and processing at this site, and over 68,000 troy ounces of gold were produced. In hardpan areas, As was found to reach as high as 4.3 wt. % (DeSisto et al., 2011; Parsons et al., 2012). Montague has been of special interest to researchers and the provincial government because of its elevated As and Hg and its direct proximity to urban and residential areas, which continue to expand closer to historic tailings (Intrinsik Corp et al., 2020, 2019b).

Six samples were collected at Montague in October 2020. Bulk geochemistry indicated a mean As level of 9868 ppm. The highest concentration observed was 16,300 ppm As. SEM analysis indicated that arsenopyrite grains were common, and all of those observed showed signs of weathering, with Fe oxide minerals growing along edges and in cracks.

3.3.2. Oldham Gold Mine District

The Oldham gold mine district is 30 km northeast of Halifax (latitude: 44.921, longitude: -63.493). Mining took place from 1862 to 1910, and again from 1936 to 1942 (Lane et al., 1989). Approximately 107,000 tonnes of ore were crushed, and over 85,000 troy ounces of gold were produced (Parsons et al., 2012). Oldham, like Montague, is in the Shubenacadie Watershed, though only a small tributary, Black Brook, flows through the site (Lane et al., 1989). Tailings can be seen on the banks of the brook as it leaves the site. We did not identify any studies indicating that tailings from Oldham have reached the Shubenacadie River, which is approximately 3 km downstream.

Six tailings samples were collected in September 2020, which had a mean As

concentration of 999 ppm and a maximum of 2362 ppm. Though the lowest As of the three sites, all samples exceeded the Canadian Council of Ministers of the Environment's soil guideline of 12 ppm As (CCME, 1997). Rims of Fe oxides were visible around weathered sulphide grains in SEM images.

3.3.3. Waverley Gold Mine District: Muddy Pond

There are multiple tailings areas in the Waverley district, however, this study focuses on the largest, called Muddy Pond. The district is located approximately 12 km north of Halifax (latitude: 44.787, longitude: -63.609). Over 150,000 tonnes of ore were crushed, producing 73,100 troy ounces of gold (Parsons et al., 2012). Unlike Montague and Oldham, which were relatively remote and required infrastructure to be built to accommodate workers, Waverley was already a small village when gold was first mined in the 1860s (Hartlen, 1988). As such, mining was more or less continuous until the 1960s. Like the two districts previously mentioned, Waverley resides in the Shubenacadie Watershed, with Muddy Pond separated from the main river by only a small wetland and tributary. This site is surrounded by residential communities, and development continues to expand.

Tailings samples from Waverley had a mean As concentration of 1921 ppm and a maximum of 2971 ppm.

3.4. Mapping Indicators of Tailings

In chapter one we described how the areas around the Goldenville and Montague gold districts were analyzed using a model built in GEE. Two main methods were tested for classifying images. First, we tested a pixel-wise classifier. Every pixel of the input image in the

target mine area was analyzed by the random forest classifier and assigned a label of tailings or non-tailings. Second, we tested an object-based method that first grouped pixels according to spectral and spatial proximity and then classified the grouped pixels as either tailings or non-tailings. More detail on each model, and their results, are available in chapter one. In this study, we refer only to the pixel-wise classification, which produced more false positives than the object-based methods.

The classification model was run 50 times for each district, and results (Figure 2) were recorded using F1-score (Chapter 1, Van Rijsbergen, 1979). Maps were also generated to illustrate the frequency at which each pixel was classified as tailings (Figure 3a and 3b). The maps displayed the land cover types that most frequently elicited false positive classifications. Results are also displayed as histograms (Figure 4a and 4b), which show that most pixels with at least one tailings classification were classified as tailings in all 50 iterations. Roads were sometimes classified as tailings; however, the main sources of error were shorelines and wetlands. False positives coinciding with roads are not discussed here, as road pixels were not misclassified as consistently as the other two classes. Roads are also easier to reject as positive by an analyst, based on context and simple visual assessment. Being able to spectrally distinguish wetlands or shorelines that contain tailings, versus those that do not, is a more difficult task for an analyst using visual clues, and would be a valuable application of the classification model.

3.4.1. Possible Causes of Positive Classification

There are three likely scenarios in which wetlands and shoreline pixels would be classified as tailings, even when the area of analysis is not near a mine district:

1. Polygons that were used to outline the extent of tailings and generate sample points (i.e., the training data) included wetlands and shoreline areas when they should not have. Masks were generated to remove pixels from training areas that contained water and vegetation, however, these masks (the water mask in particular) were imperfect. Therefore, when training the classifier, pixels consisting at least partially of wetlands and waterbodies may have been included. In this scenario, the classifier has inadvertently been trained to detect wetlands and shorelines, in addition to, or combination with, tailings.
2. Wetlands and shoreline pixels are more likely to contain mixed spectra, and the spectral signature of these mixtures resembles that of tailings. The Sentinel-2 pixels used by the classifier are 20 by 20 m. Wetlands are a mixture of shallow water and vegetation, and these signals may combine to resemble the signal of tailings. Shorelines are typically narrow features and pixels that include them will have a reflectance signal consisting of some exposed sediment and some water (and likely vegetation). This combined signal may resemble tailings when apparent reflectance is resampled to the spectral resolution of Sentinel-2.
3. The classifier was correct. Tailings were often deposited into wetlands and streams, and we should expect that tailings are still present in those areas, within and around mine sites or even up to several km downstream (Drage, 2015; Parsons et al., 2012). The minimum amount of tailings required in a pixel for the classifier to correctly identify it as tailings is unknown, and hard to quantify due to many complicating factors (grain size, sediment mixture type, etc.) (Clark et al., 2003; Goetz et al., 2009). The ability to detect

tailings deposits downstream of sites along riverbanks, coastal wetlands or estuaries would be valuable, but results in these land cover types are inconsistent. Isolating the factors causing confusion in these areas would increase confidence in the results, whether positive or negative.

To explore some of these possibilities, we have sampled materials identified by the classifier as tailings, both physically and spectrally, at five coastal and wetland sites. Sediment was collected at three estuarine areas, downstream of multiple mine sites, as well as one wetland just north of Montague.

3.4.1.1. Sediments of Estuarine Environments Downstream of Mine Districts

The estuarine sediment deposits were larger than the shorelines of lakes and riverbanks found near mine sites and provided purer pixels in the Sentinel-2 image, allowing us to control for pixel mixing. Lawrencetown, Lower East Chezzetcook, and Martinique Beaches were selected for sampling (Figure 4). These areas are east of Halifax, ranging from about 15 to 35 km along the coast. Each site consists of a narrow beach separating the ocean from salt marshes or lagoons. Samples were collected from low-energy areas, where fine sediment from upstream would be likely to be deposited. Lawrencetown and Lower East Chezzetcook are downstream of the Lawrencetown and Chezzetcook historic mine districts, respectively. These were minor districts, with Lawrencetown crushing 1534 tonnes of ore, and Chezzetcook just 73 (Parsons et al., 2012). Martinique is near the Lake Catcha historic mine district, at which 29,426 tonnes of ore was crushed. It does not appear that there are streams directly connecting this site to that mine district, making sediment transportation and deposition from there unlikely.

These sediment deposits, originating from the same bedrock as the gold mine districts,

were presumed to be a close natural mineralogical proxy for tailings in grain size and composition. According to our hypothesis, the classifier's ability to discriminate naturally occurring sand from tailings should rely primarily on the Fe absorption feature present in Fe oxides and hydroxides. If these minerals are not present, and pure pixels are still classified as tailings, that would indicate that the classifier is including minerals that resemble tailings but do not originate from mines and may not contain high levels of As or other related contaminants. If only pixels at the beach-ocean threshold are positively classified as tailings and not the purer pixels, we can extrapolate that false positives at shorelines are a result of pixel mixing. First, we explore if the estuarine sediment deposits contain those Fe oxides and hydroxides.

Grains from the three coastal sites were analyzed via SEM. A random subsample from each main sample was set in resin pucks and placed in a TESCAN Mira3 LMU SEM. Grain size and shape were observed, and we inspected for the presence of sulphides (particularly arsenopyrite) using the same method as at Montague, Oldham, and Waverley (chapter 1).

Samples from Lawrencetown and Lower East Chezzetcook consisted of sub-angular to angular coarse silt to medium sand grains (Table 2). The Martinique site appeared to be a mudflat and contained fine silt to fine sand grains that were slightly less angular than the grains of the other two sites.

No sulphide grains were observed in the Lawrencetown or Lower East Chezzetcook samples. Some sulphide grains were seen in the Martinique mudflat samples and displayed a framboidal texture. Framboidal pyrite has been observed in deep tailings but is typical of a marine environment (DeSisto et al., 2016; Wilkin and Barnes, 1997). These sulphides did not have Fe oxide or hydroxide overgrowth. Whole Fe oxide or hydroxide grains were present, but

only in small amounts. Analysis of these grains via SEM suggests a reducing environment, rather than the oxidizing environment typical of tailings.

For further confirmation of whether or not sediment deposits contained tailings, bulk geochemistry was obtained. The four samples had a mean As concentration of 16.15 ppm, still slightly above the CCME's guideline of 12 ppm, but below the provincial guideline of 31 ppm, and within the range of As expected for non-tailings sediment within the province (Parsons and Little, 2015). Geochemistry suggests that these deposits did not originate from upstream tailings.

3.4.1.2. Wetlands

Two wetland areas were analyzed, in addition to coastal sediment deposits: one at Lawrencetown Beach, and another just north of the Montague tailings area.

The Montague tailings sit on the border of two watersheds. Streams flowing west or northwest feed into the Shubenacadie watershed, while those flowing north or east flow into the Musquodoboit watershed. The wetland sampled is located in the Musquodoboit watershed, just before it feeds into Lake Major. This sample site's proximity to Montague increased the probability that tailings could be present there. The area was highly vegetated, with patches of exposed sediment that would not have been large enough to dominate a Sentinel-2 pixel.

The second wetland sample site was at Lawrencetown Beach, in the same estuarine environment as sample ES00, though three km east of it. This was a well-vegetated marsh, with patches of sandy material scattered throughout. Finding sediment to sample among the moss and humus was difficult. It would have been very unlikely to obtain pure pixels in the Sentinel-2

images at this location.

Subsamples of the wetland sediment were placed in resin pucks and analyzed via SEM. No sulphides were observed in these samples. Some Fe oxides or hydroxides were observed as whole grains but were not common.

Bulk geochemistry of these samples was determined via ICP-MS following aqua regia digestion. The Montague samples had As concentrations of 63.9 and 56.4 ppm, while the Lawrencetown sample had a concentration of 29.9 ppm. All three of these samples had higher As than any of the four coastal samples and exceeded the CCME guideline of 12 ppm As. Though the highest observed in these samples, these concentrations are still low compared to even the lowest tailings As observed, which was 160 ppm at Oldham. The lowest value observed at the main tailings area of Montague was 2085 ppm As. A study of non-tailings forest soils surrounding Montague showed a large natural As variation, that did not seem to be caused by mining (Parsons and Little, 2015). The values we observed are within the range defined in that study.

3.4.2. Comparison of Land Cover Reflectance

The five areas sampled for SEM and ICP-MS analysis were also virtually sampled to obtain mean reflectance (Figure 5) from a Sentinel-2 image using the 10 and 20 m bands (Table 1). A fifth spectral sample was obtained from a tidal region in the Minas Basin containing red sand. This sand did not originate from the same bedrock as the mine sites previously included, but its colour suggests the presence of Fe oxides. We also provide mean spectra of tailings and other land cover types around the Montague mine district for comparison. To sample the non-tailings spectra, polygons were created around the physical sampling areas, and a vegetation

mask was created. Only pixels with an NDVI value of less than 0.5 were viable for spectral sampling.

Some similarities can be observed among the non-tailings spectra. All but the Minas Basin show absorption in the red band (B4, around 665 nm), before increasing in reflectance until around the NIR region (B8 and B8A, around 750 nm) and then steadily declining throughout the SWIR range. The red band absorption is likely due to vegetation, which was present in all of these sample areas despite attempting to mask it out. This same spectral shape is observed in our forest spectrum (Figure 6, top center). The spectra of Lawrencetown, Conrad's, and the Montague wetland all match the forest spectra almost exactly, though the red band absorption is not quite as deep. This suggests a significant amount of vegetation was not successfully removed by the NDVI mask.

Our tailings spectrum (Figure 6, top left) shows a gradual increase in reflectance between the visible and NIR bands, followed by a fairly flat response for the SWIR bands. The depth of absorption at B8 is less than the standard error, and the mean value for B8A shows no absorption at all. Martinique, Minas Basin, and Chezzetcook show similar degrees of absorption at B8, though Chezzetcook has a high standard error, possibly owing to a small sample size.

The Minas Basin reflectance increases sharply until the red edge (around 700 nm), where there is an absorption feature at B6 (740 nm), followed by a decrease throughout the NIR and SWIR region.

3.5. Results and Discussion

Analysis of SEM and geochemistry did not indicate that these regions contain tailings. Sulphide minerals were uncommon at all observed sites, including in the two Montague

samples collected less than two km from the main Montague tailings area. When they were present, sulphides did not exhibit the Fe oxide or hydroxide alteration rims or remineralization that is common for sulphides found in tailings (Chapter One).

After confirming that the false positive areas do not contain tailings, we compared the spectra of these areas to determine the sources of confusion for the classifier. Random forest classifiers calculate the importance of each input variable during the training stage and use these importance measures in their decisions (Chapter One, Gregorutti et al., 2017). The classifier sets some of its training points aside (an out-of-bag sample) and uses the remaining points to try and describe the subset. If all training points contain the same bias or error, that error will be included in the classifier.

We included an additional optimization step to choose an ideal set of variables (Chapter One). We started with the Sentinel-2 20 m bands, except for B8, and the NDVI and MNDWI indexes. The model provided 10 unique variable sets, which we tested and ranked according to F1-Score. Out of these variable sets, only four included the red band, B4, which we are considering diagnostic of vegetation. The optimization step was performed using the Goldenville and Montague mine districts, which have relatively large and unvegetated tailings areas compared to many of the other districts. Tailings in those districts were less likely to contain vegetated pixels, and less likely to have pixels with a mixed forest signal from the tailings' edge. While the red band may not be important for defining pure tailings pixels, it is important in discriminating vegetated tailings from non-vegetated tailings.

Sentinel-2 has two NIR bands that overlap significantly. The narrow NIR band, B8A, is completely within the range of B8. Having multiple bands detecting the same wavelengths

would be redundant and was expected to introduce bias in the classifier's training dataset. We chose to remove B8 and keep the narrow B8A, which would be easier to interpret and was thought to better target the iron absorption feature. By observing tailings spectra at multiple sites, we can see that absorption is negligible in B8A, but a slight absorption is often visible in B8. This suggests that iron absorption is taking place in the area of B8 that does not overlap B8A, i.e., from 800 to 853 nm.

3.6. Conclusion

When we classified images, the classifier was trained on all but the target districts. When classifying the most ideal target districts (i.e., Goldenville and Montague), we lost the most valuable training areas. When those districts were classified, training data was obtained from districts that may have contained excess vegetation and mixed pixels (Figure 3a and 3b). Pixels containing vegetation exhibited a chlorophyll absorption feature around 650 nm, lowering the value of B4. The result was false positives occurring in wetland areas.

False positives along shorelines are likely due to mixed pixels. The shoreline spectrum (Figure , bottom left) closely resembles the Minas Basin tidal spectrum, with the addition of absorption at B4 (the red band at 660 nm). Shorelines of lakes and rivers are likely too narrow of geographic features to be accurately described using the 20 m bands of Sentinel-2. Pixels containing shorelines in our images are highly mixed, containing dry sediment or rocks, water, and vegetation. They do not quite cross the thresholds set by either the vegetation or water masks but should be masked out by some other means when using Sentinel-2 images.

By analyzing the mineralogy and geochemistry of areas to confirm they are receiving false positive classifications, we can compare spectra band-by-band to determine what spectral

ranges are causing confusion. The primary source of error in our classifier appears to be the inclusion of pixels in the training data that contain vegetation or, to a lesser extent, water. Removing these areas from the training data would likely improve overall results. This is difficult to do with simple NDVI and MNDWI thresholding, however. A more sophisticated masking approach may be beneficial. A higher spatial resolution would improve sampling accuracy, allowing tailings to be targeted in between patches of vegetation. Smaller pixels would likely improve the model's performance along shorelines as well, but this is a complex land cover type, and some mixing may always be present at the land-water boundary.

3.7. Figures

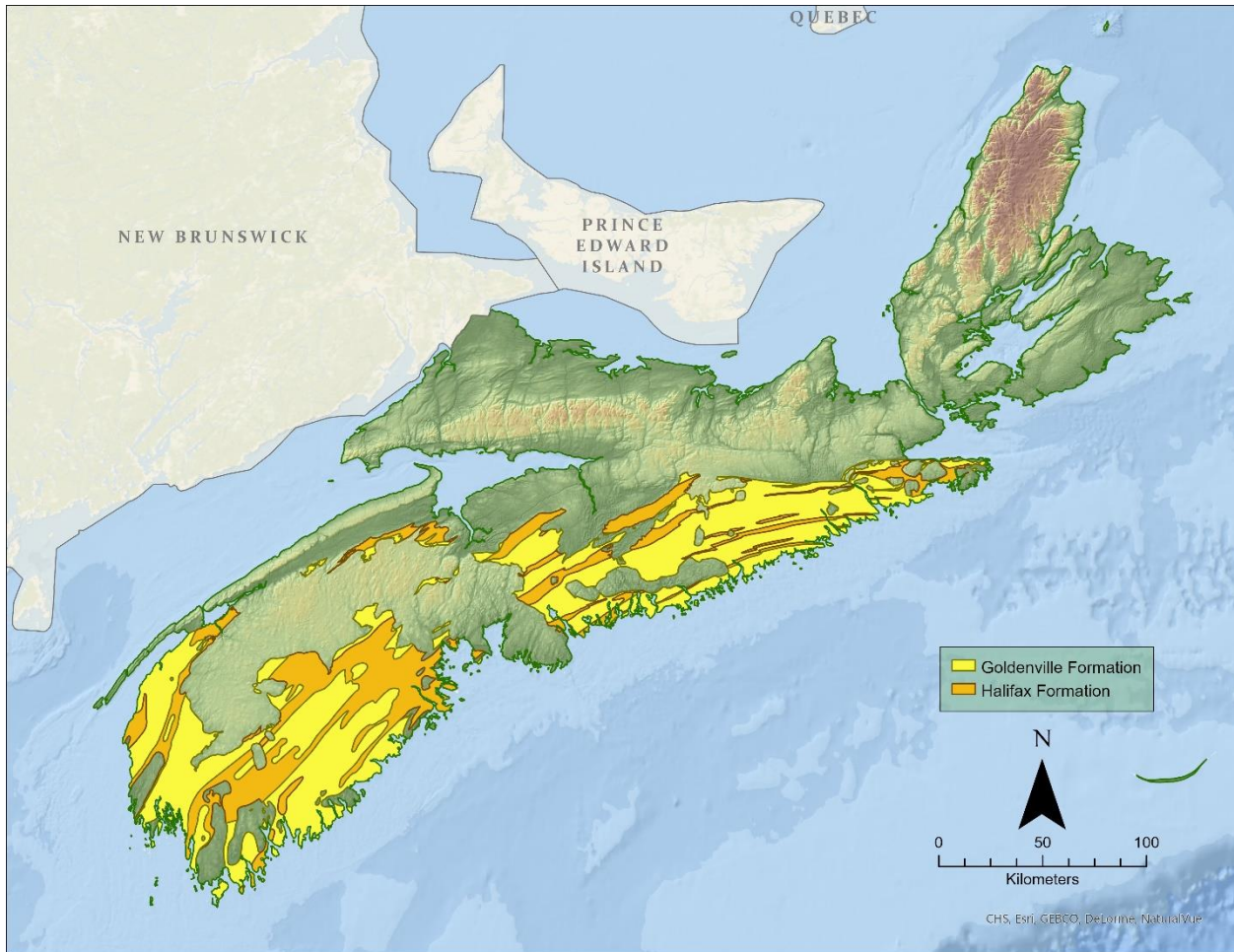


Figure 1. A map showing the province of Nova Scotia, with the Goldenville and Halifax formations overlaid. These are the main gold-bearing formations in the province.

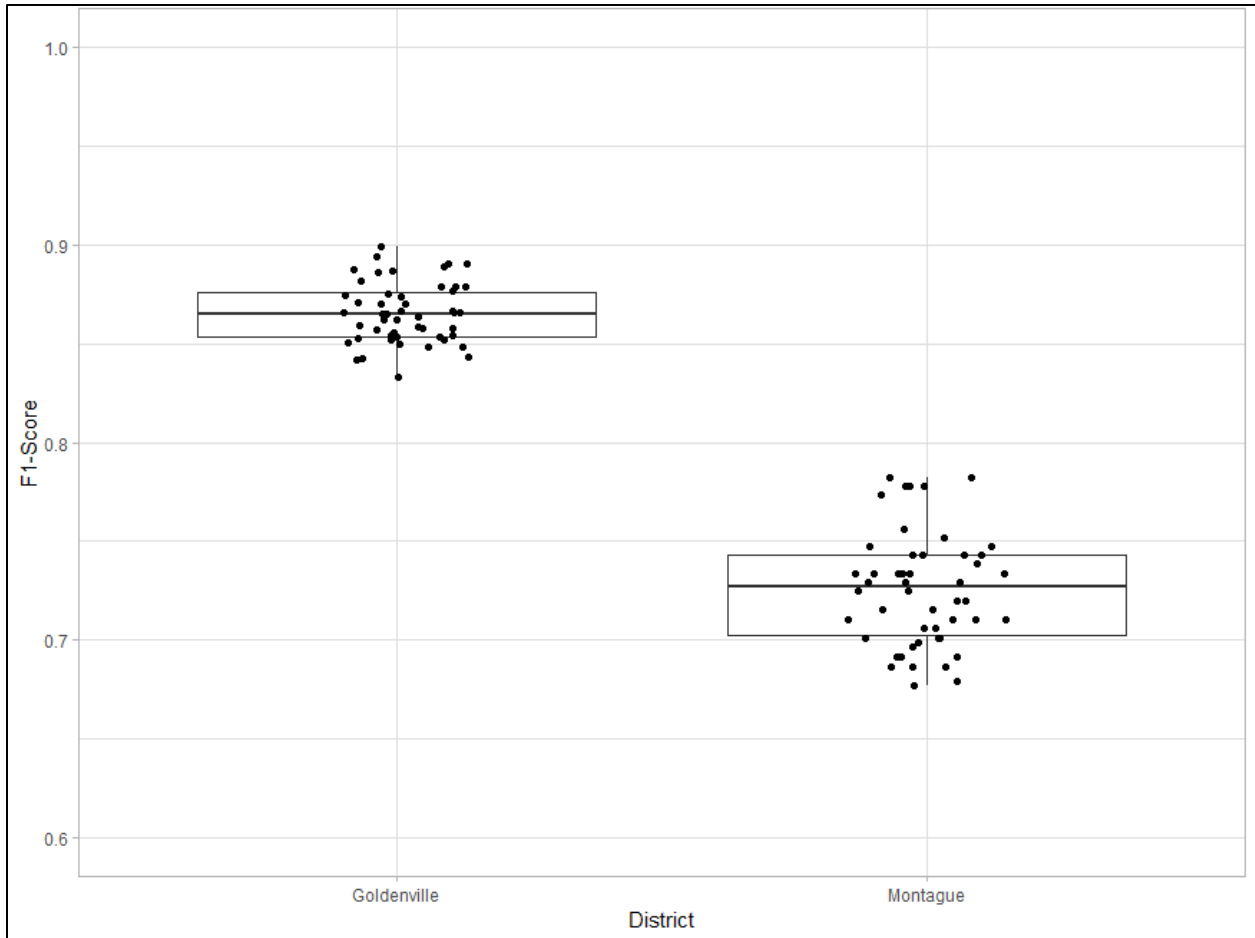


Figure 2. Box and whisker plot displaying F1-score at two districts. Values are spread out along the x-axis for clarity. The pixel-wise classification model was run 50 times each on Sentinel-2 images for the Goldenville and Montague regions, respectively.

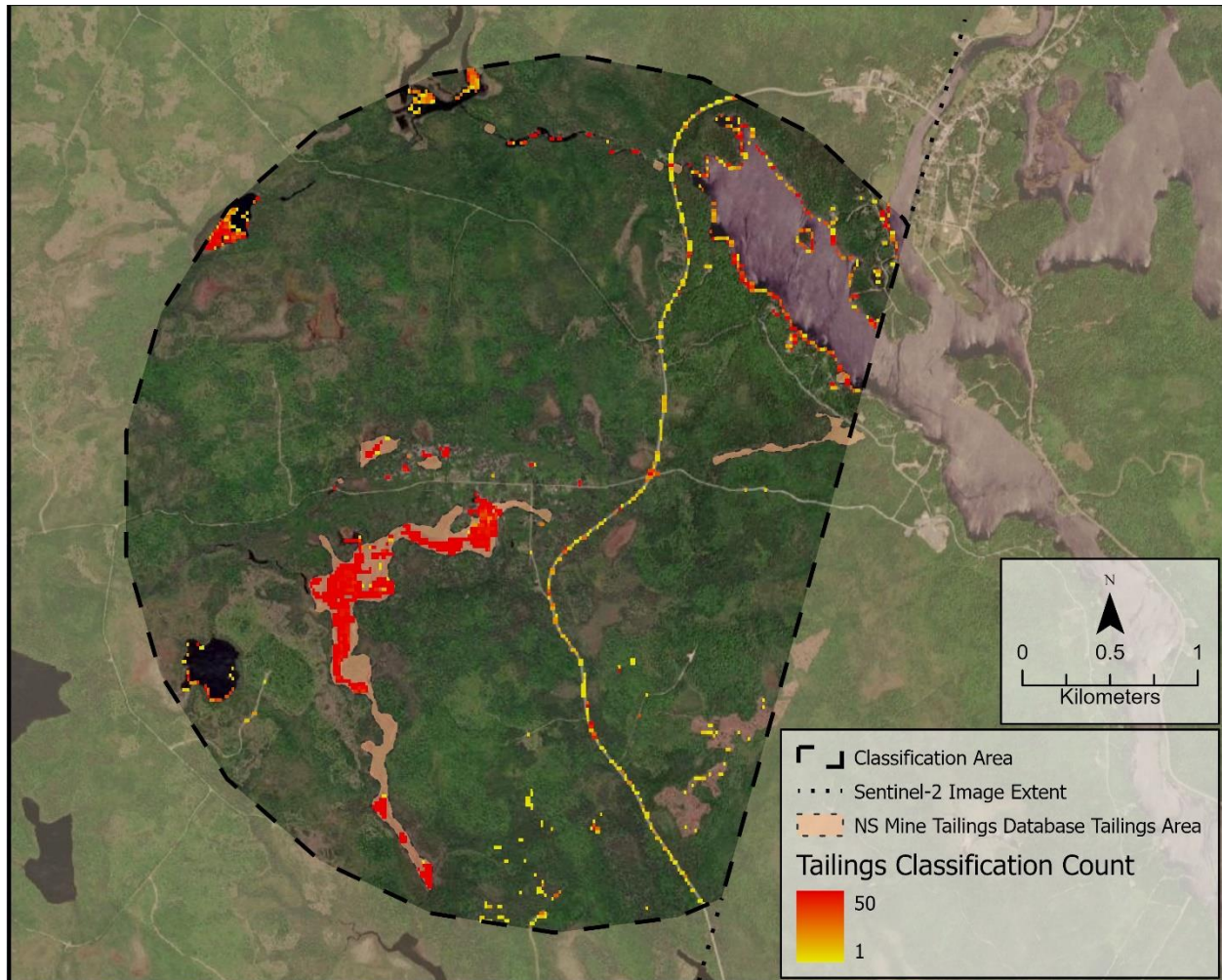


Figure 3a. Pixel-wise classifier at Goldenville displayed as a frequency. The model was run 50 times using a Sentinel-2 image, and the total count of positive classifications (i.e., the pixel was labelled as tailings by the classifier) is displayed in a range from 1 to 50. Where the basemap (satellite image) is shown, that pixel was never classified as tailings, and the count is 0. Image credit: Maxar.

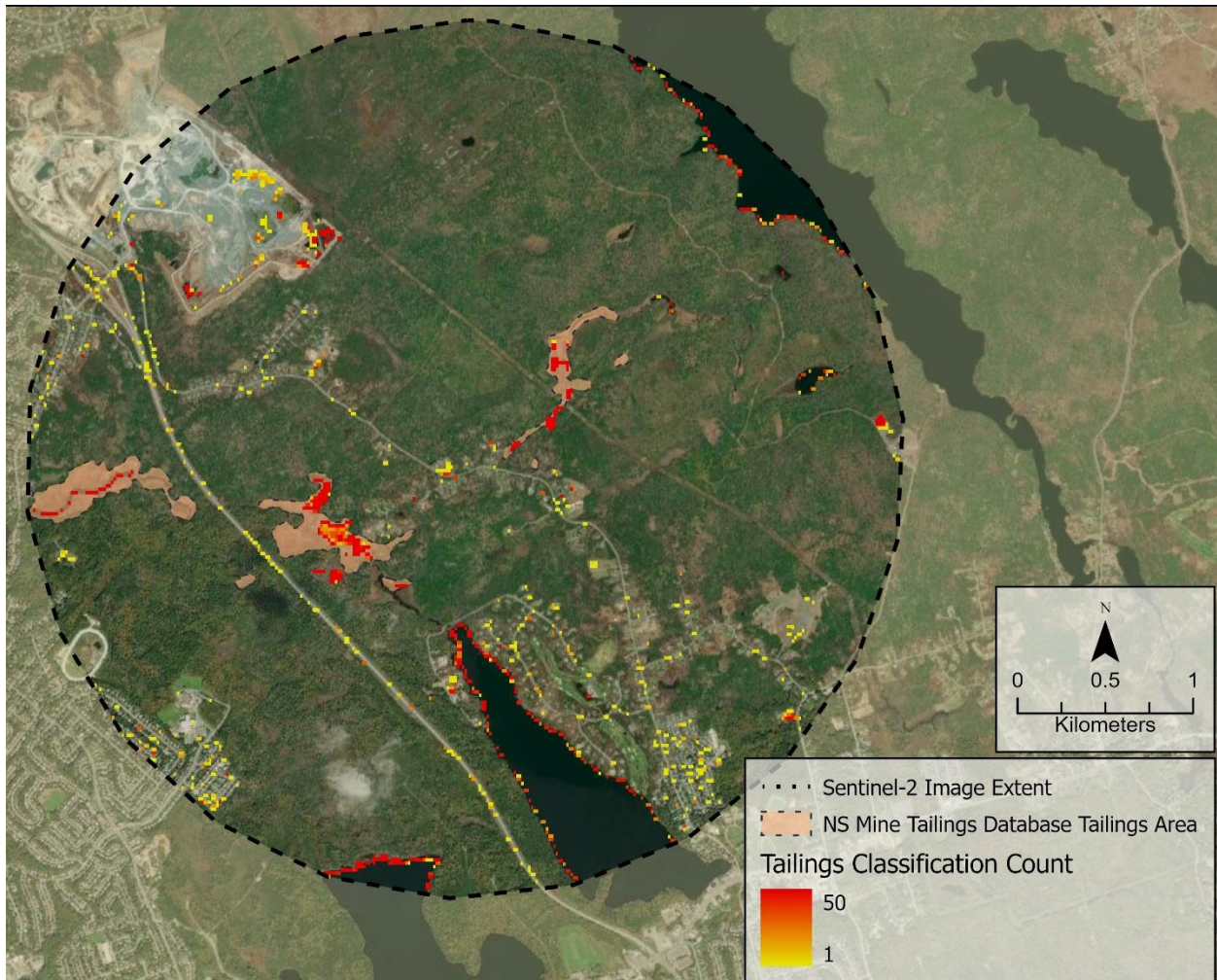


Figure 3b. Pixel-wise classifier at Montague displayed as a frequency. The model was run 50 times using a Sentinel-2 image, and the total count of positive classifications (i.e., the pixel was labelled as tailings by the classifier) is displayed in a range from 1 to 50. Where the basemap (satellite image) is shown, that pixel was never classified as tailings, and the count is 0. Image credit: Maxar.

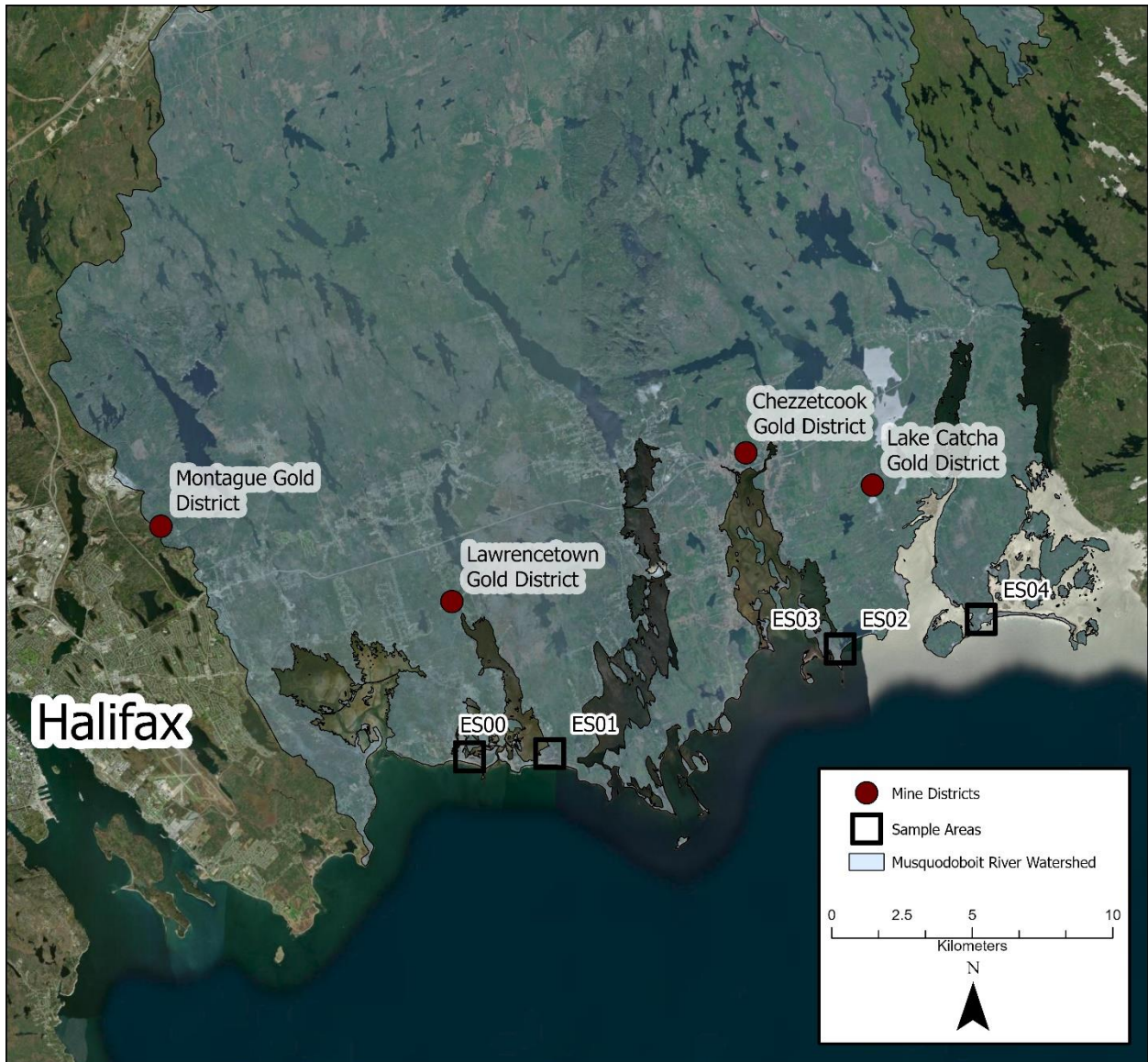


Figure 4. A map showing five sample sites in estuaries downstream of historic mine districts. All samples were collected in low energy areas, and are in the same watershed.

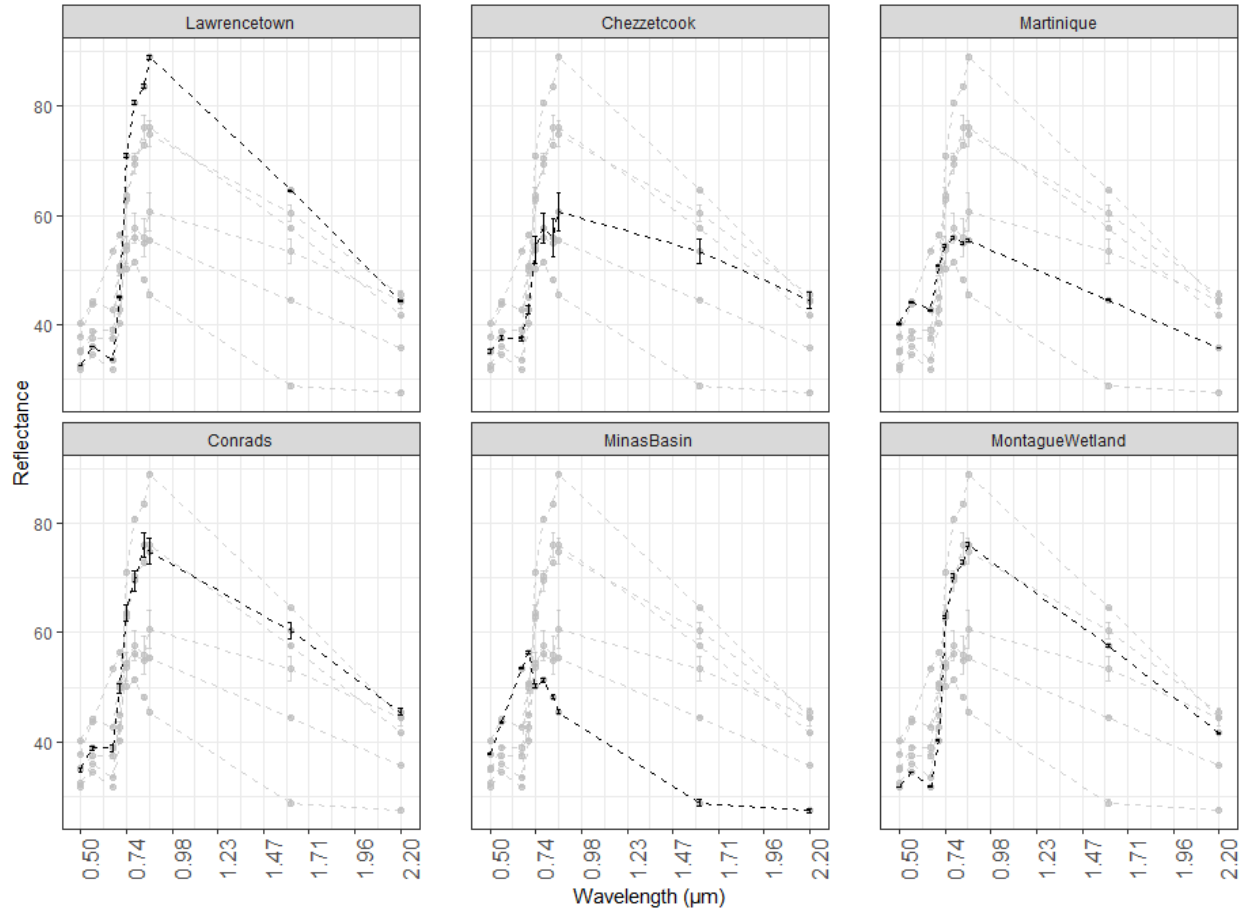


Figure 5. An array of biplots showing the mean spectrum for six non-tailings land cover types. The x value of points indicates the central wavelength of Sentinel-2 bands. Whiskers around points indicate the standard error at that band. These land cover types were often misclassified as tailings by our model.

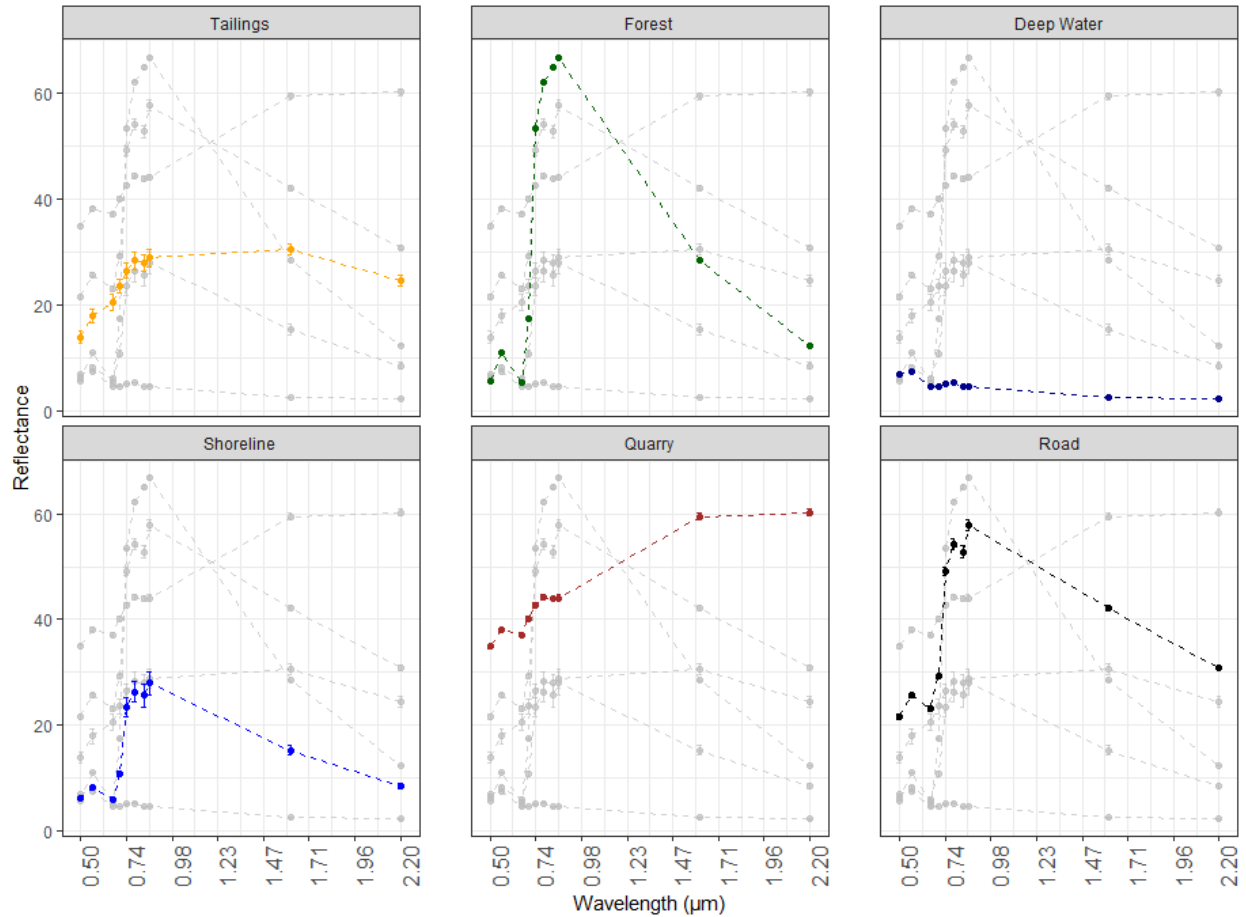


Figure 6. An array of biplots showing the mean spectrum for six land cover types found around the Montague mine district. The x value of points indicates the central wavelength of Sentinel-2 bands. Whiskers around points indicate the standard error at that band. Similar spectra, at least for a certain wavelength range, were more likely to be confused when classifying. Tailings and shorelines were the most often confused classes. Absorption at Band 4 (third point from left) indicates potential chlorophyll absorption resulting from vegetation within pixels.

3.8. Tables

Table 1. Sentinel-2 10 and 20 m bands, with bandwidth and band center. All bands were resampled to 20 m for analysis. Values are shown for Sentinel-2A for simplicity – Sentinel-2B has very similar band values.

Band Name	Bandwidth (nm)	Band Center (nm)
B2 – Blue	66	492.4
B3 – Green	36	559.8
B4 – Red	31	664.6
B5 – Vegetation red edge	15	704.1
B6 – Vegetation red edge	15	740.5
B7 – Vegetation red edge	20	782.8
B8 – NIR	106	832.8
B8A – Narrow NIR	21	864.7
B11 – SWIR	91	1613.7
B12 – SWIR	175	2202.4

Table 2. A description of tailings samples collected from four coastal locations.

Sample ID	Area	Description
ES00	Lawrencetown (Conrad's Beach)	Mixed fine sand and organic material. Seemingly dry area
ES01	Lawrencetown (wetland)	Marshy area with patches of fine sand. Thick moss, lots of organic material
ES02	Lower East Chezzetcook	Sample further from waterline. Fine to medium grey sand.
ES03	Lower East Chezzetcook	Sample closer to waterline. Fine to medium red sand at surface, with dark grey to black sand underneath
ES04	Martinique	Very fine, muddy sediment. Grey-brown at surface, with grey-blue to black sediment beneath.
MO06	Montague Wetland	A small bare patch of light brown sediment. Poorly sorted grains ranging from sand to cobbles.
MO07	Montague Wetland	Sampled from a pathway, roughly one to two meters wide. Scattered shortgrass throughout. Similar light brown sediment to MO06

3.9. References

Bates, J.L.E., 1987. Gold in Nova Scotia, Canadian Cataloguing in Publication Data. Nova Scotia Dept. of Mines and Energy, Halifax.

CCME, 1997. Canadian Soil Quality Guidelines for the Protection of Environmental and Human Health - Arsenic (Inorganic). Can. Environ. Qual. Guidel. 7.

Clark, A.J., Labaj, A.L., Smol, J.P., Campbell, L.M., Kurek, J., 2021. Arsenic and mercury contamination and complex aquatic bioindicator responses to historical gold mining and modern watershed stressors in urban Nova Scotia, Canada. *Sci. Total Environ.* 787, 147374.

<https://doi.org/10.1016/j.scitotenv.2021.147374>

Clark, R.N., Roush, T.L., 1984. Reflectance spectroscopy: Quantitative analysis techniques for remote sensing applications. *J. Geophys. Res. Solid Earth* 89, 6329–6340.

<https://doi.org/10.1029/JB089iB07p06329>

Clark, R.N., Swayze, G.A., Livo, K.E., Kokaly, R.F., Sutley, S.J., Dalton, J.B., McDougal, R.R., Gent, C.A., 2003. Imaging spectroscopy: Earth and planetary remote sensing with the USGS Tetracorder and expert systems. *J. Geophys. Res. - Planets* 108, 5131-n/a. <https://doi.org/10.1029/2002JE001847>

Cleaver, A.E., Jamieson, H.E., Rickwood, C.J., Huntsman, P., 2021. Tailings dust characterization and impacts on surface water chemistry at an abandoned Zn-Pb-Cu-Au-Ag deposit. *Appl. Geochem.* 128, 104927. <https://doi.org/10.1016/j.apgeochem.2021.104927>

DeSisto, S.L., Jamieson, H.E., Parsons, M.B., 2017. Arsenic mobility in weathered gold mine tailings under a low-organic soil cover. *Environ. Earth Sci.* 76, 773. <https://doi.org/10.1007/s12665-017-7041-7>

DeSisto, S.L., Jamieson, H.E., Parsons, M.B., 2016. Subsurface variations in arsenic mineralogy and

geochemistry following long-term weathering of gold mine tailings. *Appl. Geochem.* 73, 81–97.

<https://doi.org/10.1016/j.apgeochem.2016.07.013>

DeSisto, S.L., Jamieson, H.E., Parsons, M.B., 2011. Influence of hardpan layers on arsenic mobility in historical gold mine tailings. *Appl. Geochem.* 26, 2004–2018.

<https://doi.org/10.1016/j.apgeochem.2011.06.030>

Drage, J., 2015. Review of the Environmental Impacts of Historical Gold Mine Tailings in Nova Scotia. Open File Rep. ME 2015-004 15.

European Space Agency, 2015. Sentinel-2 User Handbook 64.

Faribault, E.R., 1900. The gold measures of Nova Scotia and deep mining / by E.R. Faribault. Together with other papers bearing upon Nova Scotia gold mines. Mining Society of Nova Scotia, Halifax, N.S.

Goetz, A.F.H., Curtiss, B., Shiley, D.A., 2009. Rapid gangue mineral concentration measurement over conveyors by NIR reflectance spectroscopy. *Miner. Eng.* 22, 490–499.

<https://doi.org/10.1016/j.mineng.2008.12.013>

Gorelick, N., Hancher, M., Dixon, M., Ilyushchenko, S., Thau, D., Moore, R., 2017. Google Earth Engine: Planetary-scale geospatial analysis for everyone. *Remote Sens. Environ.* 202, 18–27.

<https://doi.org/10.1016/j.rse.2017.06.031>

Gregorutti, B., Michel, B., Saint-Pierre, P., 2017. Correlation and variable importance in random forests. *Stat. Comput.* 27, 659–678. <https://doi.org/10.1007/s11222-016-9646-1>

Groves, D.I., Goldfarb, R.J., Gebre-Mariam, M., Hagemann, S.G., Robert, F., 1998. Orogenic gold deposits: A proposed classification in the context of their crustal distribution and relationship to other gold deposit types. *Ore Geol. Rev.* 13, 7–27. [https://doi.org/10.1016/S0169-1368\(97\)00012-7](https://doi.org/10.1016/S0169-1368(97)00012-7)

Guha, A., 2020. Mineral exploration using hyperspectral data, in: Pandey, P.C., Srivastava, P.K., Balzter, H., Bhattacharya, B., Petropoulos, G.P. (Eds.), *Hyperspectral Remote Sensing, Earth Observation*.

Elsevier, pp. 293–318. <https://doi.org/10.1016/B978-0-08-102894-0.00012-7>

Hartlen, J., 1988. *Gold! The Wealth of Waverley*. Lancelot Press, Hantsport, Nova Scotia.

Hennick, E.W., Poole, J.C., 2020. Nova Scotia Mine Tailings Database.

Hindmarsh, J., McLetchle, O.R., Heffernan, L., Hayne, O., Ellenberger, H.A., Mccurdy, R., Thiébaux, H.J., 1977. Electromyographic Abnormalities in Chronic Environmental Arsenicalism.

<https://doi.org/10.1093/JAT/1.6.270>

Intrinsic Corp, EcoMetrix, Crippen Berger, K., Wood, 2020. Human Health Risk Assessment of Sediment, Surface Water, and Fish from Barry's Run, Halifax Regional Municipality.

Intrinsic Corp, EcoMetrix, Crippen Berger, K., Wood, 2019. Conceptual Closure Study For The Historic Montague Mines Tailings Areas. Halifax, Nova Scotia. Final Report (Consulting). NS Lands Inc.

Jewell, D.A., 2021. Tailings Classification NS Repository. <https://doi.org/10.5281/zenodo.8273117>

Koch, I., McPherson, K., Smith, P., Easton, L., Doe, K.G., Reimer, K.J., 2007. Arsenic bioaccessibility and speciation in clams and seaweed from a contaminated marine environment. *Mar. Pollut. Bull.* 54, 586–594. <https://doi.org/10.1016/j.marpolbul.2006.12.004>

Lane, P.A., Pett, Robert J., Crowell, M. J., MacKinnon, D. S., Graves, Milton C., 1989. Further studies on the distribution and fate of arsenic and mercury at a site contaminated by abandoned gold mine tailings. *CANMET Spec. Publ.* 89–9, 77–107.

LeBlanc, M.E., Parsons, M.B., Chapman, E.E.V., Campbell, L.M., 2020. Review of ecological mercury and arsenic bioaccumulation within historical gold mining districts of Nova Scotia. *Environ. Rev.* 28, 187–198.

<https://doi.org/10.1139/er-2019-0042>

Mudroch, A., Clair, T.A., 1986. Transport of arsenic and mercury from gold mining activities through an aquatic system. *Sci. Total Environ.* 57, 205–216. [https://doi.org/10.1016/0048-9697\(86\)90024-0](https://doi.org/10.1016/0048-9697(86)90024-0)

Ngole-Jeme, V.M., Fantke, P., 2017. Ecological and human health risks associated with abandoned gold mine tailings contaminated soil. *PLOS ONE* 12, e0172517.

<https://doi.org/10.1371/journal.pone.0172517>

Parsons, M.B., LeBlanc, K.W.G., Hall, G.E.M., Sangster, A.L., Vaive, J.E., Pelchat, P., 2012. Environmental geochemistry of tailings, sediments and surface waters collected from 14 historical gold mining districts in Nova Scotia (No. 7150). <https://doi.org/10.4095/291923>

Parsons, M.B., Little, M.E., 2015. Establishing geochemical baselines in forest soils for environmental risk assessment in the Montague and Goldenville gold districts, Nova Scotia, Canada. *Atl. Geol.* 51, 364.

<https://doi.org/10.4138/atlgeol.2015.017>

Percival, J.B., White, H.P., Goodwin, T.A., Parsons, M.B., Smith, P.K., 2013. Mineralogy and spectral reflectance of soils and tailings from historical gold mines, Nova Scotia. *Geochem. Explor. Environ. Anal.* Vol. 14, 3–16. <http://dx.doi.org/10.1144/geochem2011-071>

Sangster, A.L., Smith, P.K., Goodfellow, W.D., 2007. Metallogenic Summary of the Meguma Gold Deposits, Nova Scotia (Special Publication No. 5), *Mineral Deposits of Canada: A Synthesis of Major Deposit-Types, District Metallogeny, the Evolution of Geological Provinces, and Exploration Methods.* Geological Association of Canada, Nova Scotia.

van der Meer, F., 2004. Analysis of spectral absorption features in hyperspectral imagery. *Int. J. Appl. Earth Obs. Geoinformation* 5, 55–68. <https://doi.org/10.1016/j.jag.2003.09.001>

van der Meer, F.D., van der Werff, H.M.A., van Ruitenbeek, F.J.A., 2014. Potential of ESA's Sentinel-2 for

geological applications. *Remote Sens. Environ.* 148, 124–133. <https://doi.org/10.1016/j.rse.2014.03.022>

Van der Werff, H., Van der Meer, F., 2015. Sentinel-2 for Mapping Iron Absorption Feature Parameters. *Remote Sens.* 7, 12635–12653. <https://doi.org/10.3390/rs71012635>

Van Rijsbergen, C.J., 1979. *Information retrieval*, 2d ed. ed. Butterworths, London ; Boston.

Walker, S.R., Parsons, M.B., Jamieson, H.E., Lanzirrotti, A., 2009. ARSENIC MINERALOGY OF NEAR-SURFACE TAILINGS AND SOILS: INFLUENCES ON ARSENIC MOBILITY AND BIOACCESSIBILITY IN THE NOVA SCOTIA GOLD MINING DISTRICTS. *Can. Mineral.* 47, 533–556. <https://doi.org/10.3749/canmin.47.3.533>

Wilkin, R.T., Barnes, H.L., 1997. Formation processes of framboidal pyrite. *Geochim. Cosmochim. Acta* 61, 323–339. [https://doi.org/10.1016/S0016-7037\(96\)00320-1](https://doi.org/10.1016/S0016-7037(96)00320-1)

Appendix A: Raw Data

Table 1. Geochemical analysis of all sediment samples. Table presented in two parts, showing results of 37 elements analysed via ICP-MS. Also available online, DOI: 10.6084/m9.figshare.23989908

Analyte	Mo	Cu	Pb	Zn	Ag	Ni	Co	Mn	Fe	As	U	Au	Th	Sr	Cd	Sb
Unit	PPM	PPM	PPM	PPM	PPB	PPM	PPM	PPM	%	PPM	PPM	PPB	PPM	PPM	PPM	PPM
MDL	0.01	0.01	0.01	0.1	2	0.1	0.1	1	0.01	0.1	0.1	0.2	0.1	0.5	0.01	0.02
Sample																
WV00S	0.16	11.37	48.56	187.9	54	34.2	15.9	2596	1.27	2055.8	0.2	36.2	2.4	38.4	0.6	1.19
WV00B	0.04	13.39	58.98	142.7	65	13.7	6.8	384	1.61	3740.4	0.3	25.7	2.9	30.2	0.64	0.85
WV01S	0.09	14.67	66.65	328.5	63	19.9	6.2	463	1.46	2970.9	0.2	49.4	2.9	20.3	0.88	2.7
WV01B	0.13	25.42	152.97	345.5	226	21.1	8.3	367	2.19	6142.6	0.3	200.6	3.9	25.9	1.4	5.71
WV02S	0.08	15.22	71	237.3	93	16.3	5.6	478	1.4	1753.3	0.3	113	3.1	45.5	0.78	1.54
WV02B	0.05	19.67	91.22	220.9	157	16.2	5.3	459	1.44	1885.5	0.3	281.2	3.4	32.8	1.01	0.99
WV03S	0.09	5.85	43.63	134.7	68	11.6	5.3	821	1.82	902.9	0.2	83	2.6	18.1	0.35	0.55
WV03B	0.24	32.34	294.53	505.3	470	46.9	12.9	802	3.66	5688.4	0.6	624	5.1	38.2	2.17	3.26
OH06S	1.09	45.91	61.47	144.1	213	33.7	16.1	945	3.41	2362.2	0.4	835.2	4.7	22.5	0.26	3.07
OH06B	0.59	36.86	53.22	116.4	112	29.8	11.8	326	2.64	749.2	0.4	198.4	5.1	19.9	0.2	1.55
OH07S	0.63	46.55	70.52	133.4	183	36.7	15.6	532	2.87	827.2	0.5	473.2	5.6	34.7	0.22	1.52
OH07B	0.44	47.13	92.16	122.9	205	39.3	18.5	739	2.92	1011.2	0.6	339.8	5.6	33.1	0.26	1.28
OH08S	0.95	30.82	45.77	122.1	88	31.4	12.7	766	2.69	590.8	0.5	304.1	5.8	43	0.21	0.75
OH08B	0.58	46.45	69.52	124.3	158	36.8	14.8	722	2.82	160.7	0.5	581.1	7.5	32	0.24	0.61
OH09S	3.19	48.75	66.76	153.3	109	30	11.8	781	2.73	307.8	0.5	95.4	5.2	19.2	0.38	0.88
OH09B	1.44	70.57	76.13	158.7	136	37	14.1	540	2.61	554.2	0.5	215.6	6.7	38.2	0.39	1.21
OH10S	0.59	52.6	62.72	120	140	34.1	15.2	449	2.77	612	0.5	863.8	5.9	15.6	0.32	0.81
OH10B	0.63	55.98	72.53	125.6	117	35.2	16.5	487	2.91	970.2	0.5	347.8	5.7	15.5	0.51	1
OH11S	1.08	49.08	68.51	169.1	133	41.8	18.3	1251	3.12	1295.1	0.5	161.4	6.1	63.6	0.43	0.82

OH11B	0.82	84.04	111.21	203.2	208	53.7	21.3	676	3.84	367.1	0.6	281.3	7.3	34.3	0.51	1.85
MO00S	0.71	59.45	54.61	110.7	124	28.5	10	448	4.05	12500	0.6	235.5	6	19.5	0.14	13.3
MO00B	0.69	102.45	33.61	168.7	105	36.5	17	615	3.84	5629.3	0.7	209.2	6.6	18	0.3	5
MO01S	0.46	52.18	44.86	94.4	84	26.2	10.5	415	3.6	9042.4	0.6	340.7	6.8	20.3	0.1	9.24
MO01B	0.36	54.54	31.62	108.1	78	31.7	11	519	3.32	5481.1	0.7	116.6	7.1	28.1	0.13	4.95
MO02S	0.54	119.85	79.12	257.1	229	57.4	28.1	746	4.95	16300	0.7	536.5	7.4	34.5	0.46	14.76
MO02B	0.32	53.92	40.15	113.4	85	28.5	10.2	453	3.67	8405	0.6	286.3	6	17.8	0.18	9.35
MO03S	1.01	59.22	37.69	124.3	121	41	13.7	519	4.19	4682	0.8	303.2	7.8	25.2	0.15	6.78
MO03B	0.48	59.89	45.34	133.9	137	41.2	16.1	606	3.85	5802	0.8	451.2	8.5	28.9	0.21	7.12
MO04S	0.67	24.84	73.68	75.2	188	24.8	8.9	315	4.38	14600	0.7	395	6.8	9.7	0.07	16.84
MO04B	0.49	54.78	48.87	115.3	200	38.3	43.4	740	3.6	6443.1	0.8	1103.7	7.8	10.3	0.27	8.19
MO05S	0.54	36.92	20.12	85	56	22.6	7.3	327	2.98	2085	0.6	165.2	6	11.3	0.09	2.03
MO05B	0.61	45.19	25.23	89.6	54	21.8	7.3	279	3.42	2394.1	0.7	159.7	6	10.7	0.1	2.3
MO06B	0.44	15.91	20.94	51.1	56	16.8	4.6	222	2.95	63.9	0.5	2.1	6.7	5.5	0.08	0.19
MO07B	0.33	10.99	15.81	51.8	120	10.1	3.1	167	2.26	56.4	0.3	2.3	2.7	3.7	0.08	0.18
ES01B	0.77	7.21	10.11	16.2	26	7.5	2.7	222	1.59	29.9	0.5	1	1.2	11.3	0.06	0.24
ES00B	0.5	4.8	6.06	23.4	22	7.7	2.9	139	0.8	3.4	0.5	<0.2	1.7	37.9	0.04	0.06
ES02B	0.44	7.09	6.34	31.5	11	9.3	4.4	255	1.64	17.4	0.6	<0.2	4.1	24.1	0.02	0.14
ES03B	0.78	7.76	6.38	28.7	9	9.4	4.3	243	1.89	26	0.6	<0.2	4.1	27.8	0.04	0.18
ES04B	3.93	18.47	21.23	63	109	24.3	8.6	334	2.71	17.8	1.9	5.8	4.1	47	0.53	0.15

Analyte	Bi	V	Ca	P	La	Cr	Mg	Ba	Ti	B	Al	Na	K	W	Sc	Tl	S	Hg	Se	Te	Ga
Unit	PPM	PPM	%	%	PPM	PPM	%	PPM	%	PPM	%	%	%	PPM	PPM	PPM	%	PPB	PPM	PPM	PPM
MDL	0.02	1	0.01	0.001	0.5	0.5	0.01	0.5	0.001	20	0.01	0.001	0.01	0.1	0.1	0.02	0.02	5	0.1	0.02	0.1
Sample																					
WV00S	0.28	6	0.31	0.034	8.2	6.4	0.3	29.9	0.003	<20	0.49	0.048	0.07	0.6	0.7	0.03	0.03	939	<0.1	0.05	1.4
WV00B	0.33	5	0.16	0.035	10.5	6.2	0.32	21.3	0.003	<20	0.56	0.012	0.07	0.5	0.7	0.03	<0.02	1249	<0.1	0.08	1.5
WV01S	0.38	5	0.19	0.033	10.7	6.6	0.34	27.7	0.003	<20	0.59	0.007	0.09	1.1	0.8	0.04	0.03	1324	<0.1	0.07	1.5
WV01B	0.94	6	0.22	0.048	13.4	10	0.43	23.9	0.003	<20	0.74	0.005	0.08	2.7	0.9	0.04	0.09	6827	0.1	0.14	1.9
WV02S	0.49	5	0.64	0.034	10.8	7.9	0.41	25.6	0.003	<20	0.57	0.007	0.08	1.5	0.7	0.03	<0.02	2956	<0.1	0.06	1.5
WV02B	0.63	5	0.38	0.038	11.9	7.5	0.42	22.1	0.003	<20	0.58	0.005	0.08	1.8	0.7	0.03	0.03	3518	<0.1	0.06	1.6
WV03S	0.31	6	0.31	0.039	9.3	7	0.36	42.3	0.002	<20	0.59	0.006	0.05	2.4	0.7	0.03	0.02	3868	<0.1	0.04	1.6
WV03B	2.01	11	0.56	0.057	15.9	20.2	0.92	48.4	0.004	<20	1.42	0.003	0.12	7.3	1.5	0.08	0.4	25368	<0.1	0.24	3.8
OH06S	0.5	15	0.32	0.058	21.4	17	0.65	45.6	0.044	<20	1.21	0.007	0.23	13.8	1.6	0.21	0.11	6219	0.3	0.23	3.8
OH06B	0.38	15	0.21	0.056	25.1	15.5	0.65	35.8	0.045	<20	1.18	0.005	0.23	5.2	1.6	0.21	0.07	3293	<0.1	0.11	3.7
OH07S	0.48	17	0.75	0.054	26.1	17.7	0.74	49.4	0.052	<20	1.34	0.008	0.35	3.3	1.8	0.26	0.03	3241	<0.1	0.07	4.1
OH07B	0.6	17	0.77	0.057	26.8	18.8	0.75	52.9	0.055	<20	1.36	0.008	0.37	1.2	2.1	0.26	0.02	9469	<0.1	0.09	4.1
OH08S	0.29	15	0.74	0.06	26.3	15.6	0.69	43.7	0.044	<20	1.21	0.006	0.21	1.8	1.6	0.22	0.03	2307	<0.1	0.05	3.6
OH08B	0.42	16	0.39	0.064	33.5	18.6	0.75	43.9	0.055	<20	1.35	0.006	0.29	10.8	2	0.23	<0.02	1954	<0.1	0.05	4.1
OH09S	0.37	17	0.31	0.061	25.9	17.3	0.68	51.3	0.044	<20	1.3	0.011	0.23	1.4	1.8	0.2	0.05	2454	<0.1	0.04	3.9
OH09B	0.47	16	0.89	0.055	31.9	17.6	0.69	42.9	0.047	<20	1.23	0.008	0.32	2.2	1.9	0.22	0.1	3464	<0.1	0.06	4
OH10S	0.35	16	0.15	0.053	25.6	17.3	0.69	43.2	0.052	<20	1.26	0.007	0.32	0.5	1.8	0.25	<0.02	1683	<0.1	0.06	4
OH10B	0.39	16	0.14	0.053	26.9	17.5	0.7	47.6	0.055	<20	1.27	0.007	0.34	3.3	1.8	0.25	<0.02	1977	<0.1	0.07	4
OH11S	0.4	18	2.99	0.06	29.8	20.7	0.79	72.1	0.06	<20	1.39	0.006	0.3	2	2.2	0.32	0.05	2498	<0.1	0.06	4.5
OH11B	0.61	22	0.9	0.071	35.5	26.9	1.02	57.4	0.074	<20	1.77	0.008	0.45	2.1	2.6	0.37	<0.02	4628	<0.1	0.1	5.4
MO00S	0.9	18	0.26	0.045	22.3	18.1	0.83	59	0.06	<20	1.42	0.01	0.5	1.3	1.7	0.29	0.05	404	<0.1	1.2	4.1
MO00B	0.64	18	0.27	0.046	26.4	22.9	0.89	61.6	0.062	<20	1.52	0.01	0.54	0.4	2.1	0.29	<0.02	490	<0.1	0.57	4
MO01S	0.67	15	0.27	0.044	25.5	16.1	0.82	47.1	0.056	<20	1.3	0.006	0.44	1.3	1.6	0.25	0.06	427	<0.1	0.92	3.7

MO01B	0.58	16	0.47	0.045	26.4	16.8	0.93	57.5	0.061	<20	1.39	0.009	0.49	0.8	1.8	0.27	0.05	729	<0.1	0.57	4.1
MO02S	1.26	22	0.28	0.059	25.8	18.2	0.97	69	0.07	<20	1.6	0.011	0.4	1.1	1.9	0.29	0.29	1801	<0.1	1.91	4.5
MO02B	0.65	17	0.24	0.045	22.2	16.7	0.87	51.2	0.066	<20	1.4	0.006	0.48	1.7	1.7	0.28	0.04	293	<0.1	0.87	3.9
MO03S	0.69	18	0.47	0.051	34.1	22.3	0.97	61.2	0.075	<20	1.58	0.015	0.52	0.9	2.1	0.32	0.04	1078	<0.1	0.59	4.5
MO03B	0.77	19	0.47	0.058	33.6	19.9	1.02	63.8	0.08	<20	1.53	0.011	0.56	0.5	2.1	0.34	0.02	844	<0.1	0.84	4.2
MO04S	1.17	19	0.11	0.048	25	18.4	0.81	59.3	0.068	<20	1.47	0.006	0.51	2.3	1.9	0.3	0.09	2804	<0.1	1.57	3.9
MO04B	0.77	18	0.11	0.049	30	18.4	0.83	59.1	0.063	<20	1.5	0.006	0.49	0.5	1.9	0.29	0.04	5195	<0.1	1.62	4
MO05S	0.35	15	0.13	0.04	23.8	16.4	0.72	55.8	0.057	<20	1.25	0.008	0.41	0.4	1.5	0.22	<0.02	2474	<0.1	0.23	3.6
MO05B	0.59	15	0.12	0.043	23.3	17.7	0.74	48.8	0.058	<20	1.25	0.005	0.4	0.4	1.5	0.23	<0.02	3017	<0.1	0.29	3.6
MO06B	0.16	24	0.05	0.04	17.1	19.9	0.41	50.8	0.035	<20	1.75	0.008	0.14	0.9	1.8	0.15	0.02	121	0.7	0.02	4.4
MO07B	0.12	22	0.06	0.036	13.4	20.5	0.26	33.5	0.025	<20	1.57	0.005	0.08	0.9	1.3	0.1	0.03	60	0.7	<0.02	3.5
ES01B	0.06	23	0.12	0.033	11.6	12.2	0.17	22.8	0.04	<20	0.39	0.015	0.06	<0.1	1	0.03	0.02	100	<0.1	<0.02	1.8
ES00B	0.03	11	0.27	0.031	5.8	9.1	0.58	17	0.016	43	0.47	2.336	0.17	0.1	1.1	0.04	0.44	12	0.1	<0.02	1.5
ES02B	0.04	27	0.38	0.047	11.7	13	0.36	27.3	0.104	<20	0.74	0.035	0.12	0.1	2.2	0.06	<0.02	38	<0.1	<0.02	3.2
ES03B	0.03	26	0.37	0.046	11	12.7	0.32	26.9	0.09	<20	0.65	0.095	0.12	0.2	2	0.05	0.04	53	<0.1	<0.02	2.9
ES04B	0.17	31	0.33	0.109	15.5	26.3	0.88	47.9	0.032	44	1.26	2.583	0.36	0.2	2.9	0.28	1.32	61	1	<0.02	4

Appendix B: Additional Maps

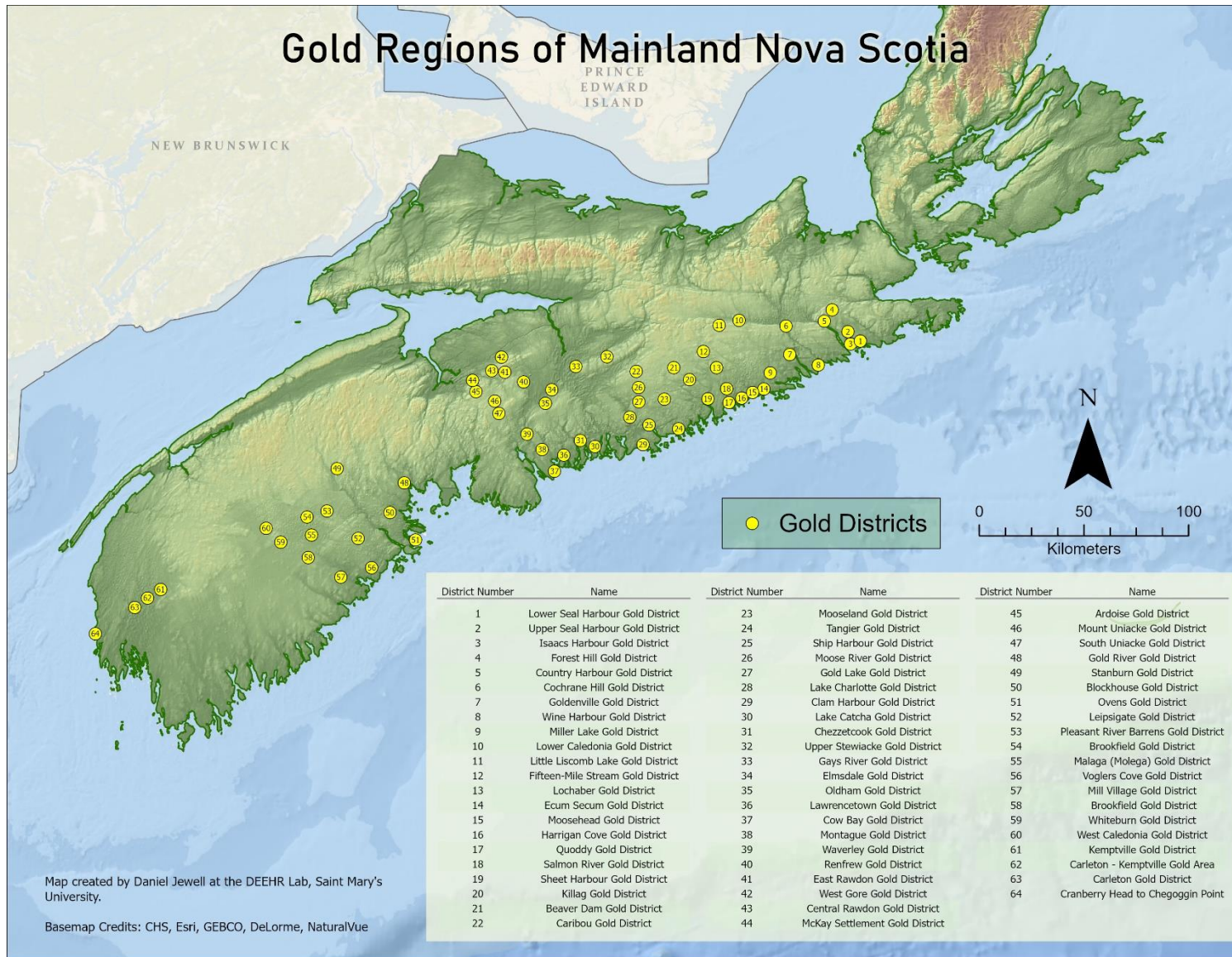
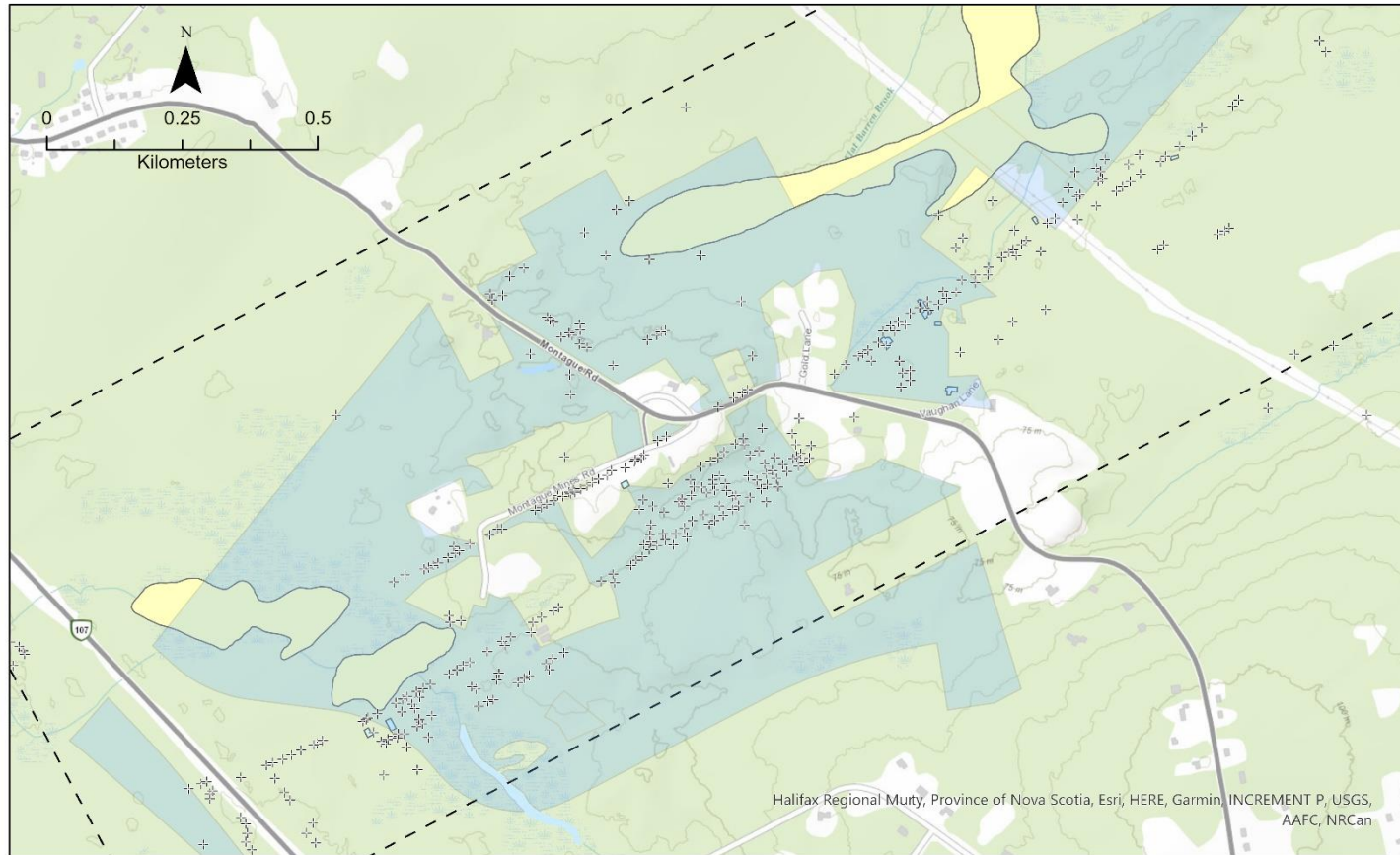


Figure 1. A map displaying all 64 historic gold mine districts in Nova Scotia

Montague Gold Mine District



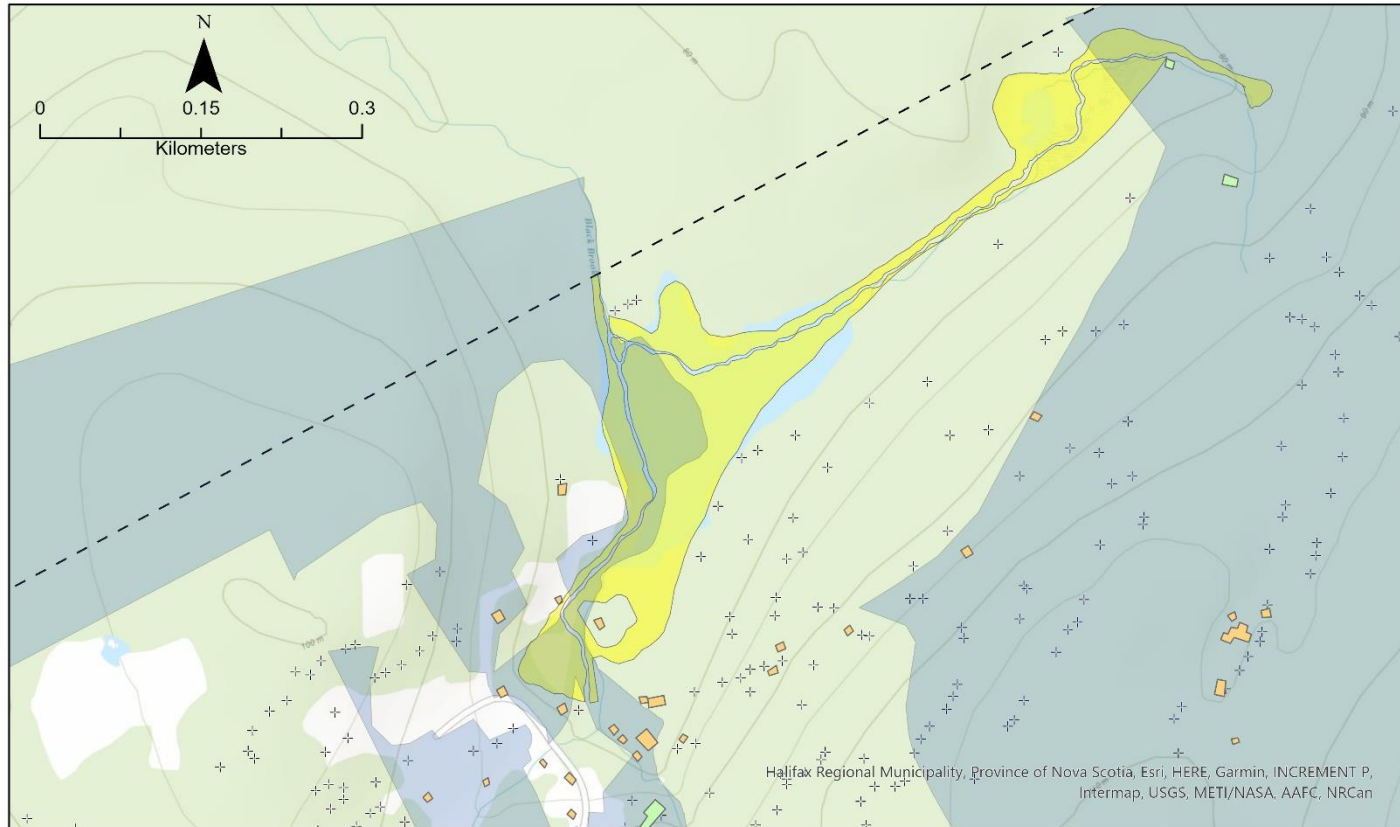
- + Mine Shafts (NSAMOD)
- Crown Land
- Buildings
- Tailings
- - - District Boundary

Crown land data for this map from the Nova Scotia Open Data Portal. Crusher, tailings, shaft (Faribault), and district boundary based on NS DNR Map, and is a digitized version of Geological Survey of Canada (GSC) Map 642, Oldham Gold District, compiled by E. R. Faribault, 1898. Shafts (NSAMOD) downloaded from the Nova Scotia Abandoned Mine Opening Database, subject to the NS Open Government License.

This map is for DEEHR group reference purposes only.

Figure 2. A map showing the Montague Gold Mine District and associated data found in the Nova Scotia Mine Tailings Database

Oldham Gold Mine District



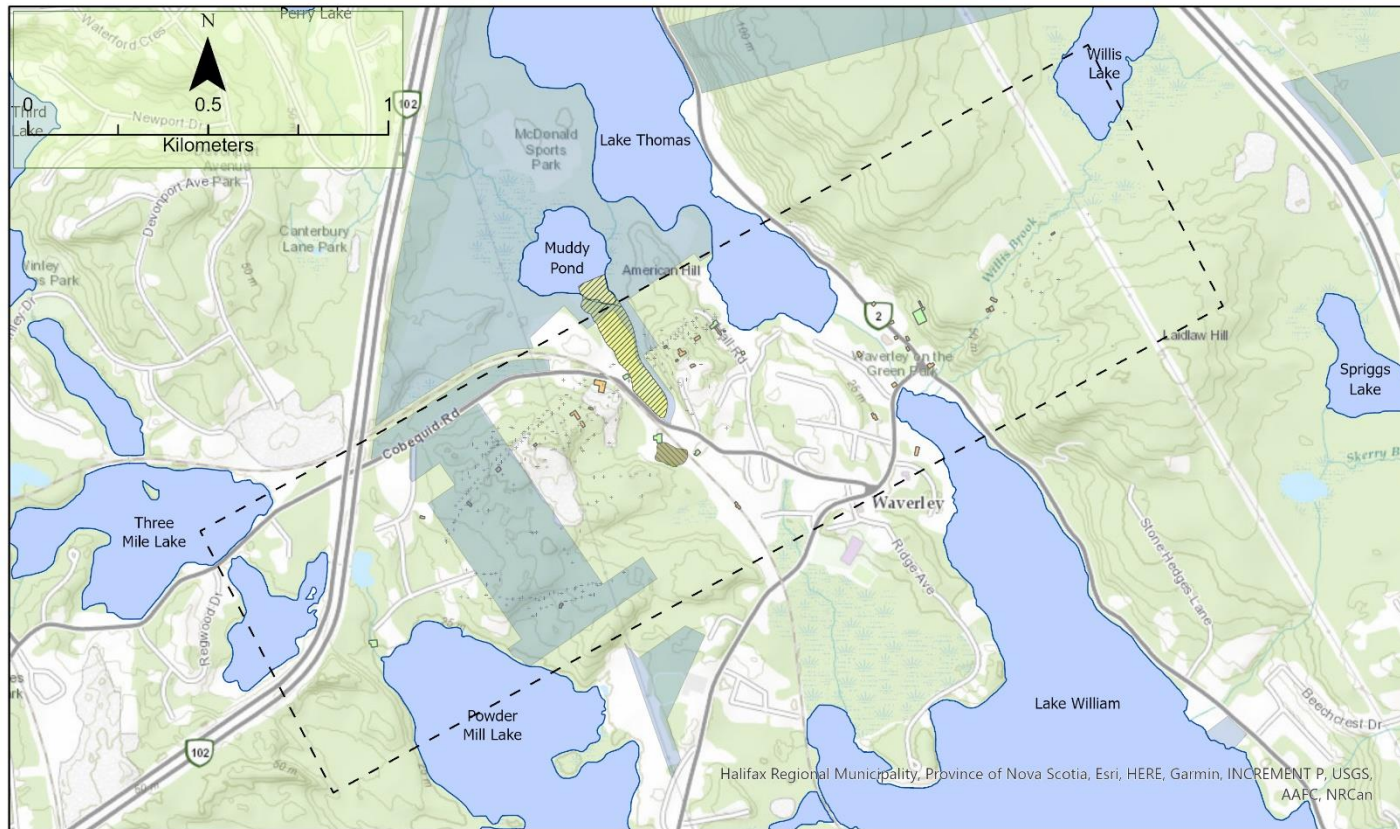
- Building (Other)
- Building (Crusher)
- Crown Land
- Tailings
- District Boundary
- + Shafts (NSAMOD)

Crown land data for this map from the Nova Scotia Open Data Portal. Crusher, tailings, shaft (Faribault), and district boundary based on NS DNR Map. and is a digitized version of Geological Survey of Canada (GSC) Map 642, Oldham Gold District, compiled by E. R. Faribault, 1898. Shafts (NSAMOD) downloaded from the Nova Scotia Abandoned Mine Opening Database, subject to the NS Open Government License.

This map is for DEEHR group reference purposes only.

Figure 3. A map showing the Oldham Gold Mine District and associated data found in the Nova Scotia Mine Tailings Database

Waverley Gold Mine District (Muddy Pond)



- | | | |
|-----------------------|-------------------|------------------|
| • Shafts (NSAMOD) | Tailings | Buildings |
| ⌈ ⌋ District Boundary | ▨ 2019 Fieldwork | ■ Crusher |
| ■ Crown Land | ▨ Historical Maps | ■ Other |
| ■ Lakes | | |

Crown land data for this map from the Nova Scotia Open Data Portal. Crusher, tailings, and district boundary based on NS DNR map and is a digitized version of Geological Survey of Canada (GSC) Map 721, Waverley Gold District, compiled by E. R. Faribault, 1898. Shafts (NSAMOD) downloaded from the Nova Scotia Abandoned Mine Opening Database, subject to the NS Open Government License. 2019 field map of tailings by Peter Opra.

Cartography by Daniel Jewell, Saint Mary's University, 2021

Figure 4. A map showing the Waverley Gold Mine District and associated data from the Nova Scotia Mine Tailings Database

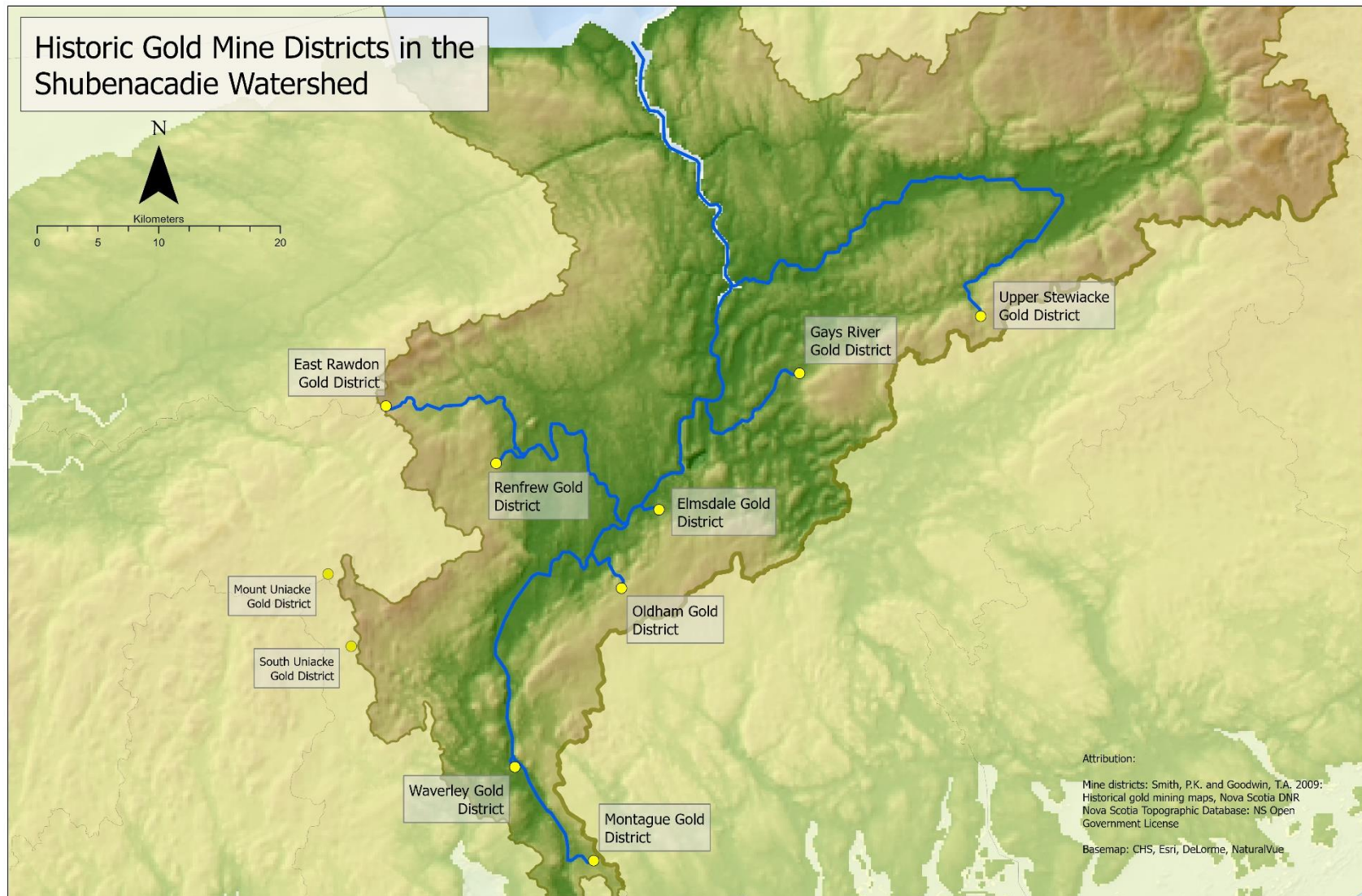


Figure 5. A map of all gold districts within, or on the border of, the Shubenacadie Watershed. This watershed includes the Montague, Waverley, and Oldham Gold Mine Districts. It feeds directly into the Atlantic Ocean.